Examining the Effects of Activator Compounds on hERG Cardiac Potassium Channel Protective Currents Conducted in Response to Premature Stimulations

by

Jacob Kemp

BSc., Simon Fraser University, 2016

Thesis Submitted in Partial Fulfillment of the
Requirements for the Degree of
Master of Science

in the
Department of Biomedical Physiology and Kinesiology
Faculty of Science

SIMON FRASER UNIVERSITY
Summer 2020

Declaration of Committee

Name:	**Jacob Kemp**
Degree:	**Master of Science**
Thesis title:	**Examining the effects of activator compounds on hERG cardiac potassium channel protective currents conducted in response to premature stimulations**
Committee:	**Chair: Sam Doesburg** Associate Professor, Biomedical Physiology and Kinesiology
	Thomas Claydon Supervisor Professor, Biomedical Physiology and Kinesiology
	Peter Ruben Committee Member Professor, Biomedical Physiology and Kinesiology
	Glen Tibbits Committee Member Professor, Biomedical Physiology and Kinesiology
	Edgar Young Examiner Associate Professor, Molecular Biology and Biochemistry

Ethics Statement

The author, whose name appears on the title page of this work, has obtained, for the research described in this work, either:

a. human research ethics approval from the Simon Fraser University Office of Research Ethics

or

b. advance approval of the animal care protocol from the University Animal Care Committee of Simon Fraser University

or has conducted the research

c. as a co-investigator, collaborator, or research assistant in a research project approved in advance.

A copy of the approval letter has been filed with the Theses Office of the University Library at the time of submission of this thesis or project.

The original application for approval and letter of approval are filed with the relevant offices. Inquiries may be directed to those authorities.

Simon Fraser University Library
Burnaby, British Columbia, Canada

Update Spring 2016

Abstract

The human ether-a-go-go-related gene (hERG) encodes the rapid delayed rectifier cardiac potassium channel. Vital for repolarization of the myocardium and termination of the cardiac action potential, loss of function in hERG K^+ channels can result in Long QT Syndrome Type II (LQTS2). Additionally, hERG channels have been shown to mediate robust repolarizing currents in response to premature depolarizations, reflective of channels remaining in the open state into the refractory period. Thought to be protective against afterdepolarizations, loss of function in this regard may leave individuals susceptible to arrhythmia. Recently, several small molecule activators of hERG have been discovered. The effects of these compounds on the protective currents mediated by hERG channels have yet to be studied. The work presented in this thesis examines the effects of both Type I and II hERG channel activators on protective currents mediated by hERG channels, in the context of an inherited mutation.

Keywords: hERG; Cardiac; Arrhythmia; LQTS; Activators

Acknowledgements

I would like to thank all those involved in this academic journey. Without the friends, family, and colleagues that I have been blessed with, this Thesis would not exist. I would also like to extend a special thank you to my senior supervisor, Dr. Tom Claydon, without whom this endeavour would simply not have been possible.

Table of Contents

List of Tables

List of Figures

List of Acronyms

hERG	Human Ether-a-go-go-related Gene
LQTS	Long QT Syndrome
LQTS2	Long QT Syndrome Type 2
AP	Action Potential
TEVC	Two-electrode Voltage Clamp
CiPA	Comprehensive *in vitro* Pro-arrhythmia Assay
iPSC	Inducible Pluripotent Stem Cell
GFP	Green Fluorescent Protein
FBS	Fetal Bovine Serum
Kv	Voltage-gated Potassium Channel
TdP	Torsades des Pointes
PAS	Per-Arnt-Sim
CNBHD	Cyclic Nucleotide Binding Homology Domain
EAD	Early Afterdepolarization
CHO	Chinese Hamster Ovary
HEK	Human Embryonic Kidney
QT_c	Heart Rate-corrected QT Interval

Chapter 1. Introduction

1.1. Ion Channels Overview

Ion channels are membrane-embedded proteins that span the lipid bilayer of the cell membrane. Acting as a conduit for charged particles to cross this lipid barrier, ion channels are expressed in all cells and are vital to excitability and excitable behaviour of tissues. Many different types of ion channels exist, and they are largely categorized first by the ion which permeates them most readily: Na^+, K^+, Ca^{++}, or Cl^-. Among ion channels that allow permeation of the same ion, further diversity exists according to the behaviour exhibited by the channel. Classified according to gating mechanism, ion channels can allow for ion permeation in response to changes in membrane potential, ligand binding, or coupling to other proteins. Voltage-gated potassium (Kv) channels are a diverse group of such proteins that selectively allow potassium ions to cross the cell membrane in response to a change in voltage. Kv channels have been shown to mediate outward repolarizing currents in many different physiological settings, including the heart. Vital for repolarization of the cardiac action potential (AP), Kv channels are largely responsible for terminating the cardiac AP (Matsuura et al., 1987). With such an important role in normal physiology, it would be expected that abnormal function of these Kv channels can result in potentially life-threatening arrhythmias. Indeed, loss of function of the gene product of the human ether-a-go-go-related gene (hERG)(Sanguinetti et. al., 1995; Trudeau et. al., 1995), has been shown to be responsible for Long QT syndrome Type II (LQTS2)(Curran et. al., 1995), which can lead to the potentially lethal arrhythmia, Torsades des Pointes (TdP). Thus, the importance of understanding both the structure and function of such a protein is apparent, as it better informs research into potential therapies. With this in mind, the subject of this thesis relates to the function of the hERG channel, and whether loss of function can be rescued using small molecule activators of the channel.

The proceeding introduction is a summary on the gating of hERG channels, and how loss of function due to inherited mutation or acquired drug block results in LQTS2. A brief synopsis of small molecule activators will follow, discussing the background of hERG channel activators and the problems facing their adoption as a viable therapy. This background will inform the thesis work presented here, which investigates the loss of

function observed in inherited LQTS2, and how it may be selectively rescued using small molecule activators.

1.2. hERG Discovery and Physiology

Much like all other ion channels, the story of the discovery of hERG begins with Hodgkin & Huxley's seminal work on action potential conductance in giant squid axons, and their ties to ion conductance across lipid membranes (Hodgkin & Huxley, 1952a, 1952b, 1952c, 1952d). Forming the bedrock upon which the field of electrophysiology is built, these papers tied the excitable behaviour of tissues to the coordinated movement of sodium and potassium ions via what we now know to be ion channels (Hodgkin & Huxley, 1952a, 1952b, 1952c). The first such potassium channel to be discovered and studied was the *Shaker* K^+ channel first identified in *Drosophila melanogaster (Papazian et al., 1987)*. Often referred to as the canonical voltage gated ion channel, *Shaker* is representative of a family of Kv channels that are broadly similar between one another in terms of structure and function. Until 1969, all identified Kv channels were assumed to be in this family, as their sequence similarity differed by at most, 35% (Warmke et al., 1991). However, in 1969, the discovery of *eag* exposed those assumptions as inaccurate (Kaplan & Trout, 1969). First identified in a mutant *Drosophila*, a shaking leg phenotype presented upon application of ether (Kaplan & Trout, 1969). The underlying protein was identified in 1991 when Warmke et. al. published the first report that tied the *eag* gene to a potassium channel polypeptide similar to the *Shaker* superfamily (Warmke et al., 1991). Following up on the study on *eag*, a human hippocampus cDNA library was screened using a mouse *eag* cDNA probe. This probe identified several genes with sequence similarity to that of *eag*. One such gene that was isolated and sequenced afforded the human-*eag*-related construct, the human ether-a-go-go-related gene (hERG)(Warmke & Ganetzky, 1994). This gene product was shown to have a 49% similarity in amino acid composition within the hydrophobic core with that observed in both *eag* and *elk* (ether-a-go-go-like) genes, and it was determined to be more closely related to these genes than those of the *Shaker* superfamily. For this reason, it was termed the ether-a-go-go-related gene. In humans, this gene is located on chromosome 7, and it has been shown that hERG channels, now known also as Kv11.1 following standardized nomenclature designation (IUPHAR), are expressed widely throughout the body, including the heart, brain, liver, pancreas, and microglial tissue of the brain (Curran et al., 1995; Warmke & Ganetzky, 1994; Zhou et al.,

1998). While this went a long way in determining where hERG channels fit into the Kv family of ion channels, it accomplished little in the way of functional characterization of the protein.

Beginning in 1987, a parallel, but independent line of inquiry was investigating repolarization of cardiac tissue that occurs during an AP by examining the constituent ionic currents mediated during repolarization. Prior to this point, it was thought that a single outward potassium current, I_K, was responsible for repolarizing the myocardium and terminating the ventricular action potential (Noble & Tsien, 1969). However, using isolated guinea pig ventricular myocytes, it was shown that I_K was a complex current comprising at least two components that could be pharmacologically separated by the application of the benzenesulfonamide Class III antiarrhythmic agent, E-4031 (Matsuura et al., 1987). Now able to isolate the component currents of I_K, studies were rapidly undertaken to characterize these currents and better understand their physiological significance. The portion of I_K sensitive to E-4031 was subsequently named the rapid cardiac delayed rectifier current, I_{Kr} (Sanguinetti & Jurkiewicz, 1990). Named for its rapid activation relative to other delayed rectifiers, it was shown that I_{Kr} fully activated at potentials positive to 0 mV (Sanguinetti & Jurkiewicz, 1990). While unable to explicitly identify the ion channel(s) underlying the current, these early functional studies discovered characteristics of hERG channel function now considered to be identifying hallmarks of the presence of the channel. Further interrogations of the I_{Kr} current led to the discovery that the molecular correlate of the current is indeed the hERG channel first identified by Warmke et. al. in 1994 (Sanguinetti et al., 1995; Trudeau et al., 1995). As observed in I_{Kr}, hERG channel conductance is maximal at potentials positive to 0 mV, at which point hERG channels show a progressive decrease in current amplitude due to a strong rectification mechanism. Identical to I_{Kr}, hERG channels also show susceptibility to block by E-4031 (Sanguinetti et. al., 1995; Trudeau et al., 1995). Further evidence is derived from the currents recorded from hERG channels, which are characterized by slow activation, and a much more rapid inactivation process at depolarized potentials that forms the basis of rectification. Channels rapidly recover from the inactivated state and an exceedingly slow deactivation process occurs following repolarization to more negative potentials (Sanguinetti et al., 1995; Trudeau et al., 1995). Of note, these functional studies were carried out after the cloning of the hERG gene, and so were carried out not in isolated guinea pig cardiomyocytes, but rather in single cell heterologous expression systems. As a result of

these unusual gating kinetics, hERG channels pass a bolus of outward current during phase three repolarization of the cardiac action potential upon recovery from inactivation. This outward repolarizing current is vital for the termination of the cardiac AP, and inherited mutations that disrupt the delicate balance of gating kinetics delay repolarization and lead to the potentially life threatening LQTS2 (Curran et al., 1995; Perrin et al., 2008). More recently, it has been posited that hERG channels may also exhibit a protective function mediated by the profoundly slow deactivation process (Lu et al., 2001, 2003). With a population of hERG channels remaining open well into the refractory period, they are kinetically unconstrained from passing repolarizing currents. As a result, in response to premature depolarization, hERG channels can pass a robust repolarizing current that may prevent the onset of arrhythmia (Du et al., 2010; Lu et al., 2001, 2003). Termed the protective current, the arrhythmogenic implications of a loss of function in this regard remain poorly understood. Should a loss of protective current lead to increased risk of arrhythmia, it stands to reason that dysfunction of hERG channel deactivation may alter the amplitude of hERG repolarizing current available during the refractory period. With this in mind, the protective current mediated by hERG channels may provide a novel therapeutic target for the treatment of LQTS2 that is more targeted than the oft-used β-adrenergic receptor blockers (β blockers).

1.3. hERG channels and the Cardiac Action Potential

The cardiac ventricular AP is a complex waveform that is made up of several constituent ionic currents (Fig. 1.1). These currents act in a highly coordinated fashion to produce the canonical waveform shown in Figure 1 that is responsible for excitation of the myocardium and subsequent contraction. Phase zero depolarization is mediated by an inward sodium current that acts to rapidly depolarize the membrane and propagate the action potential produced at the sinoatrial node. This is followed by a brief repolarization, termed phase one transient repolarization, and this is mediated by an outward potassium current, $I_{K,to}$, or the transient outward current. What follows is one of the defining features of the ventricular cardiac action potential, the plateau phase (phase two). This key determinant of AP duration allows for contraction to occur in a coordinated manner such that one action potential produces one wave of contraction, without the summation that is observed in skeletal muscle. The plateau phase is produced by an inward calcium current via the L-type calcium channel, along with a small electrogenic ‘current’ produced by the

sodium-calcium exchanger, NCX. These inward currents are somewhat balanced by early contributions of the delayed rectifiers, which produces the flat plateau observed in ventricular APs. Following the plateau phase, phase three repolarization is predominantly mediated by two outward potassium currents, which act to repolarize the membrane and terminate the AP. These outward potassium currents are referred to as the delayed rectifier currents, with I_{Ks} being the slow component, and I_{Kr} being the rapid component mediated by hERG channels (Sanguinetti et al., 1995; Trudeau et al., 1995).

The role of hERG channels in terminating the cardiac AP arises as a result of complex gating kinetics that produce a resurgent current during phase three repolarization (Sanguinetti et al. 1995; Trudeau et al. 1995). Similar to the voltage gated sodium channel responsible for the upstroke during phase zero, hERG channels activate in response to membrane depolarization. However, due to strong rectification produced by hERG channel inactivation, little current is passed until repolarization begins and recovery from inactivation into the open relaxed state occurs (Fig. 1.2A, C). This bolus of current then decays due to a combination of channel deactivation and the electromotive force for potassium ion movement approaching zero as the membrane repolarizes. Upon termination of the action potential, phase four occurs, termed the refractory period. In the early stages of this period, myocytes are thought to be in refractory, meaning that triggering of another action potential is less likely due to sodium channel inactivation. However, in the later stages of the refractory period, sodium channel recovery from inactivation and hERG channel deactivation results in termination of the refractory period, i.e. myocytes are able to be excited again by membrane depolarization. Thus, the refractory period could be separated into early phase four, whereby the myocardium is in refractory and unlikely to produce another AP in response to membrane depolarization, and late phase four, whereby the myocardium is able to become excited, but a subsequent action potential has not arrived as yet to start phase zero.

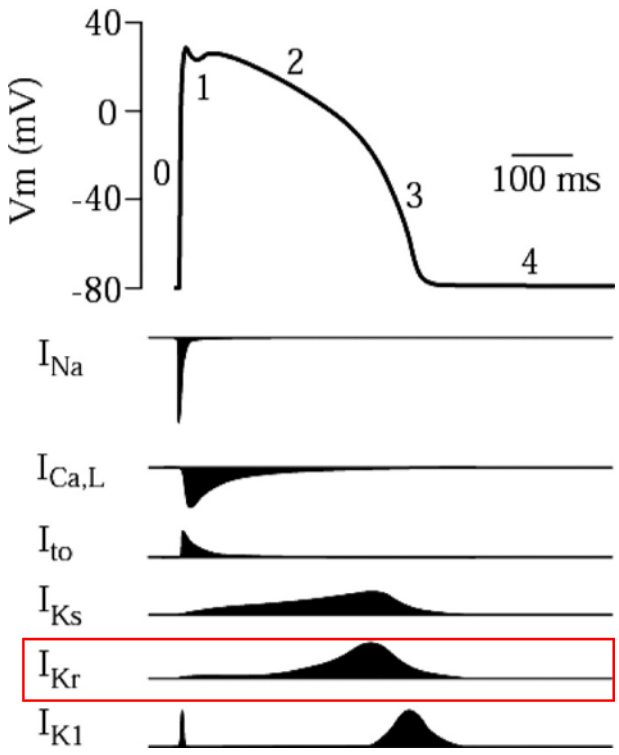

Figure 1.1 The cardiac action potential and its constituent currents.
(Boukens et al. 2009, *Circ Res*)

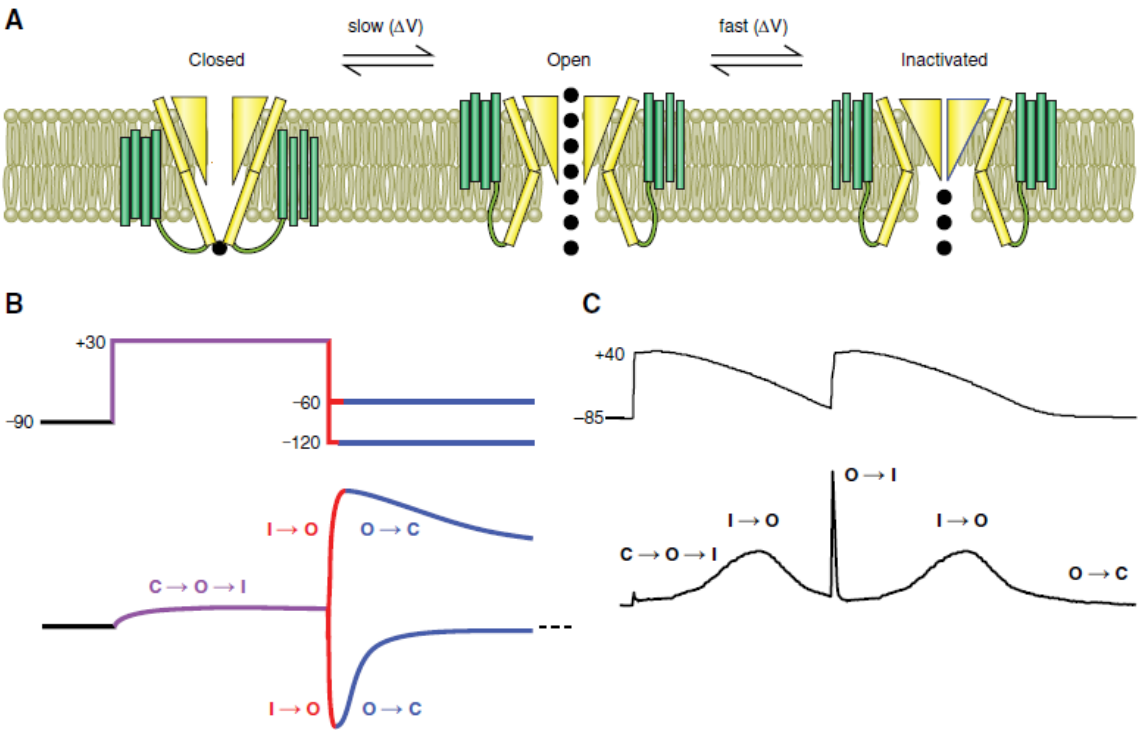

Figure 1.2 hERG channel gating scheme.
A. Schematic showing gating transitions observed in hERG channels. **B.** Top, protocol showing two test pulse potentials commonly used to observe hERG 'hooked' tail currents. Bottom, tail currents elicited in response to the two test potentials shown at top. **C.** Bottom, I_{Kr} current evoked in response to the protocol shown at top. Dominant gating transitions are shown over each region (Vandenberg et al. 2012, *Phys Rev*).

1.4. hERG Channel Structure

Until recently, the structure of hERG was largely inferred from functional studies, and the solving of crystal structures of a variety of other K^+ channels, including prokaryotic, eukaryotic, ligand gated, and voltage gated channels (Doyle, 1998; Jiang et al., 2002a, 2002b, 2003; Long, 2005a, 2005b; Zhou, 2001). While each of these studies identified common structure-function features between distantly related potassium channels, it was clear that the unusual gating behaviour exhibited by hERG channels was likely due to novel structural determinants. However, x-ray crystallography was unable to provide an answer as to the structure of the channel. As cryo-electron microscopy gained traction as a technique to elucidate protein structure, things shifted seismically. In 2017, the first structure of an open-state hERG channel was published by Dr. MacKinnon's group (Wang & MacKinnon, 2017). A landmark publication, it detailed several key features of hERG channels that differentiate them from both closely related *eag* (Kv10) and *elk* (Kv12)

channels, but also the more distantly related *Shaker* family (Kv1-9), which until then had served as a homology model for voltage dependent gating in hERG. Confirming the predicted fourfold symmetry of a prototypical Kv channel, hERG channels displayed four identical subunits with each subunit containing six transmembrane domains (S1-S6) and one pore helix (Sanguinetti & Tristani-Firouzi, 2006; Wang & MacKinnon, 2017; Warmke & Ganetzky, 1994). Transmembrane helices S1-S4 comprise the 'voltage-sensor' of the subunit, which is responsible for sensing changes in potential across the membrane (Bezanilla, 2000), while S5-S6 make up the pore domain, with an intervening pore helix between them. The remainder of this section will discuss elements of hERG channel structure and their functional consequences.

1.4.1. The Voltage Sensing Domain

As mentioned previously, the voltage sensor comprises the first four transmembrane segments, S1-S4 (Bezanilla, 2000). Responsible for sensing changes in membrane potential, the voltage sensing domain is the structural determinant of voltage sensing behaviour in all voltage-gated channels (Bezanilla, 2000). In *Shaker* channels, membrane depolarization results in the electrostatic repulsion of the S4 transmembrane segment, driving its displacement away from the intracellular leaflet and resulting in a conformational change that initiates channel opening (Stuhmer et. al. 1989, Perozo et. al. 1992, Stefani et. al. 1994, Bezanilla et. al. 1994). In hERG, this electrostatic repulsion is due to the presence of five key gating charges found in the S4 transmembrane helix (Liu et al. 2003, Subbiah et al., 2004). Spaced at regular intervals of one charge every three amino acids, these positive gating charges are not only responsible for voltage sensing but they also have been shown to contribute to the overall stability of the channel by interacting with acidic residues of S2 and S3 to form salt bridges (Liu et al. 2003, Subbiah et al. 2004, Zhang et al. 2005).

With broad similarity between hERG and *Shaker* in the context of gating mechanisms, it was assumed the two channels likely exhibited similar voltage sensing capabilities and transmitted this signal to the pore in a similar fashion. Indeed, it was later shown that the extent to which S4 moves in hERG was broadly similar to that observed in *Shaker* channels (Elliott et al., 2009). However, with the solving of the crystal structure of a mammalian *Shaker* family channel in 2005 (Kv1.2), and its comparison with the hERG structure published in 2017, it became clear that while both families respond to changes

in membrane potential, the manner in which this signal is transduced to the pore differs markedly (Long, 2005a, 2005b; Wang & MacKinnon, 2017). Indeed, with the publication of the cryo-EM structure of hERG, it was confirmed that unlike *Shaker* family Kv channels, hERG channels, along with *eag* and *elk* channels (Wang & MacKinnon, 2017; Whicher & MacKinnon, 2016), are non-domain swapped. This means that unlike in *Shaker*, where the voltage sensing domain of one subunit transmits its signal to the pore of an adjacent subunit via a short α-helical S4-S5 linker segment, hERG channels display an alternate signal transduction mechanism, whereby the voltage sensor is coupled to the pore of the same subunit. Inherently, this raises the question of how this voltage signal is transduced from the voltage sensor to the pore, as while hERG channels contain an S4-S5 linker, it is shorter than that observed in *Shaker* family Kv channels and it seems unlikely that mechanical transduction to the pore could be achieved in a non-domain swapped channel (Wang & MacKinnon, 2017).

It has been posited that voltage sensors in hERG and EAG1 transmit force through the S5-S6 interface, as there are multiple anti-parallel contacts between S5 and S6 that are consistent between the structures of hERG and EAG1 (Codding & Trudeau, 2019; Wang & MacKinnon, 2017; Whicher & MacKinnon, 2016). Indeed, it is thought that voltage sensor movements in hERG channels are transmitted at least in part by S4 mediated displacements of S5, that are then transmitted directly to the S6 helix due to its adjacent positioning and tight association (Codding & Trudeau, 2019; Wang & MacKinnon, 2017). It is worth noting that these interactions differ markedly from gating observed in *Shaker* family channels. Indeed, it has been posited that these interactions are relatively weak, and so may contribute to the slow activation observed in hERG channels (Codding & Trudeau, 2019). Further, the effects of this mechanism on the pore gave rise to the idea that the pore of hERG opens in a manner similar to that of a camera iris, whereby transmission of the voltage signal from S5 to S6 results in an outward radiation of the S6 helices to open the pore (Wang & MacKinnon, 2017). However, the idea that this means the S4-S5 linker serves no function in hERG is misplaced, as there is evidence that the S4-S5 linker forms specific interactions with the base of the S6 helix that have been shown to stabilize the closed state of the channel (Ferrer et al., 2006; Hull et al., 2014; Tristani-Firouzi et al., 2002; Van Slyke et al., 2010). Further, it has been shown that the length and flexibility of the S4-S5 linker have key implications for not only stability of the channel, but gating transitions between states (Hull et al., 2014; Van Slyke et al., 2010). As such, while

this linker is less ordered and thought to be unable to transduce force to the pore in hERG due to hypothesized structural limitations, it still retains functional features that contribute to the normal functioning of the channel. The role of the S4-S5 linker in hERG is however under consideration because of experiments conducted under split channel conditions, whereby the voltage sensor and pore were not covalently linked, which showed split hERG channels displayed WT-like function (de la Peña et al., 2018). The disruption of the S4-S5 linker shifted the voltage dependency of activation to more negative potentials, and the sigmoidal shape characteristic of activation time course was abolished. Deactivation kinetics were also slowed markedly. Taken together, this indicates a role for the S4-S5 linker in regulating the stability of the closed state of the channel, potentially as a signal integrator (de la Peña et al., 2018; Ng et al., 2012).

1.4.2. The Pore

The pore domain of ion channels is the conduit through which ions pass from one side of the cell membrane to the other. Comprising the S5-S6 helices, along with the intervening S5-P-loop helix, the pore receives the electromechanically coupled signal from the voltage sensor, and responds by transitioning to the open conducting state (Bezanilla, 2000). More detailed insights into structure-function relationships of the pore were discovered as the crystal structures of several different potassium channels were solved (Doyle, 1998; Jiang et al., 2002a, 2002b, 2003; Long, 2005a; Zhou, 2001).

With the publication of the crystal structure of KcsA, key mechanisms underlying potassium selectivity were elucidated and posited to be similar for most potassium channels due to key sequence similarities in the pore domain (Doyle, 1998). Of note, the narrow selectivity filter with the canonical sequence, TVGYG, was discovered to be only 12 Å long, with the remainder of the pore being wider, and largely lined by inert hydrophobic residues (Doyle, 1998). This large water filled cavity is the centre towards which the negative dipole of the four pore helices are oriented. This has the advantage of making the water filled cavity relatively electronegative, facilitating K^+ ion movement into the pore cavity and lowering the electrostatic barrier for ion movement across the membrane (Doyle, 1998). Taken together, this means that through structural features of the pore, K^+ ions only interact strongly with the channel along the 12 Å selectivity filter – the structure essentially results in the shortening of the distance the ion has to travel across the membrane to the length of the selectivity filter (Doyle, 1998). The crystal

structure of KcsA also afforded an answer to one of the larger questions surrounding ion selectivity in monovalent cation channels – namely, how is it that potassium channels are able to conduct larger potassium ions (Pauling radius 1.33 Å) with exquisite selectivity (as high as 10,000:1) relative to the smaller sodium ion (Pauling radius 0.95 Å) (Doyle, 1998). The answer was shown to lie within the structure of the selectivity filter, with its signature TVGYG sequence. Rather than the side chains, it was discovered that the backbone carbonyl groups of the selectivity filter are responsible for the coordination of potassium ions (Doyle, 1998). Indeed, one backbone carbonyl from each of the four channel subunits acts to dehydrate the incoming potassium ion, replacing the lost water molecules with the negative dipole of the carbonyl oxygen (Doyle, 1998; Zhou, 2001). This was unexpected, as it was thought that amino acid side chains were responsible for ion coordination rather than the carbonyl oxygens, which were shown to act as a surrogate hydration shell, lowering the free energy barrier for ion dehydration and conductance. This precise coordination allows for an energetically favourable dehydration of the potassium ion and permits its conductance across the membrane (Doyle, 1998; Zhou, 2001). With four such coordination sites identified, it was shown that only two are occupied at any given time at physiological K^+ concentrations (Doyle, 1998). The functional implications of this are significant, as the electrostatic repulsive forces between the two cations have been posited to lower the energy barrier for conductance, as the ion entering the coordination centres of the pore will repel the ion in the selectivity filter across the membrane and into the extracellular compartment. These characteristics of the pore region of potassium channels have been shown to be broadly similar between different families, with some distinguishing characteristics unique to each channel (Doyle, 1998; Jiang et al., 2002a, 2002b, 2003; Wang & MacKinnon, 2017; Zhou, 2001). With the publication of the cryo-EM structure of the open state hERG channel, our understanding of these subtle differences and their implications became more complete.

Several features of hERG channel function are unique, differentiating the channel from other Kv channels. Such key characteristics include the rapid, voltage dependent inactivation process, the non-domain swapped channel architecture, subtle differences in the canonical selectivity filter sequence, e.g. GFG rather than GYG, and the high affinity for a wide variety of compounds across diverse molecular classes; all of which are unique to hERG channels (Doyle, 1998; Perrin et al., 2008; Sanguinetti et al., 1995; Trudeau et al., 1995; Vandenberg et al., 2012). The Wang & MacKinnon structure provided several

structural explanations for the behaviours mentioned above that have illuminated further studies into the nuances of hERG function. Of note is that the central cavity found in all potassium channels is atypically small in hERG, and surrounded by four deep hydrophobic pockets (Wang & MacKinnon, 2017). It has been suggested that these pockets may be what confers sensitivity to such a wide variety of pharmaceutical compounds, as they are non-existent in most other K^+ channels and constricted shut in the closely related EAG1 channel (Wang & MacKinnon, 2017). This is consistent with key residues that have been identified and associated with high affinity drug block in hERG, as they are present within the hydrophobic pockets and central cavity just below the selectivity filter (Chen et al., 2002; Mitcheson et al., 2000; Perry et al., 2004; Wang & MacKinnon, 2017). Additionally, the smaller cavity of hERG has implications for drug binding. Particularly susceptible to block by cationic compounds and conjugated acids, the smaller central cavity would amplify the electrostatic potential, making it more negative relative to other channels (Wang & MacKinnon, 2017). This would favour the binding of such compounds and could partly explain the diversity of compounds that block hERG channels.

Publication of an open state hERG structure using cryo-EM also highlighted a subtle difference in the selectivity filter. The canonical selectivity filter sequence specific to potassium channels is TVGYG; however, in hERG it is SVGFG (Sanguinetti et al., 1995; Wang & MacKinnon, 2017). Additionally, the positioning of the side chain at F627 is subtly but indisputably different from other potassium channels. This residue has been posited as being key for rapid voltage dependent inactivation, as mutational analysis revealed that hERG S631A does not inactivate appreciably and F627 in these non-inactivating channels is positioned like other K^+ channels that do not inactivate appreciably (Wang & MacKinnon, 2017). This would suggest that the unusual selectivity filter sequence with phenylalanine in place of tyrosine may be responsible for hERG channel inactivation. However, tying one residue to the entire inactivation process may be inappropriate, as it has been shown that inactivation is a complex, multi-step process that includes molecular rearrangements throughout the channel, reminiscent of a Japanese puzzle box (Wang et al., 2011). Thus, several other domains of hERG have functional significance with regards to not only inactivation, but activation and deactivation processes.

1.4.3. Cytosolic N- & C-terminal Domains

hERG potassium channels contain two soluble intracellular domains per subunit: the N- and C-terminal domains (Sanguinetti et al., 1995; Wang & MacKinnon, 2017). The N-terminal tail contains the Per-Arnt-Sim (PAS) domain, and has been shown to interact with the cyclic-nucleotide binding homology domain (CNBHD) of the C-terminal tail to mediate channel deactivation (Codding & Trudeau, 2019; Gustina & Trudeau, 2011, 2012). Numerous mutations have been shown to impact deactivation gating in both the N-terminal PAS domain and the CNBHD domain, consistent with poor tolerance for even relatively conservative mutations (Gustina & Trudeau, 2009, 2011, 2012; Vandenberg et al., 2012). Interrogation of the interaction between the PAS domain and the CNBHD revealed that an intrinsic ligand exists within the CNBHD that serves to bind with the PAS domain and mediate slow deactivation in hERG channels (Codding & Trudeau, 2019; Gustina & Trudeau, 2011, 2012). Disruption of this interaction via deletion of either cytosolic domain or point mutation results in accelerated deactivation kinetics, reflective of the effect of the interaction on the stability of the open state (Codding & Trudeau, 2019; Gustina & Trudeau, 2011).

1.5. hERG Channel Gating

Since its first measurement, hERG gating has been a subject of great interest, as even apparently small shifts in gating kinetics can result in loss of function and LQTS2 (Curran et al., 1995). Typical of voltage gated channels, hERG channels activate in response to membrane depolarization in a voltage dependent manner. However, this activation is atypically slow relative to *Shaker* family channels, and is actually overshadowed by the rapid, voltage dependent inactivation process observed in hERG channels (Sanguinetti & Tristani-Firouzi, 2006). With both processes occurring over the range of depolarized potentials typical of a cardiac action potential, the exceedingly rapid inactivation occurs on a faster time scale than activation and results in little appreciable outward current when the myocardium is depolarized. Indeed, almost instantaneously upon activation, channels shift into a non-conducting inactivated state (Liu et al., 1996; Sanguinetti & Tristani-Firouzi, 2006; Vandenberg et al., 2012). Upon repolarization, channels begin to recover from inactivation, transitioning back into the open conducting state, before slowly undergoing deactivation and closing in the refractory period

(Sanguinetti et al., 1995; Trudeau et al., 1995). This gating scheme gives rise to the characteristic bolus of outward current observed during phase three repolarization that is mediated by hERG channels and largely responsible for terminating the cardiac AP (Matsuura et al., 1987; Sanguinetti & Jurkiewicz, 1990). With this vital function in mind, it is clear that understanding the nuances of hERG gating is vital to understanding the consequences of inherited mutation or high affinity drug block. The remainder of this section will briefly detail the gating processes of hERG.

1.5.1. Activation

hERG is a voltage-gated ion channel, meaning that in response to a change in transmembrane potential the channel senses the voltage, couples this signal to the pore, and opens in response (Bezanilla, 2000). Activation gating refers to the transition from closed to open states in response to this signal coupling. hERG is unique in that its activation process is exceedingly slow relative to other Kv channels such as *Shaker* (Piper et al., 2003; Sanguinetti et al., 1995; Smith & Yellen, 2002; Trudeau et al., 1995). With an order of magnitude separating the time constants of the two channels, it is clear that hERG channels activate differently from *Shaker* channels. Based on gating currents and evidence collected using the voltage clamp fluorimetry technique, it appears that this slow activation is due to slow voltage sensor movement, and it is this slow voltage sensor movement that is the rate limiting step in hERG channel activation (Piper et al., 2003; Smith & Yellen, 2002). It is worth mentioning here that hERG channel activation is a multi-step pathway, and that mathematical modelling has revealed the presence of a voltage-independent step that manifests as a sigmoidal relationship when plotting activation kinetics (Wang et al., 1997). Additionally, structure-function studies have revealed that activation gating is not limited to rearrangements of the voltage sensor, and have suggested that the S4-S5 linker may play a role in activation (de la Peña et al., 2018). However, the nature of this role is unclear, as previous studies were based on domain-swapped channel architecture, and the new evidence demonstrating non-domain swapped architecture has yet to reconcile with data showing S4-S5 linker perturbation of activation (Wang & MacKinnon, 2017). For example, with the discovery of the non-domain-swapped architecture of hERG, structural implications for activation become evident. Namely, it is unlikely that the short S4-S5 linker can act as a ‘lever’ to mediate pore opening in hERG as in *Shaker*. However, the data supporting a role for the S4-S5 linker

is compelling, and further studies are required to tease out the role of the S4-S5 linker in activation. In any case, Wang & MacKinnon have posited a possible mechanism describing electromechanical coupling in hERG channels, whereby S4 mediated rearrangements of the pore are transmitted via S5 to the pore through close opposition and packing of the S5 and S6 helices (Wang & MacKinnon, 2017). This highlights that S4 movement is the primary driver of activation, but perhaps the structural constraints imposed by non-domain swapped architecture could play a role in the slow movement of S4.

1.5.2. Inactivation

hERG channel gating is best described as a sequence of intricate processes that differs in many respects from most Kv channels. As mentioned above, activation gating in hERG channels is slow relative to *Shaker* channels. In addition to channel activation in response to membrane depolarization, hERG also undergoes a rapid, voltage dependent inactivation process that results in little functional current at depolarized potentials (Sanguinetti et al., 1995; Trudeau et al., 1995). Occurring in response to depolarization, inactivation renders the channel non-conducting. It is for this reason that during phase two of the cardiac AP, hERG mediates little appreciable current, and does not begin to do so again until membrane repolarization causes the channels to recover from inactivation into the open state (Sanguinetti et al., 1995; Trudeau et al., 1995). hERG is unique in that this inactivation is not only voltage dependent, but exceedingly rapid. Indeed, inactivation occurs over a more rapid time scale than activation, such that upon activation channels essentially immediately inactivate (Sanguinetti et al., 1995; Trudeau et al., 1995). As both activation and inactivation occur in response to membrane depolarization, the question as to how this change in voltage is sensed is raised. Evidence indicates that as with activation, the S4 transmembrane segment serves as the voltage sensor, albeit a different region from that observed with activation (Piper et al., 2005). Further irregularities in hERG inactivation gating involve the mechanism by which the channel inactivates.

Canonically, transitions to the inactivated state can occur as a result of N- or C-type inactivation. N-type inactivation is so named as it is mediated by the cytosolic N-terminal domain forming an association with the pore domain and physically occluding the conduction pathway (Hoshi et al., 1990). Rapid in time course, N-type inactivation is abolished with the removal of the N-terminal domain (Hoshi et al., 1991). The much slower

C-type inactivation is so named as it involves the collapse of the outer mouth of the pore, occluding the conduction pathway (Lopez-Barneo et al., 1993). In *Shaker*, inactivation is N-type and rapid, but removal of the N-terminus will result in C-type inactivation (Hoshi et al., 1991). Inactivation gating in hERG closely resembles C-type, as opposed to N-type inactivation (Sanguinetti & Tristani-Firouzi, 2006). Removal of the N-terminus does not abolish inactivation, while mutations in the outer pore region and S5-P-loop linker have been shown to significantly alter the process (Schönherr & Heinemann, 1996; Smith et al., 1996; Spector et al., 1996). However, limiting the mechanism behind inactivation to one region is inappropriate, as molecular rearrangements observed with inactivation occur all across the channel in a specific sequence (Wang et al., 2011). hERG inactivation gating is both complex and vital for normal cardiac function, as evidenced by various mutations that result in either long QT (E637K) or short QT syndrome (N588K) (Hayashi, 2002; Brugada et al., 2004), as a result of inhibiting or enhancing, respectively, hERG inactivation. While the functional consequences of perturbing hERG inactivation may be clear, why hERG channel inactivation is so rapid and voltage dependent has yet to be understood.

1.5.3. Deactivation

Upon repolarization of the membrane, hERG channels recover from inactivation and shift from the inactivated state to the open conducting state (Sanguinetti et al., 1995; Trudeau et al., 1995). This open state is inherently stable, and as such closure of the channel occurs exceedingly slowly, allowing for hERG to pass its physiologically relevant current during phase three cardiac repolarization (Sanguinetti et al., 1995; Trudeau et al., 1995; Vandenberg et al., 2012). Thus, slow deactivation is what gives rise to the canonical bolus of hERG current that is largely responsible for terminating the cardiac AP. Interestingly, the slow deactivation observed in hERG may also reflect slow movement of the voltage sensor, as in activation gating (Smith & Yellen, 2002). Evidence suggests that the voltage sensor transitions into a stable activated state, the relaxed state, which limits deactivation (Goodchild et al., 2015; Lacroix et al., 2011; Thouta et al., 2017; Villalba-Galea et al., 2008). There is also compelling evidence that both the N- and C-terminal cytosolic domains play key roles in mediating channel closure (Codding & Trudeau, 2019; Gustina & Trudeau, 2011, 2012). Specifically, mutations in the PAS domain and CBNHD were associated with altered deactivation (Gustina & Trudeau, 2009, 2011, 2012). With

this in mind, it was thought that perhaps an interaction occurs between these domains that somehow mediates channel closure. Indeed, recent evidence has confirmed that the CBNHD acts as an 'intrinsic ligand', associating with the PAS domain to mediate slow channel closure (Codding & Trudeau, 2019). Perturbation of this interaction through mutation or chimeric channels has been shown to accelerate deactivation significantly (Codding & Trudeau, 2019; Gustina & Trudeau, 2009, 2011, 2012; Liu & Trudeau, 2015). This suggests that the stability of the open state may be tied to N- and C-terminal interactions, and that destabilizing the open state accelerates channel closure (Chen et al., 1999; Goodchild et al., 2015; Gustina & Trudeau, 2011). This idea that destabilizing the open state results in accelerated deactivation is supported by experiments conducted in low pH. Protons have been shown to destabilize the relaxed state of the voltage sensor, promoting the destabilization of the open state, resulting in accelerated deactivation (Shi et al., 2014). In any case, it is clear that the slow deactivation gating observed in hERG channels is regulated by both relaxation of the voltage sensor and by the N- and C-terminal interactions. While slow deactivation has long been known to be important for the characteristic resurgent current mediated by hERG channels, it is increasingly thought that slow deactivation may also play a role in arrhythmia suppression, as explored below.

1.6. Slow Deactivation and the Protective Current

Since first being associated with LQTS2, the role of hERG in arrhythmia suppression and susceptibility has been extensively examined. Pharmacological inhibition of I_{Kr} reduces repolarization and prolongs the APD, creating a substrate for incidence of early afterdepolarizations (EADs) and arrhythmia (Kannankeril et al., 2010). Through its distinct gating kinetics, there is also evidence for a role in arrhythmia suppression with regard to premature beats. This hypothesized function has led to the idea that hERG channels mediate a protective current, specifically as a result of the particularly slow deactivation kinetics (Lu et al., 2001). Both square wave and dynamic action potential clamp experiments revealed that hERG channels pass robust repolarizing currents in response to premature stimulation (Lu et. al., 2001). First conducted at physiological temperature in Chinese Hamster Ovary (CHO) cells expressing hERG channels, square wave depolarizations followed by a second 'premature' square wave depolarization revealed that this protective current varies with both coupling interval and strength of depolarizing pulse (Lu et al., 2001). Investigation of the transient peak current in response

to premature stimulation revealed a biphasic distribution of current amplitudes, peaking at approximately APD_{90} (Lu et al., 2001). It is worth mentioning here that this is the approximate timing of the ventricular effective refractory period, suggesting functional significance. The currents in response to premature stimulation were noted to be instantaneous, with a slow decay. Reflective of channels already residing in the open state, channels do not require activation, inactivation, and subsequent recovery from inactivation to mediate current, and can therefore be said to be kinetically unconstrained. This suggests that the slow deactivation in hERG channels results in a population of channels remaining open well into the refractory period (Lu et al., 2001). Indeed, kinetic analysis revealed that the rising phase of protective currents reflected channels undergoing recovery from inactivation, while the decaying phase correlated well with deactivation gating (Lu et al., 2001). Taken together, there is compelling evidence that slow deactivation in hERG results in open channels during the refractory period that are able to pass robust repolarizing currents in response to any premature depolarization (Lu et al., 2001). These protective currents have understandably generated significant interest, as a loss of function in this regard would theoretically leave the myocardium susceptible to afterdepolarizations and premature beats (Du et al., 2010; Lu et al., 2001, 2003; Melgari et al., 2014; Perry et al., 2016).

Consistent with changes to the electrochemical driving force for ionic movement, the protective currents mediated by hERG channels are regulated by changes in ionic distribution across the membrane and in response to acidosis (Du et al., 2010; Melgari et al., 2014). Experiments conducted at low pH using an action potential voltage waveform revealed that a pH of 6.3 was sufficient to reduce outward current relative to control conditions (Du et al., 2010). Examination of the effects of low pH on hERG channel gating revealed that activation parameters were unchanged, while inactivation and deactivation showed a statistically significant shift in voltage dependence (Du et al., 2010). However, the statistically significant shift in inactivation gating was only 1 mV, and so the functional significance of this effect was minimized by the authors (Du et al., 2010). In contrast, application of low pH recording solution was sufficient to significantly accelerate deactivation in WT hERG (Du et al., 2010). Consistent with earlier reports linking deactivation kinetics with protective current mediated in refractory, extracellular acidosis resulted in significant reductions in protective current magnitude at all coupling intervals tested (Du et al., 2010). This may have profound implications when considering heart

failure and myocardial ischemia. Acidosis is a known consequence of both conditions, and a loss of function at a time when cardiac conduction is already impaired could be catastrophic. Another environmental condition that can affect protective current is hypokalemia. Known to result in reduced outward I_{Kr} during an AP waveform, it was shown that hypokalemia may also reduce protective current via reduced channel conductance despite the increase in the electrochemical driving force for potassium movement (Melgari et al., 2014).

With such diverse conditions affecting protective current via effects on hERG gating processes, questions surrounding the effects of inherited mutations and drug block on hERG protective currents are inherently raised. Experiments presented in this thesis with dofetilide show that high affinity drug block abolishes protective current in hERG channels. This stands to reason, as drug-block in hERG is associated with occlusion of the pore, and so with no accessory ion permeation pathways, it is expected that hERG protective current would also be abolished. However, the picture becomes less clear when discussing inherited mutations.

Inherited mutations in hERG have been shown to result in both loss of function and LQTS2, and gain of function and SQTS1, respectively (Brugada et al., 2004; Curran et al., 1995; Modell & Lehmann, 2006; Perrin et al., 2008; Sun et al., 2011). However, the mechanism by which mutations exert these effects are diverse. Mutations in hERG have been shown to exhibit altered gating that drives the observed loss of function (Vandenberg et al., 2012). Largely mediated by a left shift in the voltage dependence of inactivation, and thus its enhancement, outward current during depolarized potentials is reduced, ultimately leading to a prolonged AP and LQTS2 (Sanguinetti & Tristani-Firouzi, 2006). However, mutations affecting other gating processes have also been determined to result in a loss of function. Accelerated deactivation is such an example (Chen et al., 1999). The vast majority of hERG mutations; however, result in abnormal protein folding, and so are not expressed at the membrane and result in haploinsufficiency, or exert a dominant negative effect when incorporated into heterotetramers at the membrane (Vandenberg et al., 2012). Thus, pharmacological chaperones that were able to improve membrane expression were long hypothesized to be a potential therapy for affected patients. However, rescue of defective trafficking via incubation of *Xenopus* oocytes at low temperature revealed that even when expressed at the membrane, less than half of those tested showed WT-like gating characteristics with regard to protective current (Perry et

al., 2016). Co-expression with WT ameliorated these effects but did not abolish them. As such, in cases where mutations affect both expression and gating, the authors suggest that a combination of therapies targeting both expression and gating is required for rescue of function (Perry et al., 2016). Taken together, these observations show that the impact of mutations on the protective current in the physiological context are unclear and that mutations in the hERG protein affect the protective current through both deficient membrane expression and abnormal gating. Therefore, small molecule activators of hERG that potentiate channel function may provide benefit in both cases. My thesis focuses on addressing these questions.

1.7. hERG Loss of Function results in LQTS2

Long QT Syndrome is characterized by a prolonged heart rate-corrected QT (QT_c) interval on the electrocardiogram, in the absence of any obvious structural heart disease (Schwartz et al., 2012). Associated with an elevated risk of seizure and sudden cardiac death due to the lethal arrhythmia Torsade des Pointes (TdP), the first sign is often a syncopal episode (Schwartz et al., 2012). A complex syndrome, LQTS has been associated with inherited mutations in approximately fifteen different genes (Kapplinger et al., 2009; Schwartz et al., 2009, 2012). In addition to this inherited form of the syndrome, acquired LQTS2 may occur through high affinity block of hERG channels and makes up the majority of clinical cases. Of the genes associated with the inherited form of the syndrome, *KCNH2* (hERG) has been implicated in approximately 25-30% of cases (LQTS2), and almost all cases of acquired LQTS (Schwartz et al., 2009; Tester, 2014).

With regard to *KCNH2*, acquired LQTS results from physical occlusion of the pore due to high affinity drug block of its associated ion channel, hERG. As mentioned previously, hERG channels are the molecular correlate of the rapid delayed rectifier current and are largely responsible for the repolarization of the myocardium during phase three repolarization and termination of the cardiac AP (Sanguinetti et al., 1995; Trudeau et al., 1995). Regardless of the cause, both the inherited and acquired forms of the syndrome result in loss of repolarizing current and a delayed repolarization of the myocardium. This manifests as a prolongation of the cardiac action potential, and by extension, the QT interval, which leaves affected individuals susceptible to early-afterdepolarizations and subsequent development of TdP (Benhorin & Medina, 1997). The predominance of the acquired form of the syndrome has led to the adoption of

comprehensive screening procedures during drug development aimed at identifying compounds that block hERG channels.

With an estimated prevalence of 1:2500 people, the diagnosis and management of LQTS presents with several challenges, not least of which is the lack of effective treatment options. Most often, patients with clinically relevant LQTS will be prescribed β-blockers, a non-specific therapy that limits the dispersion of repolarization and subsequent risk of arrhythmia. However, many patients receiving β-blockers will experience breakthrough cardiac events such as syncope or sudden cardiac death regardless of the treatment received (Chockalingam et al., 2012). Notably, anti-arrhythmic compounds were suggested as a potential therapy, but many of these actually blocked hERG channels and resulted in an exacerbated phenotype, particularly the Class III antiarrhythmics (Spector et al., 1996). Severe cases of LQTS that are at high risk for sudden cardiac death may receive an implantable cardioverter defibrillator, as they have been shown to be effective at preventing or aborting arrhythmia (Cho, 2016). However, these devices are not without their drawbacks and are not appropriate for all patients. Cost-prohibitive, cardioverter defibrillators are not universally effective. Both lead failures and erroneous shocks can occur, neither of which are desirable in patients presenting with abnormal heart rhythm (Cho, 2016).

Further complicating the diagnosis and management of LQTS is the diversity of penetrance of the syndrome. While descriptive, the term ‘Long QT Syndrome’ is inappropriate for some patients who are genotype positive, as they show no obvious clinical signs. It has been shown that approximately 10-15% of patients presenting with a genotype-positive LQTS mutation will not display a prolonged QT interval (Giudicessi & Ackerman, 2013; Szabo et al., 2011). These cases of concealed LQTS present several challenges to clinicians with regard to risk stratification and suggest that characterization of each patients’ phenotype may be appropriate. Notably, in many cases where a disease-causing mutation has been identified, it is identified as being novel. Further complicating the picture is the presence of clinically relevant polymorphisms, such as K897T. Shown to have variable effects on hERG protein function, polymorphisms appear to exert differential effects on hERG function depending on other pathogenic mutations that may be found within the same gene (Anson et al., 2004; Bezzina, 2003). Taken together, the complexity of LQTS cannot be understated, and it is apparent that treatment options are lacking in diversity and efficacy. This is largely due to the high affinity of hERG for a wide variety of

molecular classes that can result in occlusion of the pore and acquired LQTS2 (Hancox et al., 2008). While block of hERG is a well-known phenomenon, it has been posited that there may be compounds that potentiate hERG function, although these would likely be quite rare in light of hERG channel promiscuity. Indeed, with the discovery of RPR260243 in 2005, it was confirmed that hERG agonists existed (Kang et al., 2005). The clinical value of these activators has yet to be fully realized, but their potential use as treatment options for LQTS is tantalizing. The following sections will discuss general characteristics of known hERG channel activators.

1.8. hERG Channel Agonists

hERG channels are susceptible to high affinity block by a wide variety of compounds across diverse molecular classes. This is a functional consequence of two aromatic residues; Y652 and F656, acting as binding sites, along with inactivation and possibly the previously discussed hydrophobic pockets (Chen et al., 2002; Mitcheson et al., 2000; Perry et al., 2004; Wang & MacKinnon, 2017). Additionally, the pore helix dipoles' orientation results in a negative dipole in the intracellular cavity that promotes the binding of positively charged compounds or those with a positive dipole (Wang & MacKinnon, 2017). These features render hERG particularly susceptible to drug block, although the mechanism and binding site for blockers appears to be consistent regardless of molecular class (Chen et al., 2002; Mitcheson et al., 2000; Perry et al., 2004; Vandenberg et al., 2012). Just as problematic as inherited mutation induced loss of function, high affinity drug block of hERG can reduce I_{Kr} and lead to acquired LQTS2. This has led to the inclusion of a hERG screen used in pharmaceutical research that has identified and removed compounds from development that block hERG channels. Regardless of the mechanism underlying loss of function, it has been posited for some time that pharmacological intervention using a hERG channel agonist may provide therapeutic benefit for patients with LQTS2. Interestingly, scans of these molecular libraries afforded a surprising discovery – small molecules that potentiate, rather than inhibit, hERG function. The first activator discovered was RPR260243 (Kang et al., 2005), a compound that was found to slow hERG channel deactivation. Since then, a number of other activators have been identified with effects on other gating parameters in addition to deactivation (Casis et al., 2006; Gerlach et al., 2010; Kang et al., 2005; Zeng et al., 2006; Zhang et al., 2012; Zhou et al., 2005). However, it is noteworthy that each individual

activator appears to have a distinct mode of action that has been posited as reflective of unique binding sites for each activator (Kang et al., 2005; Vandenberg et al., 2012; Zhang et al., 2012; Zhou et al., 2005). While each activator is unique in its mechanism of action, stratification of activators into classes according to the gating parameter affected is appropriate. Type I activators are classified as compounds that exhibit a slowing of deactivation kinetics (Vandenberg et al., 2012). Type II activators predominantly attenuate inactivation, with depolarizing shifts in the voltage dependency profoundly disrupting the C-type inactivation process and leading to large outward currents during phase two of the cardiac action potential (Casis et al., 2006; Gerlach et al., 2010; Vandenberg et al., 2012; Zhang et al., 2012; Zhou et al., 2005). The profound effects observed with application of Type II activators have led to the idea that an over-correction of loss-of-function may be possible, resulting in a drug-induced Short QT Syndrome (Perry et al., 2020). Still other activators do not fall neatly into either of these categories and so additional classes have been put forth, although these are poorly defined, and classification is largely limited to Type I or II (Rasmusson & Anumonwo, 2015; Vandenberg et al., 2012; Zeng et al., 2006). While the utility of some activators as viable pharmaceutical compounds has been called into question, discarding activators as a whole would be inappropriate. For example, Type I activators, such as RPR260243, might be expected to have minimal effects on outward currents during phase two of the cardiac action potential, which would be reflected in a largely unaffected action potential waveform, and this is an idea included in my thesis work. The remainder of this section will briefly discuss several key activators, and their potential utility in rescuing loss of function.

1.8.1. Type I hERG Channel Activators and RPR260243

RPR260243 was the first hERG channel agonist to be discovered (Kang et al. 2005) using high throughput scans of pharmaceutical compound libraries. Patch clamp electrophysiology revealed that RPR260243 slowed deactivation kinetics in a voltage- and temperature-dependent manner (Kang et al. 2005). With little effect on steady-state activation parameters and inactivation gating, hERG current magnitude remained unchanged. Interestingly, it was shown that RPR260243 had no significant effect on action potential duration or morphology in guinea pig myocytes, but when applied in the context of a dofetilide-induced AP prolongation using ventricular wedge preparations, RPR260243 was able to shorten APD_{90} (Kang et al. 2005). This provided evidence that RPR260243

may be appropriate for further study as a potential therapeutic agent. Later reports have shown that at elevated concentrations (>10 μM) RPR260243 does have a small but significant attenuating effect on inactivation gating and the kinetics of activation (Perry et al., 2007). However, these effects are quite small relative to the observed effects on deactivation kinetics. Indeed, while outward current amplitude increases with concentration of RPR260243, tail currents essentially do not decay at RPR260243 concentrations exceeding 10 μM (Kang et al., 2005; Perry et al., 2007). Taken together, it is clear that RPR260243 is a Type I activator, primarily affecting deactivation kinetics. Arguably, RPR260243 is the only true Type I activator currently known, as other activators with similar effects on deactivation also display profound effects on other gating parameters (Casis et al., 2006; Gerlach et al., 2010; Zhang et al., 2012; Zhou et al., 2005). RPR260243 was also shown to display specificity for hERG, with no observed effects on human cardiac sodium channels or KvLQT1/mink channels. Tested against L-type calcium currents recorded from guinea pig myocytes, RPR260243 was shown to have a small blocking effect at concentrations exceeding 10 μM (Perry et al., 2007). This effect was also observed on the *erg3* human brain potassium channel at 30 μM, which is of particular interest considering its close similarity to hERG (Perry et al., 2007).

The 2007 report by Perry et. al. was also instrumental in identifying the putative binding site for RPR260243. Previous reports had identified the binding site for two activators of KCNQ1 as being located in the S5-S6 region, and so mutagenesis scanning was undertaken in the same region of hERG, as well as the S4-S5 linker. Channel expression and recording in the presence of 3 μM RPR260243 revealed that mutation of 4 key residues rendered the channel essentially insensitive to RPR260243 (Perry et al., 2007). L553A, F557L, N658A, and V659A mutations were able to prevent the effects on both deactivation and inactivation induced by RPR260243. Located in two clusters at the base of S5 and S6, tucked just behind the S4-S5 linker, these residues form a small hydrophobic pocket and were identified as the putative binding site for RPR260243 (Perry et. al. 2007). A later report using concatenated tetramers confirmed the idea that this indicates the presence of four identical but distinct binding sites per channel (Wu et al., 2015). The location of the binding site at the interface of the voltage sensor domain and the pore domain provides a potential mechanism for the slowed deactivation observed upon application of RPR260243 (Perry et al., 2007). RPR260243 present in its binding site would be expected to interfere with electromechanical coupling between the S4-S5

linker and the pore domain, resulting in the slowed deactivation (Perry et al., 2007). This provides an interesting link to the mechanism of deactivation gating, as it supports the idea that deactivation involves the S4-S5 linker (Hull et al., 2014; Thouta et al., 2017). The residues identified earlier as the putative binding site of RPR260243 are conserved between hERG and *erg3*, raising the question as to why RPR260243 acts as an antagonist for *erg3* but an agonist for hERG. TEVC recordings in *Xenopus* oocytes revealed that a single amino acid (Thr556) substitution was responsible for this differential sensitivity. However, it is worth mentioning that RPR260243 has also provided additional evidence for the role of the cytosolic N- and C-terminal domains in channel closure (Gardner & Sanguinetti, 2015). Comparison of hERG1 and rERG2 mutants revealed that seven residues localized in the C-linker and two in the adjacent cyclic nucleotide-binding homology domain can account for the difference in sensitivity to RPR260243. Known to be important for deactivation gating (Codding & Trudeau, 2019; Gustina & Trudeau, 2009, 2011, 2012), the C-terminal domain interacts with the N-terminal PAS domain as an intrinsic ligand to mediate channel closure. Mutation of these C-terminal residues fully accounted for the difference in behavior between the channels when exposed to RPR260243 (Gardner & Sanguinetti, 2015). Supporting a role for both voltage sensor relaxation and the intrinsic ligand in hERG channel deactivation, RPR260243 highlights the complexities of hERG gating and indicates that deactivation may be more complicated that initially thought, bringing to mind the 'Japanese Puzzle Box' that describes inactivation gating in hERG (Wang et al., 2011).

In addition to the utility of RPR260243 as a tool to interrogate hERG channel function, RPR260243 may provide a novel therapeutic benefit to rescue loss of function. While the effect on deactivation is profound, it is clear that even at high concentrations of RPR260243 the effect on APD is minimal (Kang et al., 2005). This has led to the idea that drugs targeting deactivation would be unable to ameliorate the prolonged APD observed in phenotypically positive cases. However, as outlined above, hERG channels deactivate incredibly slowly. So slowly in fact, that a population of channels will remain open well into the refractory period, kinetically unconstrained and able to pass robust repolarizing currents (Du et al., 2010; Lu et al., 2001, 2003; Melgari et al., 2014). Established as protective in nature, it is conceivable that these open channels pass a current directly opposing premature depolarizations, such as early or delayed afterdepolarizations (Du et al., 2010; Lu et al., 2001; Melgari et al., 2014). With this in mind, an agent acting to slow

deactivation would increase this population of channels, rendering the myocytes better able to resist an afterdepolarization and prevent degeneration into arrhythmia. The utility of RPR260243 in this regard has yet to be explored and may provide novel opportunity for the treatment of LQTS2.

1.8.2. Type II hERG Channel Activators and ML-T531

Type II activators are hERG channel agonists that primarily act by attenuating inactivation through a depolarizing shift in the voltage dependency of the process (Vandenberg et al., 2012). They are the most diverse and numerous group of activators, and several were identified and characterized soon after RPR260243 (Casis et al., 2006; Gerlach et al., 2010; Potet et al., 2012; Zhang et al., 2012; Zhou et al., 2005). Consistent with initial reports, each activator seems to have a distinct action on hERG, and again this is likely reflective of the fact that they have distinct binding sites (Kang et al., 2005; Potet et al., 2012; Vandenberg et al., 2012; Zhou et al., 2005). One of the most well-studied of these agonists is PD-118057, which has been shown to increase single channel open probability and attenuate inactivation (Mao et al., 2013; Zhou et al., 2005). Additionally, relative to RPR260243, the effects of PD-118057 are functionally significant, as PD-118057 significantly shortens dofetilide-induced APD prolongation at much lower concentrations, and even in the absence of a repolarization deficiency (Zhou et al., 2005). A sizeable depolarizing shift in the voltage dependency of inactivation would be expected to increase current during phase two of the cardiac AP, and could potentially lead to Short QT Syndrome (Perry et al., 2020). In light of these concerns surrounding overcorrection using Type II activators that target inactivation, the therapeutic potential of hERG channel activators is under question. However, the discovery of compounds that can shorten APD and the QT interval is a tantalizing therapeutic prospect that should be explored thoroughly.

In light of the variable penetrance of the syndrome, it seems unlikely that at this stage a ‘silver bullet’ compound will be discovered that can be used to treat all cases of acquired and inherited LQTS2. Rather, with the advent of the Comprehensive *In Vitro* Proarrhythmia Assay (CiPA) and the idea that a simple hERG-block screen is insufficient to assess the arrhythmogenicity of a compound, it makes sense that different activators may be appropriate in different contexts. This would require robust characterization of both the patient’s LQTS2 phenotype and the effect of the activator on that given mutation. In

terms of practicality, this is consistent with the confounding role of hERG in drug development, due to the susceptibility of the channel to high affinity block by diverse molecular classes. However, with personalized medicine gaining traction and the advent of inducible pluripotent stem cell technologies, these barriers are diminishing. With all this in mind, testing a Type II activator within the context of reduced protective current would be informative. The ideal Type II activator used in such a case would be one that has a relatively specific effect on inactivation gating. A potential candidate activator is ML-T531, which has been shown to significantly increase outward currents during depolarized potentials in hERG channels, reflective of an approximately 30 mV depolarizing shift in the voltage dependency of inactivation in the presence of 10 µM ML-T531 (Zhang et al., 2012). Although less-well studied than other Type II activators, ML-T531 has a dominant effect on inactivation, although there is a modest slowing of deactivation kinetics (Zhang et al., 2012). With an EC_{50} of 5.71 µM in inducible pluripotent stem cells (iPSCs) and 3.13 µM in CHO cells, ML-T531 is a particularly potent activator, similar to PD-118057 (Zhang et al., 2012). While both NS-1643 and ICA-105574 are Type II activators and are well described, their effects are more diverse than those of ML-T531 (Casis et al., 2005; Gerlach et al., 2010). Indeed, there is some evidence that NS-1643 may have some blocking action in addition to its potentiating effects (Casis et al., 2005). It was observed that mutation of the Y656 residue known to be important for binding of blocking compounds rendered the channel sensitive to the activating effects of NS-1643 at all observed voltages, unlike WT channels (Casis et al., 2005). While ICA-105574 does not show blocking effects, it does act to slow deactivation kinetics (Gerlach et al., 2010). Additionally, the effect of ICA-105574 on inactivation is so potent, it essentially renders the channel unable to inactivate under physiological conditions (Gerlach et al., 2010). For these reasons, and to keep drug effects as specific as possible, ML-T531 appears to be an excellent candidate for further study in the context of this thesis. This study will assess the effects of the Type II hERG channel activator, ML-T531, on protective currents mediated by hERG channels in response to premature depolarizations.

1.9. Study Aims

The protective current mediated by hERG channels has been the subject of inquiry for some time. Thought to be protective in nature, loss of function in this regard has been observed due to inherited mutations and is thought to potentially leave affected individuals

more exposed to premature depolarizations and subsequent arrhythmia (Perry et al., 2016). This study aims to assess the effects of hERG channel agonists on the protective currents mediated by hERG channels, and to determine whether loss of function in this regard can be rescued by the application of an activator. The study will be divided into two stages.

1.9.1. Hypothesis 1: The Type I hERG channel activator, RPR260243, will increase protective current magnitude during the refractory period by slowing deactivation kinetics.

The first stage of this study will focus on the Type I hERG channel activator, RPR260243, and the effects on protective currents mediated by WT hERG channels and hERG R56Q mutant channels. The hERG R56Q mutation causes significantly accelerated deactivation kinetics, consistent with other mutations in the N-terminal PAS domain region. Accelerated deactivation kinetics would be expected to reduce channel availability during the refractory period, and would result in loss of protective current. I predict that application of the Type I hERG channel activator, RPR260243, will slow deactivation and increase channel availability during the refractory period, thereby increasing protective current magnitude and provide rescue of function caused by the R56Q mutation. This study will assess the effects of the R56Q mutation on protective currents mediated by hERG channels, and whether a loss of function in this regard may be rescued with the application of RPR260243.

1.9.2. Hypothesis 2: The Type II hERG channel activator, ML-T531, will increase protective current magnitude during the action potential, with limited effects on protective currents mediated during the refractory period.

The second stage of this study will focus on the Type II hERG channel activator, ML-T531, and the effect of its application on protective currents mediated by WT hERG and hERG R56Q mutant channels. ML-T531 acts primarily to attenuate inactivation gating, increasing outward currents at depolarized potentials (Zhang et al., 2012). Application of ML-T531 and measurement of protective currents mediated by hERG channels will allow for comparison of the actions of RPR260243 and ML-T531 on protective currents mediated by hERG channels. I hypothesize that the Type I activator, RPR260243, via its effect on deactivation kinetics, will primarily act on protective currents mediated during the

refractory period, while ML-T531 will act to primarily increase peak protective current magnitude, with limited effects on protective currents mediated during the refractory period.

Chapter 2. Materials & Methods

Acknowledgement: All experiments conducted at 21 °C, i.e. those in the *Xenopus* oocyte system, were carried out by the author. Patch clamp studies performed in HEK cells at 37 °C were carried out by Ravichandra Venkateshappa. Analyses, data handling and figure generation of patch clamp data recorded at 37 °C were done by the author. Mathematical modelling was carried out by Dr. Dominic Whittaker, under supervision of Dr. Gary Mirams, of the University of Nottingham. Figures depicting modelling data and outputs from the modelling experiments were generated by Dr. Whittaker. The author would like to take this opportunity to thank these individuals for their contributions, without which, this work would be incomplete.

2.1. Molecular Biology

For expression in *Xenopus* oocytes, hERG1a wild-type (WT) or mutant channel cDNA, subcloned into a pBluescript SKII expression vector, was linearized using the *XbaI* restriction enzyme to create a template for cRNA synthesis using the mMessage mMachine T7 Ultra cRNA Transcription Kit (Ambion, Austin, TX). Mutations were generated by conventional overlap extension PCR using mutagenic primers synthesized by Sigma-Genosys (Oakville, ON, Canada) and confirmed by sequencing (Eurofins MWG Operon, Huntsville, AL). For expression in Human Embryonic Kidney cells (HEK-293), hERG1a WT or R56Q mutant channel cDNA was subcloned into the pcDNA3 vector and used to co-transfect cells along with pcDNA vector containing the gene encoding green fluorescent protein (GFP).

2.2. hERG channel expression in *Xenopus laevis* oocytes and human embryonic kidney cells

Experiments were conducted at 21 °C in *Xenopus* oocytes and at 37 °C in HEK-293 cells. This approach allowed for examination of the effects of the mutation at both physiological and room temperature. The *Xenopus* oocyte system was selected for its robustness, which allows for stable recordings of large macroscopic currents over long durations. However, the *Xenopus* oocyte system cannot accommodate experiments at physiological temperatures. Additionally, using data recorded at 21 °C to model effects at

37 °C may be inappropriate, as hERG channel gating processes exhibit different Q_{10} values, meaning different gating parameters respond differently to changes in temperature. To address this, we used HEK-293 cells to collect data at 37 °C and streamlined the voltage protocols such that most of the relevant information could be collected from an 80 s recording. Previous reports had established that the *in silico* approach used by Beattie et. al. could recapitulate channel behaviour at 21 °C (Beattie et al., 2018). However, the versatility of this modelling approach with regard to temperature has yet to be established, and so our approach here allowed us the opportunity to challenge the robustness of the model to recapitulate behaviour at physiological temperature.

2.2.1. Expression of channels in *Xenopus* oocytes

Xenopus laevis frogs were terminally anaesthetized by immersion in 2 g/L tricaine solution (dissolved in dd H_2O, 1.1 g/L Hepes, titrated to pH 7.4) for 25 minutes before ovarian lobes were surgically removed. In agreement with the policies and procedures of the Simon Fraser University Animal Care Committee and the Canadian Council of Animal Care, euthanasia was assessed using multiple observations and severing of the spinal cord to confirm euthanasia. Ovarian lobes were treated with Type IA collagenase (1 mg/mL in $MgOR_2$ solution [in mM: 96 NaCl, 2 KCl, 20 $MgCl_2$, and 5 HEPES; titrated to pH 7.4 with NaOH]) for 45 minutes before manual removal of the follicular layer and isolation of stage V-VI oocytes. Surgically isolated stage V-VI oocytes from *Xenopus laevis* frogs were then injected with 50 nl hERG cRNA using a Drummond digital microdispenser and stored in SOS^+ solution (in mM: 96 NaCl, 2 KCl, 1.8 $CaCl_2$, 1 $MgCl_2$, 5 HEPES, 5% horse serum, 2.5 sodium pyruvate, and 100 mg/L gentamicin sulphate, titrated to pH 7.4 with NaOH) for 1-4 days at 19 °C before recording ion currents using the two electrode voltage clamp technique.

2.2.2. Expression of channels in HEK-293 cells

HEK-293 cells were cultured in DMEM culture media supplemented with 10% fetal bovine serum (FBS, Sigma-Aldrich) at 37 °C with 5% CO_2. For transfection, HEK-293 cells were plated onto 25 mm glass coverslips. After 14-16 h, cells were transfected with 2 µg WT or R56Q mutant hERG in pcDNA along with 0.5 µg GFP in pcDNA using 3.75 µL lipofectamine 3000 according to the manufacturer's instructions (Invitrogen). Transfected

cells were incubated for 24-48 h following which cells exhibiting green fluorescence were selected for whole cell patch clamp recording.

2.3. Data Acquisition

2.3.1. Two-Electrode Voltage Clamp

The two-electrode voltage-clamp technique was used to record from injected *Xenopus* oocytes with an OC-725C amplifier (Warner Instruments, Hamden, CT) and Digidata 1440 interface (Axon Instruments). This technique uses two intracellular electrodes to measure macroscopic currents generated by the movement of ions through ion channels across the membrane. One intracellular electrode precisely measures the transmembrane potential by comparing the tip potential with that recorded at a silver chloride bath electrode positioned adjacent to the oocyte, which serves as the reference electrode in this system. The measured transmembrane potential is relayed to an OC-725C amplifier that compares the measured potential at the membrane with that of the command output generated by digital voltage protocols. The Digidata 1440 interface serves to convert this digital command protocol into an analog signal recognizable by the amplifier. The amplifier compares the actual potential with the desired command output, and delivers a signal via the second intracellular electrode that injects current required to change the membrane potential by an amount proportional to the difference between the command and measured transmembrane potentials. This injected current represents the passage of ions across the membrane, and is acquired as our signal of interest. This signal is analog in nature and must be converted into a signal that the amplifier is able to interpret. This is achieved through the silver chloride electrodes housed within the borosilicate glass pipette. Electrons are transferred in both directions between the cell and the silver chloride electrode based on the equation:

$$e^- + AgCl \leftrightarrow Ag_{(s)} + Cl^-_{(aq)}$$

Effectively converting the excitable behavior into a digital signal, this signal is recorded and archived for analysis. A limitation of this system is that the current recorded is not just that which passes through our ion channels of interest. The cell membrane acts as a capacitor, and the recorded signal includes currents due to the charging and discharging of the membrane. Additionally, leak currents are component parts of the recorded signal,

due to an imperfect seal of the membrane around the impaled electrode. This was mitigated by good impalement of oocytes achieving low leak, and the discarding of cells that showed a high leak current. Capacitive currents were excluded by using square wave pulses wherever possible and excluding the first few hundred microseconds of the clamp, which shows the capacity transient. Additionally, it is worth noting that the cells are amphibian rather than mammalian, and that the clamp speed is relatively slow when compared with patch clamp or cut-open voltage clamp techniques. These concerns are addressed by our use of HEK-293 cells and the whole cell patch clamp technique. The advantage of the *Xenopus* oocyte system is that it allows stable recordings of robust currents due to the size of oocytes and their lack of endogenous ion channels, affording a high signal to noise ratio. Low resistance electrodes also permit measurement of large currents that can be used to detect phenotypic changes.

Oocytes were placed in a 1 mL bath chamber and perfused at 1 ml/min with ND96 solution containing (in mM): 96 NaCl, 3 KCl, 0.5 $CaCl_2$, 1 $MgCl_2$, and 5 HEPES, titrated to pH 7.4 with NaOH. Reagents were purchased from Sigma-Aldrich (Oakville, ON, Canada). Application of RPR260243 (Aobious Inc., MA) at different concentrations was achieved by 5 min perfusion of the compound dissolved in ND96 recording solution at the desired concentration to allow complete exchange of bath solution, followed by repetitive depolarizations to +40 mV (from a holding potential of -100 mV) at 0.2 Hz, to achieve a steady-state level of block, prior to recordings. Glass microelectrodes were made from thin-walled borosilicate glass (World Precision Instruments, Sarasota, FL) with a tip resistance of 0.2-0.8 MΩ when filled with 3 M KCl. Current signals were acquired at 10 kHz sampling frequency and were low-pass filtered at 4 kHz (−3 dB, 8 pole Bessel filter).

2.3.2. Two-Electrode Voltage Clamp Voltage Protocols

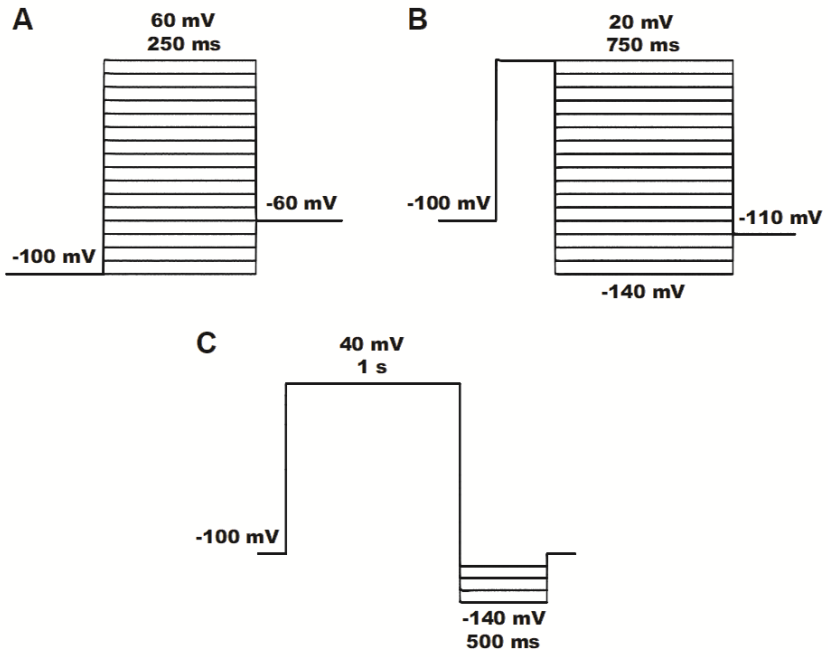

Figure 2.1. Two-Electrode Voltage Clamp Square Wave Voltage Protocols
A. Voltage protocol used to measure the voltage dependency of activation. **B**. Voltage protocol used to measure the voltage dependency of inactivation and recovery from inactivation. **C**. Whole-cell conductance protocol used to normalize protective currents and measure deactivation time constants in Chapter 3.

Activation

Data acquisition and analysis were performed using pClamp 10.2 (Axon Instruments) and SigmaPlot (Systat Software, San Jose, CA) software. The voltage dependence of channel activation was measured using a voltage clamp protocol that stepped the membrane potential from -100 to +60 mV in 10 mV increments for 250 ms (holding potential, -100 mV) before a 750 ms repolarizing step to -60 mV (Fig. 2.1A). These durations were selected due to their physiological significance. The 250 ms activating pulse is analogous in duration to a cardiac action potential, and the 750 ms test potential serves as a typical R-R interval, or an approximation of the time between heart beats at rest. These durations thus better recapitulate native channel behavior than long duration pulses lasting many seconds that allow steady state to be achieved. Peak tail currents

upon repolarization to -60 mV were measured, normalized to the maximum peak tail current recorded, and used to plot conductance-voltage (G-V) relationships.

Deactivation

Channel deactivation was measured during a voltage clamp protocol that delivered a 250 ms activating pulse to +40 mV from a holding potential of -100 mV before 750 ms repolarizing steps delivered in 10 mV increments to -140 mV before a final -110 mV step to report tail current amplitude (Fig. 2.1B). Deactivation kinetics were measured using a whole cell conductance protocol (Fig. 2.1C). An activating pulse to +40 mV from a holding potential of -100 mV was delivered for 1 s. This was followed by 500 ms repolarizing steps to a range of voltages from -110 to -140 mV. Current decay observed during the 500 ms repolarizing pulse was fit with a two-term exponential function that afforded two time constants, τ_f and τ_s, along with the amplitudes contributed by each component; A_f and A_s, respectively.

$$f(t) = \sum_{n=1}^{i} (A_{i)} * e^{\left(\frac{-t}{\tau}\right)} + C$$

The percentage contribution of the fast component to overall current decay was calculated from the relative fraction, $A_f/(A_f+A_s)$.

Inactivation

Channel inactivation was measured using the rectification method described by Sanguinetti et al. (Sanguinetti et al., 1990) from data recorded during the deactivation protocol (Fig. 2.1B). Peak current amplitudes during the 750 ms repolarizing step were plotted against voltage to obtain the fully activated I-V relationship. The rectification factor R was calculated at each potential using the current plotted in the maximal I-V relationship:

$$R = I_{hERG}/[G*n*(V_t - E_{rev})]$$

where G is the maximal conductance of hERG measured as the slope of the region of linear conductance and given in µS, n is the activation variable at +40 mV (1.0) (the proportion of channels activated at this voltage), V_t is the test potential, E_{rev} is the reversal potential of potassium, and I_{hERG} is the maximal leak subtracted current measured during the repolarizing pulses of the deactivation protocol. Rectification factor, R, is then plotted

against voltage to construct an inactivation G-V relationship. G-V relationships describing the voltage-dependence of channel activation, deactivation, and inactivation gating were fit with a Boltzmann function:

$$y = 1/(1+exp((V_{1/2}-V)/k))$$

where *y* is the normalized peak conductance, $V_{1/2}$ is the half activation, deactivation, or inactivation potential, *V* is the variable (test) voltage, and *k* is the slope factor.

Protective Current and Action Potential Waveform

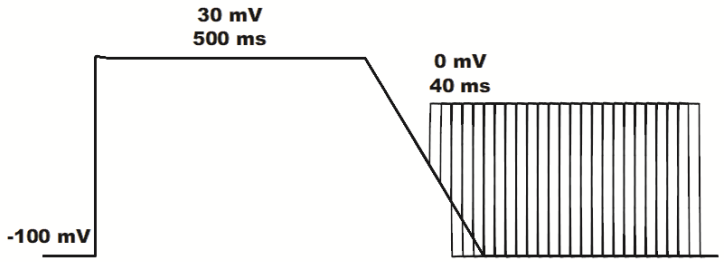

Figure 2.2. Premature Stimulation Voltage Protocol.
Voltage protocol used to quantify protective currents from Phase 3 repolarization into post-repolarization refractory.

hERG channel current passed in response to premature depolarization, described as protective current, was measured using a voltage protocol adapted from Perry et. al. (Perry et al., 2016) (Fig. 2.2). Oocytes were held at -100 mV before receiving a simplified action potential voltage waveform. Beginning at -80 ms (90% repolarization in the ramp portion of the protocol), 40 ms depolarizing steps to 0 mV were delivered at 10-20 ms intervals up to a coupling interval of 380 ms. The time at 90% repolarization was taken to be analogous to APD_{90}, and Δt from 90% repolarization is referred to as the coupling interval. Protective currents recorded in response to premature stimulation were transient and fitted with a single standard exponential function.

$$f(t) = \sum_{i=1}^{n} (A_i) * e^{\left(\frac{-t}{\tau}\right)} + C$$

Extrapolation of fits to t=0 afforded the protective current amplitude. Protective currents were normalized to whole cell conductance measured using the voltage protocol in Figure 2.1C in the same oocyte to permit comparison between constructs and conditions. In Figure 3.5E and 4.3D, data were normalized to whole cell conductance, and then normalized to the control peak protective current of the respective construct. WT and R56Q are plotted alongside one another to highlight differences in timing of the peak protective current, and the decay differences into the refractory period. Whole cell conductance was calculated using the region of linear conductance at hyperpolarized potentials, the slope of which is representative of whole cell conductance.

Membrane currents were recorded in response to action potential voltage waveforms to explore the influence of mutations and drugs on the dynamics of current flow during an action potential. Current recorded during the action potential voltage waveform shown in Figure 2.3 was normalized to the measured whole cell conductance to permit comparisons of mutation and drug effects. As part of our collaboration with Dr. Mirams' group at the University of Nottingham, we were also afforded the opportunity to work with a dynamic sine wave protocol of their own design to train kinetic modelling parameters (Fig. 2.4). The sine wave protocol delivers a voltage waveform that includes a complex oscillating sine wave. The oscillating sine wave affords rich kinetic data, allowing for the training of the Beattie model (Beattie et al., 2018), and subsequent validation against experimental repeats. All data are expressed as mean ± SEM (n=sample size). Statistical comparisons between means were conducted using student's *t*-tests or two-way ANOVA tests as appropriate, with $P < 0.05$ taken as an indicator for statistical significance. P values are given, except when lower than 0.001, which is expressed as P<0.001

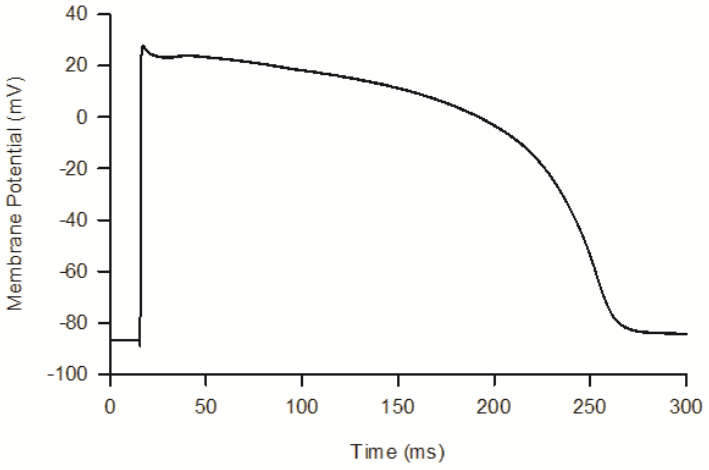

Figure 2.3. Action Potential Voltage Waveform.
Action potential waveform protocol used to explore the influence of mutations and drugs on the dynamics of current flow during an action potential.

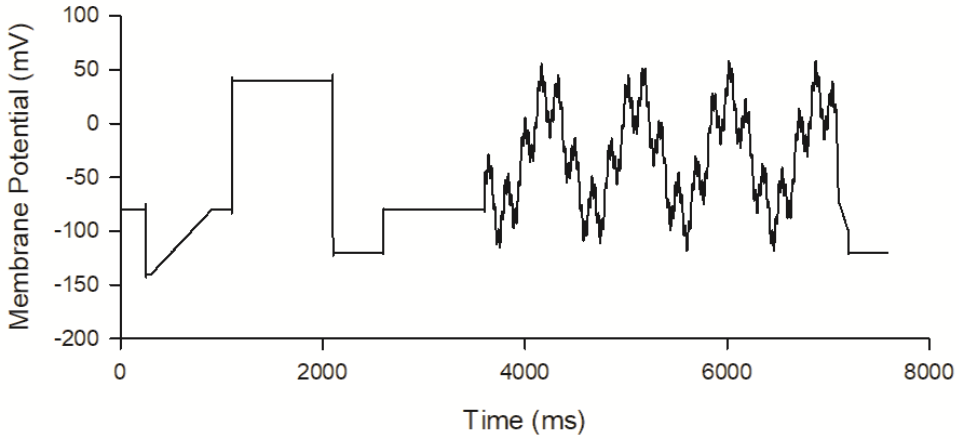

Figure 2.4. Sine Wave Voltage Protocol
Sine wave protocol used to acquire data to train the Beattie model. Cells are held at a potential of -80 mV and are subjected to a complex waveform including square wave pulses, a ramp phase, and the information rich oscillating sine wave. Data recorded in response to the protocol above are used to train the model for validation against experimental repeats.

2.3.3. Whole Cell Patch Clamp Recordings

Whole cell patch clamp recordings were performed using an Axon Instruments 200B amplifier and Digidata 1440 interface. Signals were acquired at 10 kHz sampling frequency and were low pass filtered at 4 kHz. Cells were perfused (2 ml/min) with external

solution containing (in mM):140 NaCl, 4 KCl, 1.8 $CaCl_2$, 1 $MgCl_2$,10 glucose, 10 HEPES (pH 7.4 with NaOH). Borosilicate glass capillaries (Sutter Instruments) were pulled using a P-97 puller (Sutter Instruments) to create patch electrodes, which were filled with internal solution containing (in mM): 130 KCl, 1 $MgCl_2$, 1 $CaCl_2$,10 EGTA, 10 HEPES, 5 Mg^{2+}ATP (pH 7.2 with KOH). Patch electrodes had a tip resistance of 3.7-4.5 MΩ. Series resistance was compensated 60-70%, with offline leak subtraction, using the amplifier circuitry. Bath temperature was monitored and controlled at 37 °C using a TC-344B Warner Instruments temperature controller unit with a heated platform and inline heater. Drugs were dissolved in DMSO and diluted to the desired concentration in external solution. Upon whole cell patch formation, recordings were made once the hERG tail current amplitude during a voltage step to -65 mV applied after a 2 s depolarizing step to +20 mV was stable.

2.3.4. Whole Cell Patch Clamp Voltage Protocols

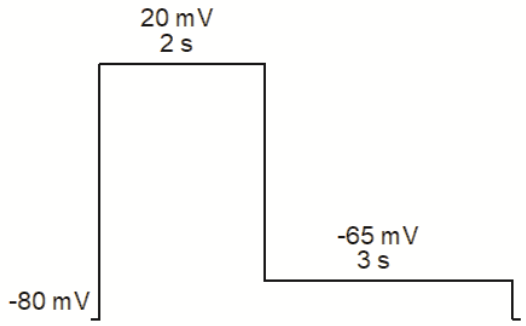

Figure 2.5. Patch Clamp Deactivation Voltage Protocol.
Voltage waveform used to record patch clamp data from HEK-293 cells. Cells were held at a potential of -80 mV before a 2 s activating pulse to +20 mV. A repolarizing step to -65 mV for 3 seconds was used to elicit hERG tail currents.

Figure 2.5 shows the protocol used to measure deactivation kinetics in patch clamp studies. Peak outward tail currents in response to this protocol were used to normalize patch data to permit comparison between constructs, as in our TEVC study. Tail current decay during the -65 mV test potential was fit with a two term exponential function to afford deactivation time constants. Figure 2.6 shows the premature stimulation protocol used to record protective currents mediated by hERG channels expressed in HEK-293 cells. Cells were held at a potential of -80 mV before a 200 ms activating pulse to 30 mV was

delivered. Beginning at a coupling interval of -30 ms, 40 ms premature depolarizations to 0 mV were delivered at 10-20 ms intervals. Currents recorded in response to premature depolarizations were fit with a single exponential function as with TEVC data, and normalized to the peak outward current elicited in response to the deactivation protocol outlined previously to permit comparison between constructs. Figure 2.7A shows the Action Potential Train Protocol, a complex waveform with a duration of 80 s that includes square wave pulses, ramp phases, the sine wave oscillation protocol, and the train of complex AP waveforms that mimic action potentials under various conditions. The duration of the protocol along with its complex waveform permits the acquisition of data that is particularly information rich. As with the Sine Wave Protocol outlined previously, we were generously provided with this stimulus waveform by Dr. Gary Mirams' group at the University of Nottingham. Both activation and inactivation voltage dependence may be derived from the protocol, with compiled modified protocols shown at inset of Figure 2.7. Additionally, the inclusion of the Sine Wave portion of the protocol allows for acquisition of information rich kinetic data that can be used to determine rate constants for the gating transitions observed in hERG channels. The action potential portion of the protocol shown in Figure 2.7B was used to derive quantitative data regarding the current mediated by both WT and mutant hERG channels during selected action potentials. Additionally, the data recorded in response to this protocol is used to train the Beattie model for validation against experimental repeats and more complex waveforms, such as the premature stimulation protocol or the AP Train.

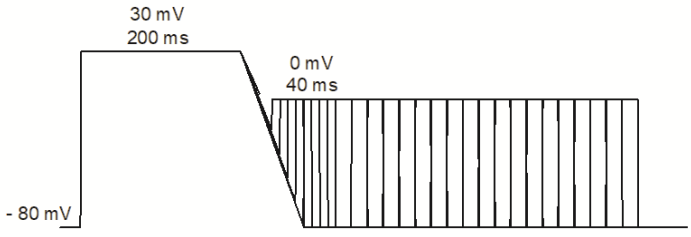

Figure 2.6. Premature Stimulation Voltage Protocol.
Voltage protocol used to record hERG protective currents in response to premature depolarizations in our patch clamp studies at 37 °C.

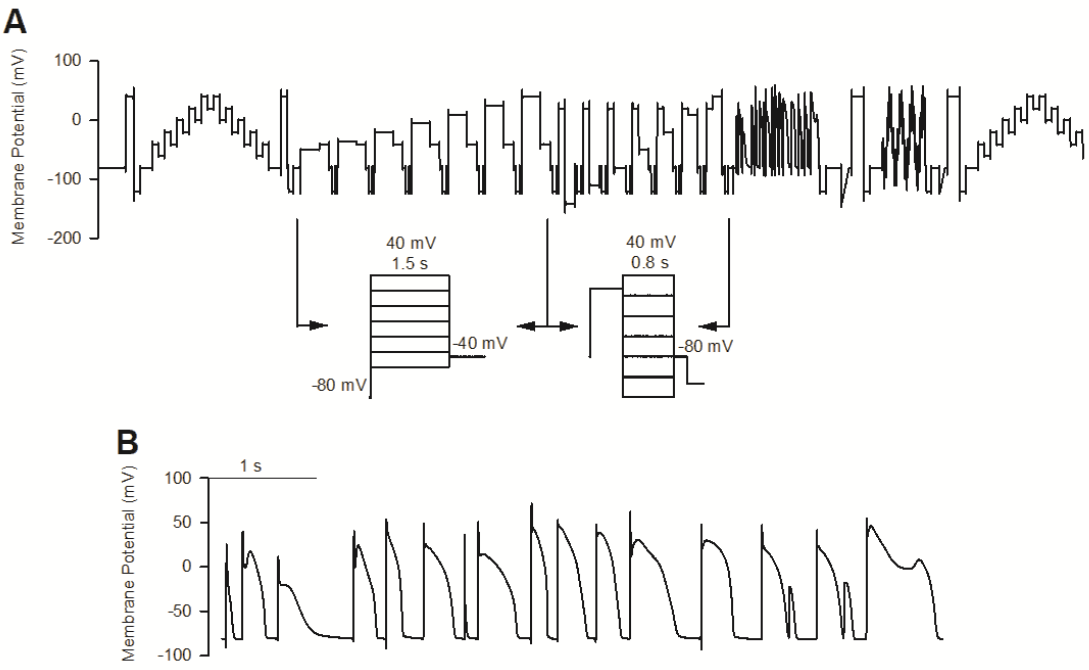

Figure 2.7. Action Potential Train Voltage Protocol.
A. Full 80 s Action Potential Train Protocol generously provided by Dr. Mirams' group. Cells are held at a holding potential of -80 mV before delivering the complex waveform. Left inset shows how the single sweep protocol may be compiled into an activation protocol, with several step potentials ranging from -50 mV to +40 mV. Tail currents elicited during the -40 mV test potential were normalized to the peak tail current elicited and fit with a single Boltzmann equation to generate activation G-V data. Right inset shows how the protocol may be compiled into an approximated deactivation protocol, used to generate an inactivation G-V curve. **B.** Immediately following the modified deactivation protocol, the train of complex AP waveforms is delivered, shown in **B**.

2.4. Mathematical Modelling

Mathematical modelling was carried out by Drs. Dominic Whittaker and Gary Mirams of the University of Nottingham using data recorded at 21 °C by the author, and 37 °C by Ravichandra Venkateshappa. Modelling was undertaken using the approach first described by Beattie et. al. (Beattie et al., 2018). Traditionally, mathematical modelling requires constraining models with data recorded at steady state conditions to yield various rate constants describing the kinetics of gating transitions as well as the voltage dependence of each process. However, these experiments are time consuming, and the model is applied to a different cell from that which it was trained. This can be problematic, as there is noted cell to cell variability in these parameters. The approach used by Beattie et. al. addresses this, as the 80 s information rich protocol described previously allows for

training of the model using the modified square wave step protocols and the sine wave oscillation, followed by validation against complex behavior in the same cell during the AP Train portion of the protocol. The rich kinetic data afforded by the sine wave results in a model that is simple relative to other models describing hERG gating. The Markov Model description of the Beattie Model is a four state model, with an inactivated, closed inactivated, open, and closed state. This differs from the Wang model, which is widely used, but emphasizes steady-state data as opposed to the kinetic data emphasized in the Beattie model (Beattie et. al., 2018; Wang et al., 1997). Also relatively simple, it is worth mentioning that the Wang model differs from the Beattie model in several key ways. While the Beattie Markov model has four states, the Wang model has five, with three closed states before transitioning to the open state, and then a fifth inactivated state. While more complex than the Beattie model, the Wang model was unable to predict experimental data as well as the Beattie model (Beattie et al., 2018). In spite of its simplicity, the predictive power of the Beattie model is significant, and appears to be due to its reliance on channel kinetics observed during the sine wave protocol (Beatie et al., 2018). Additionally, the predictive power of using a model trained in the same cell cannot be understated, as in other models kinetic data from one cell is applied to behavior recorded in a different cell. We employed the approach used by Beattie et. al., utilizing the complex AP Train protocol described previously. The step portions of the protocol shown at inset of Figure 2.7B and the sine wave oscillation were used to derive voltage dependence and kinetic data, respectively. This was used to train the model, before validation against the complex behavior observed during the train of action potentials delivered in the protocols later stages. Additionally, the model was asked to predict the more complicated waveform observed during protective current recordings in response to the premature stimulation protocol. Data is presented with model predictions alongside actual current recordings.

Chapter 3. The hERG Channel Activator, RPR260243, Reduces the Arrhythmogenic Potential of the R56Q LQTS-associated hERG Channel Mutation by Enhancing Repolarizing Drive in the Early Refractory Period

Acknowledgement: The work presented in this chapter is a modification of the work presented in Kemp et. al. (In preparation for submission). All experiments conducted at 21 °C, i.e. those in the *Xenopus* oocyte system, were carried out by the author. Patch clamp studies performed at 37 °C were carried out by Ravichandra Venkateshappa. Analyses, data handling, and figure generation of patch clamp data recorded at 37 °C were done by the author. Mathematical modelling was carried out by Dr. Dominic Whittaker, under supervision of Dr. Gary Mirams, of the University of Nottingham. Figures depicting modelling data and outputs from the modelling experiments were generated by Dr. Whittaker. The author would like to take this opportunity to thank these individuals for their contributions, without which, this work would be incomplete.

3.1. Introduction

The complexities of hERG gating are not yet fully explained. It is well known that loss of function in hERG results in insufficient repolarizing current, resulting in a prolonged cardiac AP and QT interval, and potentially, the lethal arrhythmia, TdP. However, as mentioned previously, LQTS2 displays highly variable penetrance, and the phenomena termed ‘concealed LQTS’, whereby the patient is genotype positive but phenotypically normal, can make the diagnosis and management of LQTS2 challenging (Giudicessi & Ackerman, 2013; Szabo et al., 2011). As such, better understanding of hERG channel physiology will provide a richer substrate for informing risk stratification. An example of how understanding may be improved upon is the role of hERG protective currents and how they might be manipulated by mutations to create an arrhythmia substrate, and by therapeutics to offer novel treatment options.

As mentioned previously, hERG recovers from inactivation upon membrane repolarization to pass its physiologically relevant I_{Kr} current before slowly deactivating (Sanguinetti et al., 1995; Trudeau et al., 1995). This slow deactivation has been shown to

occur over a time course sufficiently long such that channels remain in the open conducting state well into the refractory period (Lu et al., 2001). In response to afterdepolarizations, it has been shown that these open channels pass robust repolarizing currents, thereby potentially neutralizing the electrical insult (Du et al., 2010; Lu et al., 2001, 2003; Melgari et al., 2014). Termed the 'protective current' due to its hypothesized function regarding the prevention of afterdepolarization-induced arrhythmia, loss of protective current can be thought of as loss of function and potentially arrhythmogenic (Perry et al., 2016). Thus, considered selection of pathogenic mutations may be appropriate for interrogating the role of the protective current and the implications of its perturbation. A good candidate for study is the R56Q mutation, first discovered in a family with a history of sudden cardiac death (Chen et al., 1999). R56Q channels are expressed at the cell membrane, and are not trafficking deficient. Instead, biophysical analysis revealed that R56Q channels displayed significantly accelerated deactivation kinetics (Chen et al., 1999). We propose that R56Q is an ideal case with which to test the role of hERG protective current. Furthermore, we propose that selective attenuation of the protective current by the R56Q mutation as a result of enhanced deactivation kinetics may provide a possible mechanism for arrhythmia. With the rapid time course of deactivation observed in R56Q channels, the population of channels open into the refractory period would be reduced relative to WT hERG, which would reduce the protective current response to an afterdepolarization leaving mutation carriers susceptible to arrhythmia and sudden cardiac death. With the recent discovery of small molecule activators of hERG, hERG protective current could provide a novel target for pharmaceutical therapies designed to treat LQTS2. It stands to reason that the desired effect of the activator should mirror the effect of the mutation, i.e., the accelerated deactivation of R56Q would not be effectively neutralized by an activator that abolishes inactivation, but rather an activator that slows deactivation. In this chapter, I present data showing the effects of the R56Q mutation on hERG gating and the protective current in response to premature depolarizations. We show that the R56Q mutation reduces protective currents as a result of its rapid deactivation process, and that the selective slowing of channel closure through application of RPR260243 results in rescue of this loss of function.

3.2. Results

3.2.1. A PAS domain mutation accelerates channel deactivation with little effect on other gating parameters

Fig. 3.1A shows representative current traces recorded from WT hERG and hERG R56Q channels in response to the activation protocol shown in the inset. Qualitative observation highlights the significantly accelerated time course of deactivation in R56Q mutant channels relative to WT. Comparison of the activation conductance-voltage relationships (Fig. 3.1B) confirms earlier reports that activation gating is largely unaffected by the R56Q mutation. With an activation $V_{1/2}$ of -13.0 ± 1.1 and -11.4 ± 1.1 mV for WT and R56Q, respectively, there is no significant difference in activation gating between the mutant and WT hERG (Fig. 3.1B, Table 1) (Berecki et al., 2005; Chen et al., 1999). Slope factors were also not different between the two channels, indicating that the sensitivity of the channels to voltage is similar (Table 1). Figure 3.2A shows representative current traces recorded in response to the deactivation protocol shown in the inset. Comparison of inactivation gating between the channel types reveals that R56Q channels display a significantly right-shifted voltage dependence of inactivation relative to WT (Fig. 3.2B, $p < 0.05$). This modest attenuation of R56Q channel inactivation is consistent with an increase in outward current observed previously (Beattie et al., 2018; Berecki et al., 2005). Characterization of the kinetics of recovery from inactivation showed that R56Q mutant channels display an accelerated time course (Fig. 3.2C). While this was consistent with data measured at other test potentials, the clearest picture of the effects was observed at −100 mV, and this effect was rather small (Table 1).

Consistent with the phenotype of many known mutations in the PAS domain of hERG (Chen et al., 1999; Gustina & Trudeau, 2009, 2011), the most prominent phenotypic effect of the R56Q mutation is on deactivation gating, which is significantly accelerated (Fig. 3.3) (Berecki et al., 2005; Chen et al., 1999). Bi-exponential fits of current decay at –110 mV showed that the R56Q mutation significantly accelerates deactivation through effects on both τ_{Fast} and τ_{Slow} (Fig. 3.3A, B, C, D; Table 1). Of note, while the majority of current decay is mediated by the fast component in WT, this $\%A_{Fast}$ is increased significantly in R56Q from 81 ± 3.0% in WT channels to 94 ± 0.8% (Table 1). Data recorded at 37 °C show broad similarities to data recorded at 21 °C (Fig. 3.3B). One notable exception is that while no significant difference exists in the voltage dependency of

activation at 21 °C, patch clamp experiments show that R56Q exhibits a right shift in the voltage dependency of activation (Table 1). Consistent with data recorded at 21 °C, both deactivation time constants were accelerated at 37 °C. Additionally, the observed attenuation of inactivation at 21 °C was conserved.

Taken together, the R56Q mutation results in channels displaying significantly altered deactivation gating, and this is consistent with previous reports (Berecki et al., 2005; Chen et al., 1999). While a small attenuating shift in the voltage dependency of inactivation was observed, the magnitude of the effect on deactivation lends weight to the idea that the rapid channel closure typical of R56Q channels is largely responsible for the observed clinical phenotype (Table 1) (Chen et al., 1999; Lu et al., 2001). Further, qualitative comparison of the traces shown in Figure 3.1A highlight the marked difference in current decay between WT and R56Q mutant channels. The rapid decay observed in R56Q is characteristic of accelerated deactivation, and supports the idea that this is the primary pathological effect of the mutation.

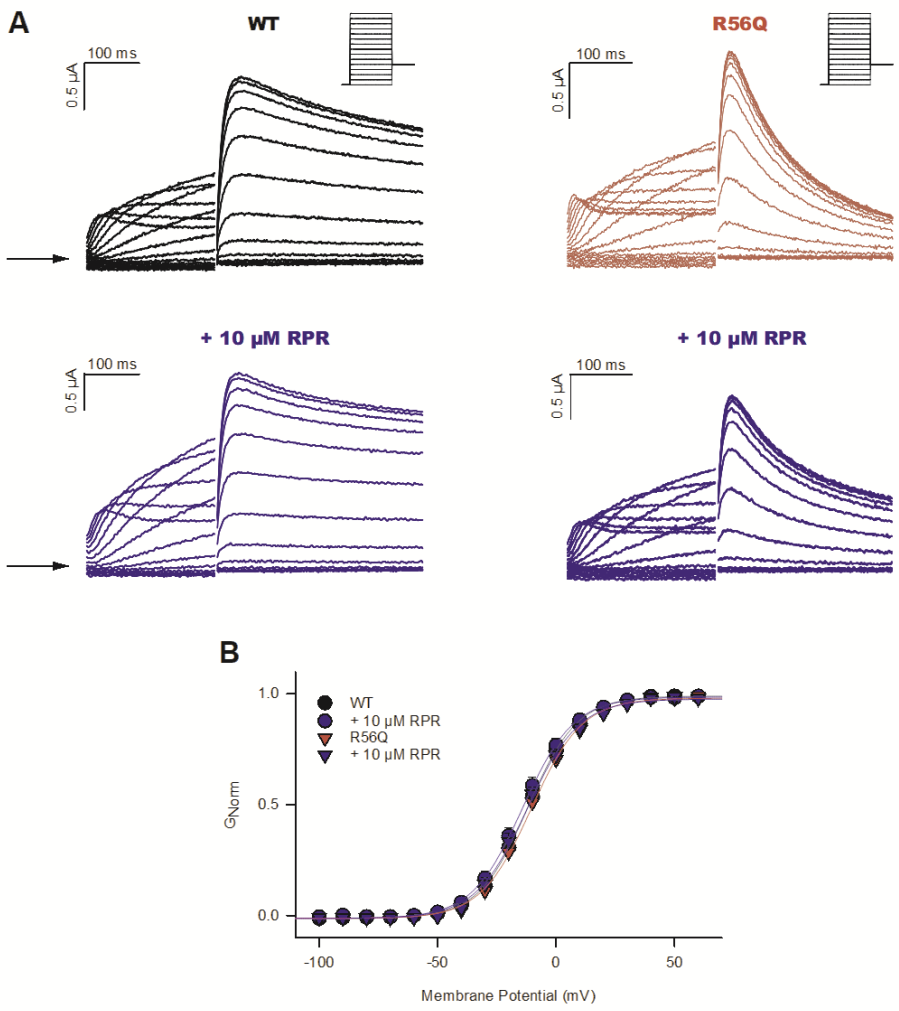

Figure 3.1. hERG channel activation is unchanged by the R56Q mutation or application of 10 µM RPR260243.

Neither R56Q nor RPR260243 have significant effects on activation gating. A. Representative current traces recorded in response to the activation protocol shown in the inset. WT and R56Q control recordings are shown at top left and right, respectively, with traces recorded in the presence of 10 µM RPR260243 shown below. B. Plot of mean activation G-V relationships in the absence and presence of RPR260243 (*n* = 7, 8 for WT and R56Q, respectively). Plots were constructed using peak tail currents measured at -60 mV and normalized to the maximal tail current value.

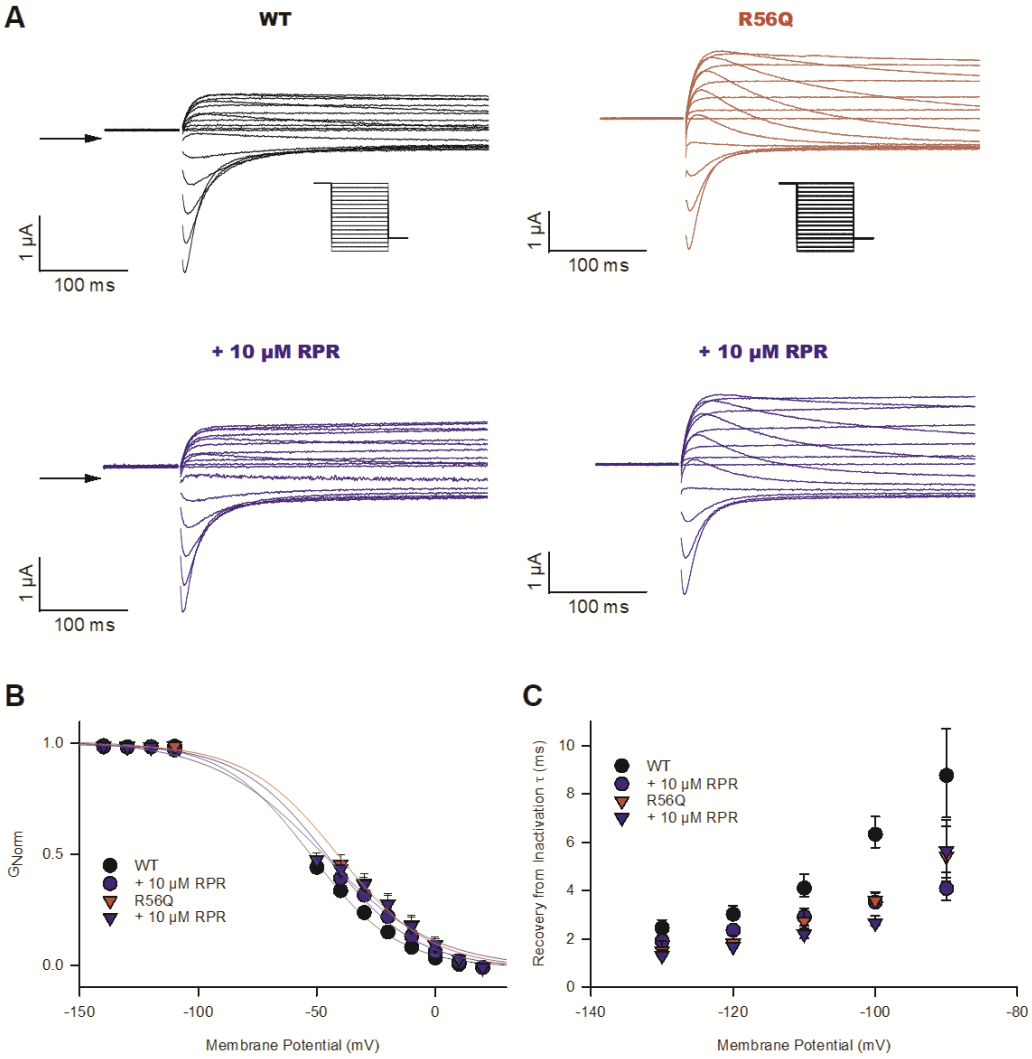

Figure 3.2 The R56Q mutation and RPR260243 have minor effects on inactivation gating.

A. Representative current traces recorded in response to the deactivation protocol shown in the inset. At top, WT and R56Q traces recorded in control conditions and in the presence of 10 µM RPR260243 as indicated. **B**. Plot of mean inactivation G-V relationships constructed by measuring peak currents during the 750 ms voltage step in panel **A,** which were used to calculate the rectification factor, R, as described in the Materials and Methods section above (*n*=5 for both WT and R56Q). **C**. Plot of mean recovery from inactivation time constants against voltage (*n*=5 for both WT and R56Q).

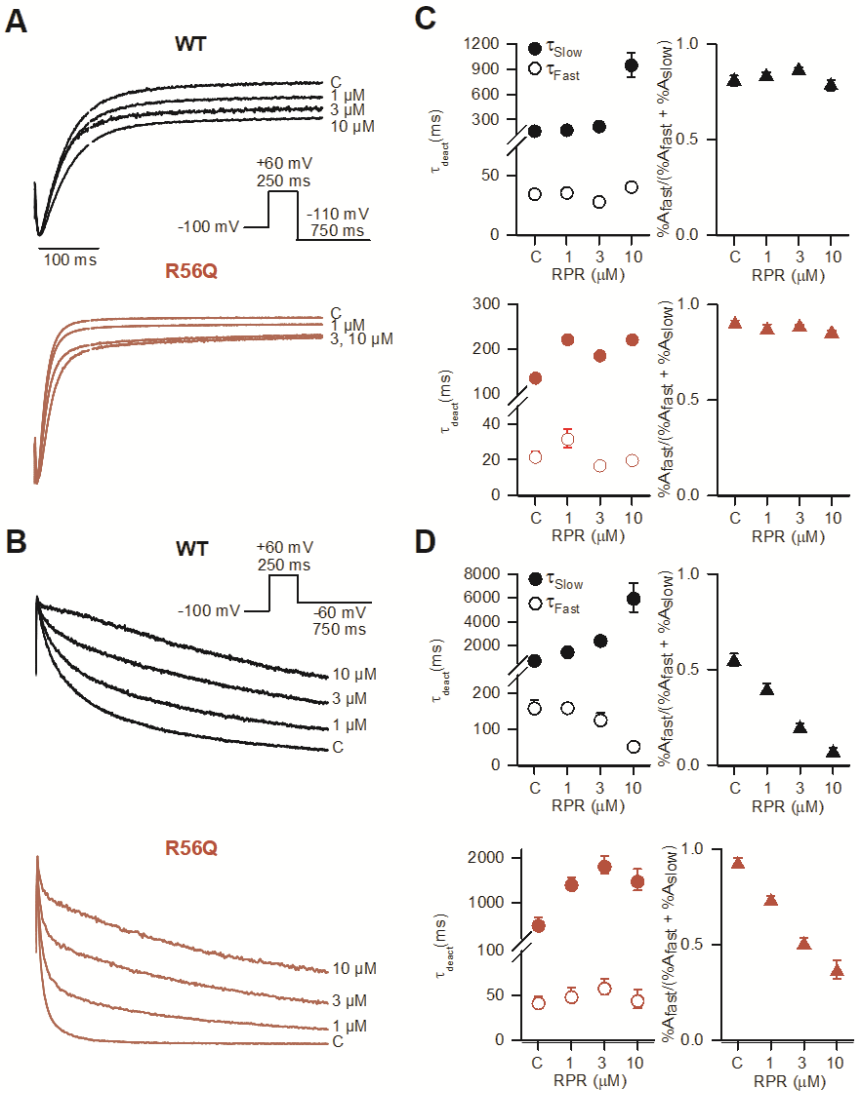

Figure 3.3 RPR260243 slows deactivation kinetics in WT and R56Q LQTS2-associated mutant channels in a concentration-dependent manner.

A., B. Typical current traces recorded in response to the voltage protocol shown at 21 °C from *Xenopus* oocytes (**A**), and at 37 °C from whole cell patch clamp of HEK cells (**B**) during control conditions (**C**) and in response to application of RPR260243 at the indicated concentration. Recordings from WT channels are shown in black, and from R56Q mutant channels in red. **C**., **D**. Plots of mean deactivation time constants (left) and their relative amplitude (right) derived from double exponential fits of current decay during deactivation at 21 °C (C; n=5 for WT, n=6 for R56Q) and 37 °C (D; n=5). Relative amplitudes are represented as the fast phase amplitude relative to the amplitude of total current decay (see Materials and Methods, as well as Table 1). The R56Q mutation accelerated both components of deactivation and increased the contribution of the fast component. RPR260243 selectively delayed the slow component of deactivation at both temperatures tested and increased its contribution at 37 °C, but not at 21 °C.

Table 1. Biophysical characteristics of WT and R56Q mutant channels in the absence and presence of RPR260243 at 21 °C and 37 °C.

		RPR	Activation		Deactivation (at -110 mV for 21 ℃, at -60 mV for 37 ℃)			Inactivation		Inactivation Recovery
			$V_{1/2}$ *(mV)*	*k (mV)*	τ_{fast} *(ms)*	τ_{slow} *(ms)*	*% A*$_{fast}$	$V_{1/2}$ (mV)	*k* (mV)	τ_{-100mV} (ms)
21°C	WT	Ctrl	-11.9 ± 1.1	10.3 ± 0.3	36.4 ± 3.1	199 ± 74	81 ± 3.0	-55.8 ± 2.7	-19.2 ± 0.4	6.3 ± 1.8
		1 µM	-	-	36.2 ± 2.7	182 ± 24	83 ± 2.0	-	-	-
		3 µM	-	-	28.5 ± 3.9	221 ± 52	86 ± 1.0	-	-	-
		10 µM	-14.1 ± 1.3*	10.6 ± 0.3	40.9 ± 1.8	953 ± 146	79 ± 3.0	-44.0 ± 3.0*	-17.6 ± 0.3	3.6 ± 0.6
	R56Q	Ctrl	-10.5 ± 1.0	10.5 ± 0.1	15.7 ± 0.5	114 ± 6.0	94 ± 0.8	-41.5 ± 3.8**	-19.6 ± 1.0	3.7 ± 0.3
		1 µM	-	-	14.9 ± 0.2	166 ± 15	95 ± 0.4	-	-	-
		3 µM	-	-	17.2 ± 0.9	188 ± 16	89 ± 0.7	-	-	-
		10 µM	-12.3 ± 1.1*	10.7 ± 0.2	20.1 ± 0.5	223 ± 8.0	85 ± 0.3	-40.5 ± 2.4	-20.4 ± 0.7	2.8 ± 0.2
37°C	WT	Ctrl	-25.8 ± 0.4	6.5 ± 0.3	161 ± 19	866 ± 128	55 ± 3.2	-34.6 ± 1.7	-21.1 ± 1.5	1.5 ± 0.1
		1 µM	-	-	162 ± 11	1595 ± 55	40 ± 2.8	-	-	-
		3 µM	-	-	129 ± 16	2526 ± 103	20 ± 2.1	-	-	-
		10 µM	-26.5 ± 0.3	6.2 ± 0.2	54.9 ± 6.0	6029 ± 1210	7 ± 1.8	-27.2 ±2.4	-19.8 ± 2.1	1.6 ± 0.1
	R56Q	Ctrl	-16.3 ± 0.7**	8.0 ± 0.6	43.5 ± 5.1	539 ± 144	93 ± 2.5	-10.8 ± 5.0**	-21.7 ± 4.3	1.4 ± 0.5
		1 µM	-	-	50.2 ± 8.2	1440 ± 124	74 ± 1.9	-	-	-
		3 µM	-	-	59.8 ± 8.5	1850 ± 193	51 ± 2.6	-	-	-
		10 µM	-21.9 ± 0.5*	7.7 ± 0.5	46.0 ± 10.0	1520 ± 238	37 ± 4.7	-15.6 ± 4.1	-20.8 ± 3.8	1.7 ± 0.6

*= sig dif compared to control (drug vs. control)
**= sig dif compared to construct (R56Q vs. WT)

3.2.2. The small molecule activator of hERG, RPR260243, slows deactivation with little effect on other gating parameters.

The first small molecule activator of hERG to be discovered, RPR260243, has been shown to slow deactivation kinetics relatively selectively (Kang et al., 2005; Perry et al., 2007). While small attenuating effects on inactivation and a slowing of activation have been reported, these are observed only at high concentrations of RPR260243 and are much smaller in magnitude than the observed effects on deactivation kinetics (Kang et al., 2005; Perry et al., 2007). Consistent with earlier observations on the effects of RPR260243, we report here that application of 10 µM RPR260243 was sufficient to slow deactivation kinetics. The effect of RPR260243 on deactivation kinetics is shown in Figure 3.3. Application of RPR260243 slowed deactivation kinetics in a dose-dependent manner, with observable effects even at 1 µM RPR260243 (Fig. 3.3A, Table 1). These effects were also observed at 37 °C, in both WT and R56Q channels. (Fig. 3.3B, Table 1). Consistent with previous reports, RPR260243 exerted its action through a specific slowing of the slow time constant (Fig. 3.3C, D)(Kang et al., 2005; Perry et al., 2007), which is reflected in a reduced $\%A_{Fast}$ value. This indicated that the percent of total current amplitude decay had shifted towards the slow component, rather than the fast component. This is particularly evident at 37 °C, but less so at 21 °C, where application of 10 µM RPR260243 significantly increased τ_{Slow} (Fig 3.3C), but the $\%A_{Fast}$ does not change to the degree observed at 37 °C. This would indicate that either the fast time constant is slowed as well at 21 °C, or the degree to which the slow component is slowed is less than at 37 °C. It is worth noting that at negative voltages the fast time constant predominated relative to the slow time constant and that test potentials were -110 and -60 mV, respectively, for experiments at 21 °C and 37 °C. This could also play a role in the discrepancy between 21 °C and 37 °C recordings. If the fast component mediates the bulk of current decay, then effects of RPR260243 on the slow time constant would be masked or underestimated even at high concentration. Further TEVC experiments at a test potential of -60 mV may provide insight, as it would be expected that the fast component of deactivation would be less dominant and therefore would better reveal effects of RPR260243 on τ_{Slow}.

Activation G-V relationships shown in Fig. 3.1B highlight that 10 µM RPR260243 produced a small hyperpolarizing shift in the $V_{1/2}$ of activation in both WT and R56Q constructs (Table 1, $p < 0.05$). While statistically significant, this approximately 2-3 mV shift

in voltage dependency is unlikely to produce functional consequences during the action potential.

Application of 10 µM RPR260243 significantly right-shifted the voltage dependency of inactivation in WT hERG from -55.8 ± 2.7 to -44.0 ± 3.0 mV, while also shallowing the slope factor, *k* (Fig. 3.2B $P<0.05$). However, when the same conditions were applied to R56Q channels, no significant shift was observed and the slope factor remained unchanged (Fig. 3.2B, Table 1). This could be due to structure-function relationships of the R56Q mutant that render it uniquely insensitive to shifts in inactivation. This is supported by evidence that shows no significant shifts in inactivation gating at 37 °C in R56Q channels (Table 1). Application of 10 µM RPR260243 also accelerated the recovery from inactivation in both WT and R56Q at -100 mV (Fig 3.2C). Acceleration of recovery from inactivation would be expected to increase outward current upon membrane repolarization; however, this effect is likely to be overshadowed by the rapid time course of deactivation in R56Q channels and the magnitude of the effect of RPR260243 on deactivation.

Taken together, the most dominant effect of the R56Q mutation on gating is accelerated deactivation. We report here that RPR260243 selectively prolonged the slow component of deactivation gating at both temperatures tested, and increased its contribution at 37 °C , but not 21 °C. Effects on inactivation gating are less clear. The initial report describing the effects of RPR260243 on hERG channels was conducted in CHO cells using patch clamp electrophysiology. The voltage dependence of inactivation was measured using a triple pulse protocol, and no significant effects were observed at 10 µM RPR260243 (Kang et al., 2005). Later reports conducted in *Xenopus* oocytes used the Rectification Method to assess this parameter and observed an approximately 28 mV depolarizing-shift in the voltage dependence of inactivation when 10 µM RPR260243 was applied to WT hERG channels. The data presented here support the idea that high concentrations of RPR260243 may attenuate inactivation in WT hERG channels. However, the magnitude of the observed effect is reduced relative to that observed previously (Perry et. al. 2007). It is worth noting that the same group observed a smaller effect in a later publication, although the effect was still significant (Perry et al., 2008). Additionally, the initial report showing effects of RPR260243 on inactivation used voltage protocols comprised of long duration pulses, and this may account for some of the observed differences between our results (Perry et al., 2007). It has been shown that the

duration of the pulse delivered can alter the kinetics of hERG channel gating, and having used physiological duration square wave pulses this could explain part of the discrepancy (Thouta et al., 2017). In any case, application of 10 µM RPR260243 resulted in significant effects on deactivation gating, with little effect on other parameters reported here. With this in mind, application of RPR260243 to R56Q mutant channels could provide targeted, selective benefit that would rescue hERG loss of function.

3.2.3. R56Q channels display reduced protective currents in response to premature stimulation, and this may be rescued by application of RPR260243.

Figures 3.4A and C show the effect of RPR260243 on WT channel currents at 21 °C and 37 °C during a voltage protocol (adapted from Perry et al., 2016) designed to mimic premature depolarizations arriving at a range of coupling intervals following an approximated action potential waveform. Peak hERG protective currents were normalized to maximal channel conductance (Fig. 3.4E and F; see Materials and Methods). Similarly to previous descriptions (Du et al., 2010; Lu et al., 2001, 2003; Melgari et al., 2014; Perry et al., 2016), we observed that premature stimulations produced robust transient repolarizing hERG protective currents in WT channels that peaked when the premature depolarization was applied at a coupling interval (Δt from 90% ramp repolarization) of 19 ± 1.3 ms (n=15) at 21 °C and -1.9 ± 4.0 ms (n=5) at 37 °C. Application of RPR260243 (Fig. 3.4B, D; Fig. 3.5G, H) had negligible effects on the amplitude and timing of the peak hERG protective current recorded at any concentration tested (P=0.16 at 21 °C, and P=0.56 at 37 °C), but significantly enhanced hERG protective current amplitudes at longer coupling intervals in a concentration-dependent manner (Fig. 3.5E and F). Notably, at a coupling interval of 100 ms, hERG protective current amplitude was increased from 0.59 ± 0.4 that of the peak hERG protective current in control conditions to 0.74 ± 0.02 upon application of 10 µM RPR260243 at 21 °C (P=0.017, n=5; one-way ANOVA with Holm-Sidak posthoc test). This effect was conserved at 37 °C, with protective currents increasing from 0.26 ± 0.04 to 0.69 ± 0.07 (P<0.001, n=5; one-way ANOVA with Holm-Sidak posthoc test). Indeed, the presence of RPR260243 markedly increased hERG protective currents even at the longest coupling interval tested (375 ms), suggesting the effect of RPR260243 on deactivation increases the number of channels residing in the open state into the refractory period, resulting in the robust increase in protective current amplitude. This effect further suggests the possibility of rate-dependent accumulation of

channels into the open state, potentially leading to increases in the early transient current observed during an AP waveform (see below).

The effect of RPR260243 application on protective currents mediated by R56Q mutant channels is shown in Figure 3.5. Relative to WT, R56Q channels displayed significantly reduced hERG protective currents at both 21 °C and 37 °C as a result of accelerated deactivation gating (Fig. 3.5A and C). Consistent with the effects of RPR260243 on WT hERG channels, R56Q protective currents mediated at longer coupling intervals were most affected by the application of RPR260243 (Fig. 3.5E-H). At a coupling interval of 100 ms, the hERG protective current in R56Q mutant channels was 0.15 ± 0.03 (21 °C, n=5) and 0.09 ± 0.01 (37 °C, n=5) that of the peak hERG protective current recorded. This hERG protective current in R56Q mutant channels was 0.18 ± 0.04 (at 21 °C) and 0.46 ± 0.07 (at 37 °C) that recorded in WT channels (Fig. 3.5G and H). Depolarizations applied at coupling intervals >100 ms elicited negligible hERG protective currents in R56Q mutant channels regardless of the temperature at which they were recorded. In addition, the peak protective current recorded in R56Q conditions occurred at a shorter coupling interval, i.e. earlier in the AP waveform, than in WT channels (Fig. 3.5G and H). The coupling interval in R56Q channels was -33.3 ± 4.2 ms compared with 18.7 ± 1.3 ms in WT channels at 21 °C (n=5, P<0.001, *t*-test) and -32.0 ± 2.2 ms compared with 0 ± 2.8 ms in WT channels at 37 °C (n=5, P<0.001, *t*-test). Furthermore, the amplitude of the peak hERG protective current recorded in R56Q mutant channels was reduced compared with that in WT channels at 21 °C (P<0.001), but not at 37 °C (P=0.271, Fig. 3.5E-H).

Application of RPR260243 resulted in a concentration-dependent increase in hERG protective currents passed by R56Q mutant channels in response to premature stimulations, albeit largely in the refractory period (Fig. 3.5B, D). The highest concentration of RPR260243 increased protective currents 4.0 ± 0.4-fold at 21 °C and 4.9 ± 0.5 fold at 37 °C at a coupling interval of 100 ms (Fig. 3.5E-H). This increase was such that the measured protective current amplitude was WT-like, or exceeded WT levels, and this effect was conserved at coupling intervals exceeding 100 ms. This rescue of the R56Q mutant protective current to WT-like levels occurred in the presence of 30 µM RPR260243 at 21 °C and 3 µM at 37 °C. Application of RPR260243 also increased the coupling interval at which the peak hERG protective current amplitude occurred in R56Q mutant channels at 21 °C and at 37 °C (Fig. 3.5E-H). Application of RPR260243 at the highest tested concentration also increased the coupling interval at which the peak hERG protective

current was mediated in R56Q mutant channels. Increases of 24.0 ± 7.5 ms and 24.0 ±4.0 ms were observed at 21 °C and 37 °C; respectively (n=5, P=0.033, paired *t*-test; n=5, P=0.004, paired *t*-test), at the concentrations outlined above, shifting values to a more WT-like coupling interval. At 21 °C, 30 µM RPR260243 also increased the peak hERG protective current in R56Q mutant channels, restoring the peak amplitude to WT-like control levels, likely via effects on inactivation gating (See Chapter 4).

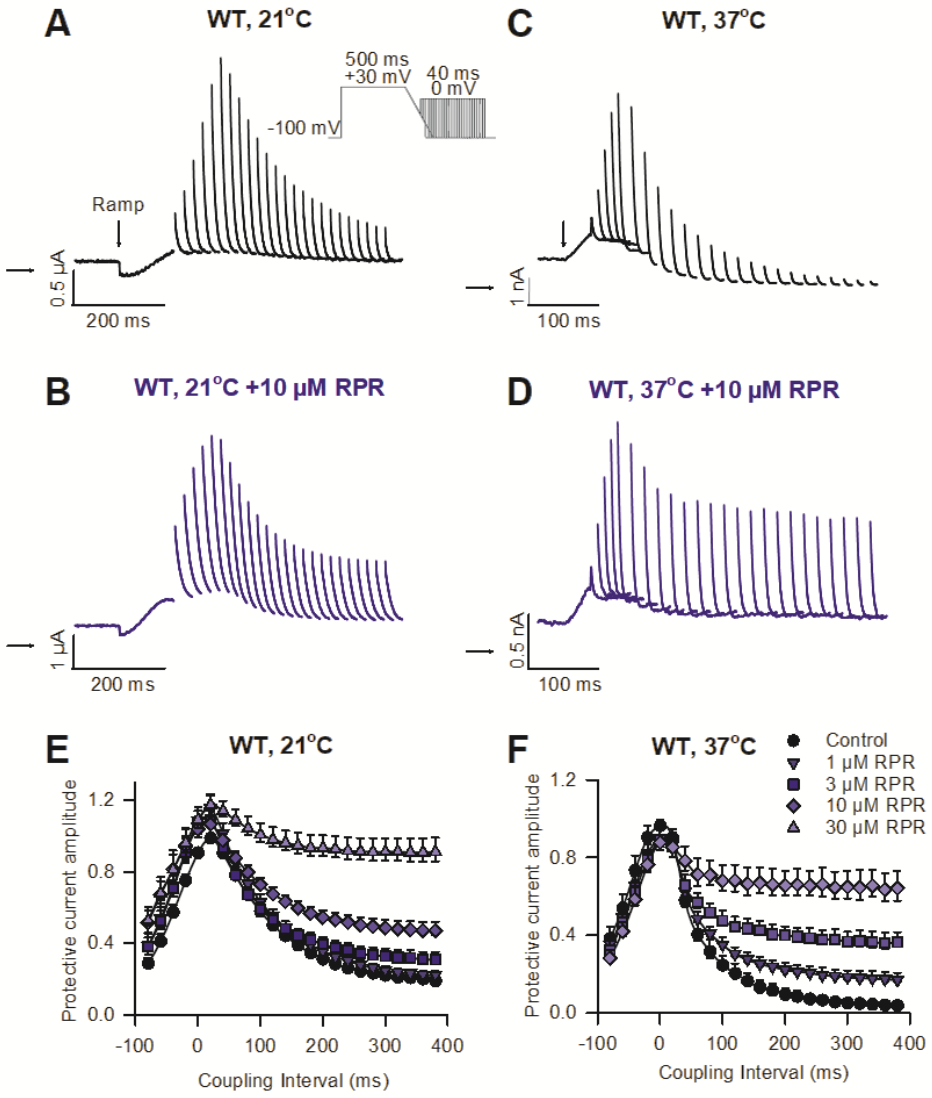

Figure 3.4 hERG protective current is increased by RPR260243 in a concentration-dependent manner.

A-D. Typical current traces recorded from WT hERG Channels in response to the premature stimulation protocol shown in the absence (black) and presence (blue) of 10 µM RPR260243 at 21 °C from *Xenopus* oocytes (**A, B**), and 37 °C from HEK cells (**C, D**). **E., F**. Mean peak current amplitudes in response to premature stimulations (protective currents) plotted against the coupling

interval recorded in the absence (black symbols) and presence (pastel blue symbols) of the indicated concentration of RPR260243 at 21 °C (E; n=5 for all data except n=4 with 30 µM) and 37 °C (F; n=5).

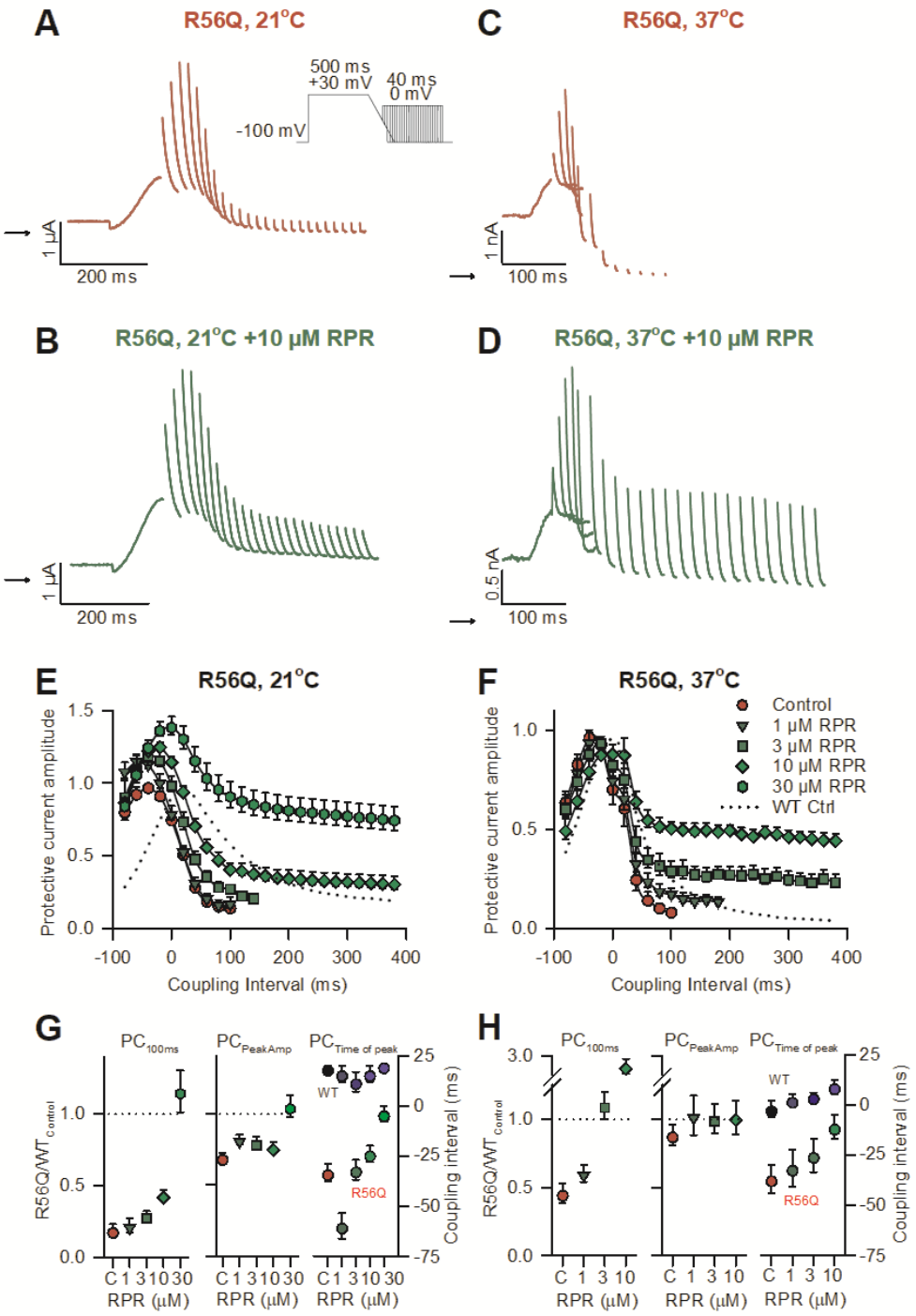

Figure 3.5 RPR260243 restores attenuated protective current in R56Q mutant channels.

A.-D. Typical current traces recorded from R56Q mutant channels in response to the premature stimulation protocol shown in the absence (blue) and presence (red) of 10 µM RPR260243 at 21 °C from *Xenopus* oocytes (**A, B**), and 37 °C from HEK cells (**C, D**). **E., F**. Mean peak protective currents plotted against the coupling interval recorded in the absence (blue) and presence (red) of the indicated concentration of RPR260243 at 21 °C (E; n=5) and 37 °C (F; n=5). WT protective current amplitudes recorded under control conditions (absence of RPR260243) from Figure 2 are also shown (dotted lines) for the purpose of comparison. **G., H**. Plots of mean protective current at a coupling interval of 100 ms (PC_{100ms}, *left*) and mean peak protective current amplitude ($PC_{PeakAmp}$, *middle*) in R56Q mutant channels as a fraction of that in WT channels in the absence (C, control; blue) and presence (red) of a range of RPR260243 concentrations at 21 °C (G; n=5) and 37 °C (H; n=5). Dashed black lines indicate WT values. *Right*, mean coupling interval at which the peak protective current was observed (*right*) in the absence and presence of RPR260243 in WT and R56Q mutant channels (n=5).

3.2.4. RPR260243 restores attenuated early transient hERG channel currents during action potential waveforms with little effect on resurgent current.

To investigate how the above findings influence repolarizing current during the action potential, we explored the effects of application of RPR260243 on hERG currents flowing during a simulated action potential voltage waveform at 21 °C and 37 °C (Fig. 3.6). Representative current traces (Fig. 3.6A) recorded in response to an action potential waveform were used to construct current-voltage relationships to examine any mutant or drug effects on I_{hERG} (the current flowing through hERG channels in the Xenopus oocyte or HEK-293 cell during the AP voltage waveform) during an action potential. These relationships show that robust transient hERG currents are passed upon initial depolarization of the membrane, and are followed by slowly developing hERG resurgent currents that peak during phase three repolarization and terminate the AP (Fig. 3.6A). Action potentials applied with increasing frequency revealed a rate-dependence to the early hERG transient current, but no significant differences were observed in the hERG resurgent current (Fig. 3.6A and B). This is consistent with previous reports that demonstrated the transient hERG current is conducted by open channels that failed to close during the previous diastolic period (Hua & Gilmour, 2004; Perry et al., 2016). Application of 10 µM RPR260243 increased WT hERG currents flowing during the action potential waveform when applied at 1 Hz at 21 °C and 37 °C (Fig. 3.6C-F). While currents were increased throughout the duration of the action potential waveform, the transient current was particularly sensitive to RPR260243 application (Fig. 3.6C). The transient hERG current amplitude was increased by 12.4 ± 2.3-fold at 21 °C and 5.3 ± 0.6-fold at 37 °C upon application of 10 µm RPR260243 relative to control (n=4, P=0.007, paired *t*-

test; n=5, P=0.035, paired *t*-test). This contrasts with the effect of RPR260243 on the resurgent hERG current, which was decidedly muted relative to effects on the early transient current. Application of 10 µM RPR260243 resulted in a 1.6 ± 0.1-fold increase at 21 °C and a 1.4 ± 0.1-fold increase at 37 °C (n=4, P<0.001, paired *t*-test; n=5, P=0.035, paired *t*-test). There was also a small change in the timing of the peak of the hERG resurgent current during the action potential waveform in the presence of RPR260243 (Fig. 3.6E and F), which reached significance at 37 °C (P=0.046), but not at 21 °C (P=0.358).

We next investigated the effect of RPR260243 application on repolarizing currents conducted during an action potential waveform in R56Q mutant channels at 21 °C (Fig. 3.7A) and 37 °C (Fig. 3.7B). Compared with WT hERG, the R56Q mutation showed little difference with regard to the peak amplitude of the hERG resurgent current and the voltage at which the peak of the hERG resurgent current occurred at both 21 °C (Fig. 3.7C) and 37 °C (Fig. 3.7D). This is consistent with previous reports that have demonstrated that the R56Q mutation exerts limited effects on hERG resurgent current during the action potential (Berecki et al., 2005; Chen et al., 1999; Gianulis & Trudeau, 2011). This contrasts with the effect of the R56Q mutation on the early transient hERG current amplitude, which showed significant reductions at both recording temperatures. Relative to WT, the transient hERG current was essentially abolished under R56Q conditions. Time-matched measurements of hERG transient currents revealed that R56Q channels mediated currents 0.06 ± 0.02 at 21 °C and 0.05 ± 0.01 at 37 °C those of the peak hERG resurgent current (Fig. 3.7A-D). Application of 10 µM RPR260243 was sufficient to restore WT-like hERG transient current in R56Q mutant channels, with an observed increase in transient current amplitude of 15.4 ± 3.7-fold at 21 °C and 10.9 ± 2.6-fold at 37 °C (n=5, P<0.001, paired *t*-test; n=5, P=0.032, paired *t*-test). In contrast, application of 10 µM RPR260243 resulted in limited effects on the peak hERG resurgent current mediated by R56Q. Peak resurgent current amplitude under RPR260243 conditions was 1.25 ± 0.08 and 1.01 ± 0.13 that observed in control conditions at 21 °C (P=0.042) and 37 °C (P=0.889), respectively. Additionally, no significant effects on the timing of the peak hERG resurgent current were observed (P=0.280 at 21 °C and P=0.313 at 37 °C).

To explore these findings further, we applied a train of action potential waveforms with heterogeneous morphology and compared the current conducted by WT and R56Q mutant channels at 37 °C. This train of complex waveforms commands voltage changes

that might be observed under a variety of conditions and locations in the myocardium, and includes the absence or presence of premature depolarizations (Fig. 3.8A). Overlay of typical currents elicited by this protocol in WT and R56Q mutant channels normalized to maximal channel conductance (Fig. 3.8B, C) shows negligible differences in the hERG resurgent current, but significant reductions in the transient hERG current caused by the R56Q mutation. This can be observed upon examination of selected action potentials (Fig. 3.8Bi, ii, iii) from which the transient hERG current relative to the hERG resurgent current was calculated (Fig. 3.8Di-iv). These analyses also revealed another significant finding, in that R56Q channels displayed significant reductions in the hERG current available in response to premature depolarizations arriving in the early refractory period. WT channels produced robust repolarizing currents in response to premature depolarizations, while in R56Q channels a 4.5-fold ($n=4$, $P<0.001$, one-way ANOVA with Holm-Sidak posthoc test) reduction in these currents was observed. This suggests a reduced protection against premature beats, and by extension an increased susceptibility to electrical insult. This is consistent with our earlier results that indicated R56Q channels mediate reduced protective currents from early in the refractory period to the most extreme coupling intervals (Fig. 3.8D). Application of 10 μM RPR260243 to R56Q mutant channels was sufficient to restore the loss of repolarizing current in response to a premature depolarization (Fig. 3.8Cii), resulting in a 4.6 ± 0.4-fold increase in current amplitude (Fig. 3.8Dii; $n=4$, $P<0.001$, one-way ANOVA with Holm-Sidak post-hoc test). Consistent with the findings in Figure 3.7, application of RPR260243 also restored the transient hERG current to WT-like levels (Fig. 3.8Ci and Di), consistent with accumulation of channels already residing in the open state upon depolarization. Of note, action potential waveforms designed to mimic EADs (Fig. 3.8Biii, Ciii), revealed that the peak amplitude of the repolarizing current mediated by R56Q channels during the EAD was reduced relative to WT hERG ($P=0.035$), and this peak occurred earlier in the action potential at more depolarized potentials ($P=0.004$) (Fig. 3.8Diii, iv). Application of 10 μM RPR260243 had little effect on these parameters (Fig. 3.8Ciii and Diii).

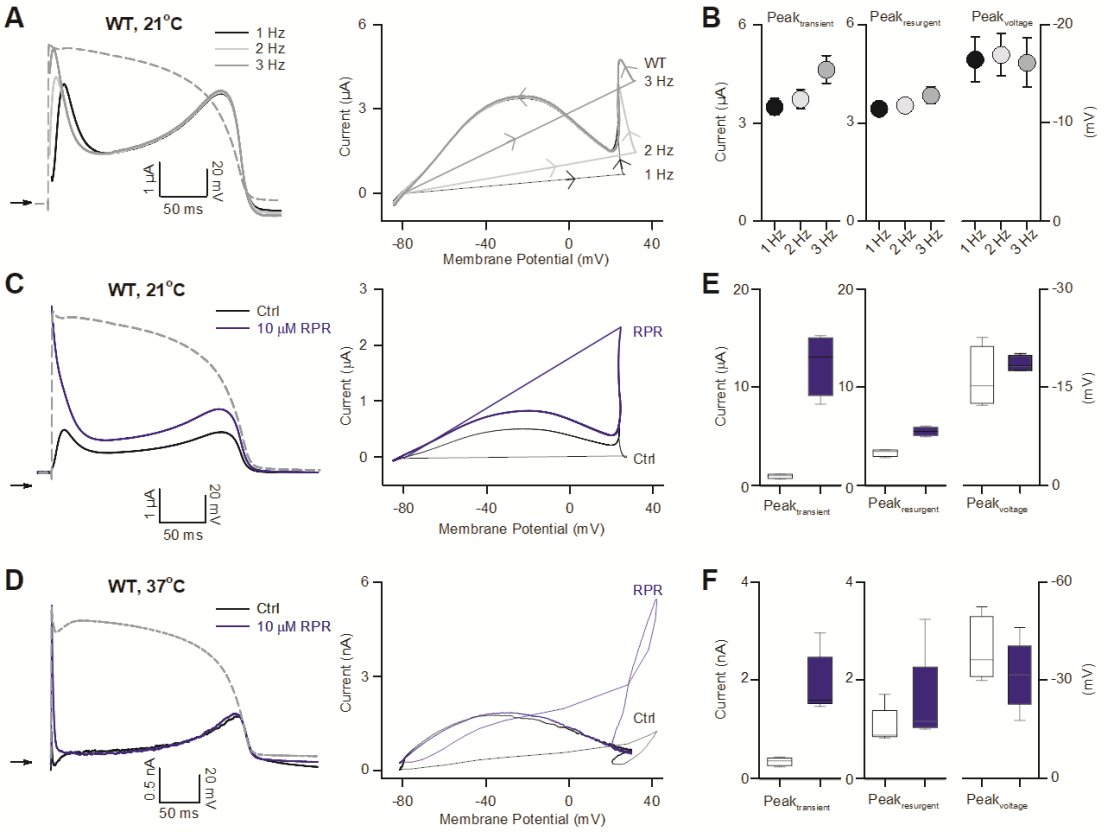

Figure 3.6 RPR260243 increases early transient hERG channel current during action potential voltage waveforms.

A. Left, typical current traces recorded from WT hERG channels at 21 °C in response to the action potential voltage waveform shown by the dashed grey line applied at the indicated stimulation frequency. Right, current-voltage relationships derived from WT hERG channel currents at the indicated stimulation frequency. **B**. Plots of the mean peak early transient current ($Peak_{transient}$, left), peak resurgent current ($Peak_{resurgent}$, middle), and mean voltage at which the peak resurgent current occurred ($Peak_{voltage}$, right) at the indicated stimulation frequency (n=4). **C., D**. Typical current traces (left) and current-voltage relationships (right) recorded from WT hERG channels in response to the action potential voltage waveform shown (grey) applied at 1 Hz in the absence (black) and presence (green) of 10 µM RPR260243 at 21 °C (C) and 37 °C (D). **E., F**. Plots of mean $Peak_{transient}$, $Peak_{resurgent}$, and $Peak_{voltage}$ in the absence (control; open boxes) and presence (green boxes) of 10 µM RPR260243 at 21 °C (E, n=5) and 37 °C (F, n=5).

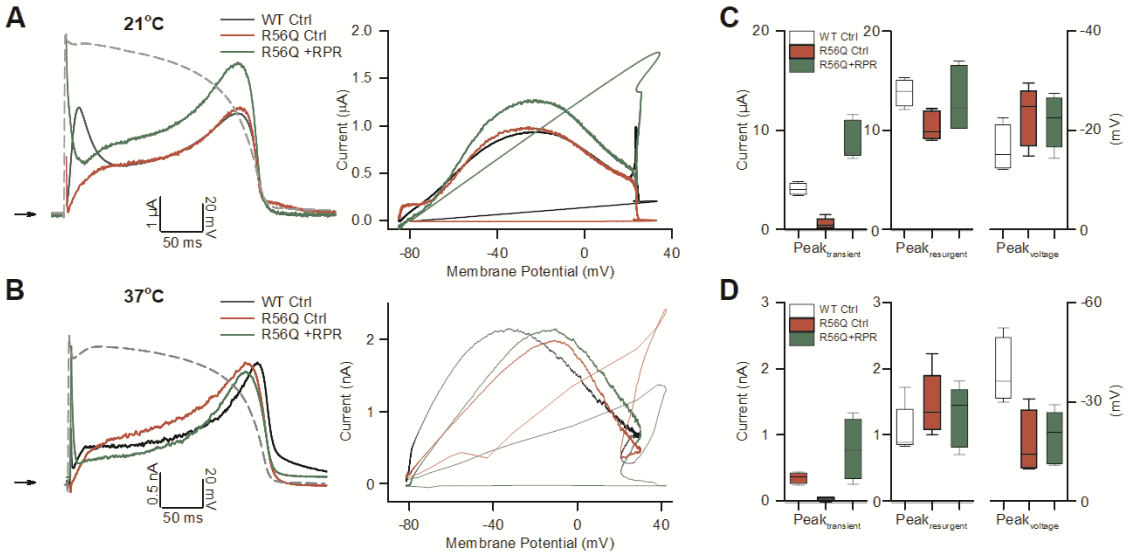

Figure 3.7 RPR260243 restores reduced early transient hERG current in R56Q mutant channels.

A., B. Typical current traces (left) and current-voltage relationships (right) recorded from R56Q mutant channels in response to the action potential voltage waveform shown (grey) applied at 1 Hz in the absence (R56Q Ctrl; blue) and presence (R56Q +RPR260243; red) of 10 µM RPR260243 at 21 °C (A) and 37 °C (B). WT data from Figure 4 are shown for the purposes of comparison (WT Ctrl; black). **C., D**. Plots of mean peak early transient current ($Peak_{transient}$, left), peak resurgent current ($Peak_{resurgent}$, middle), and mean voltage at which the peak resurgent current occurred ($Peak_{voltage}$, right) in R56Q mutant channels in the absence (control; blue boxes) and presence (red boxes) of 10 µM RPR260243 at 21 °C (C, n=5) and 37 °C (D, n=5). WT data from Figure 4 are shown for the purposes of comparison (open boxes).

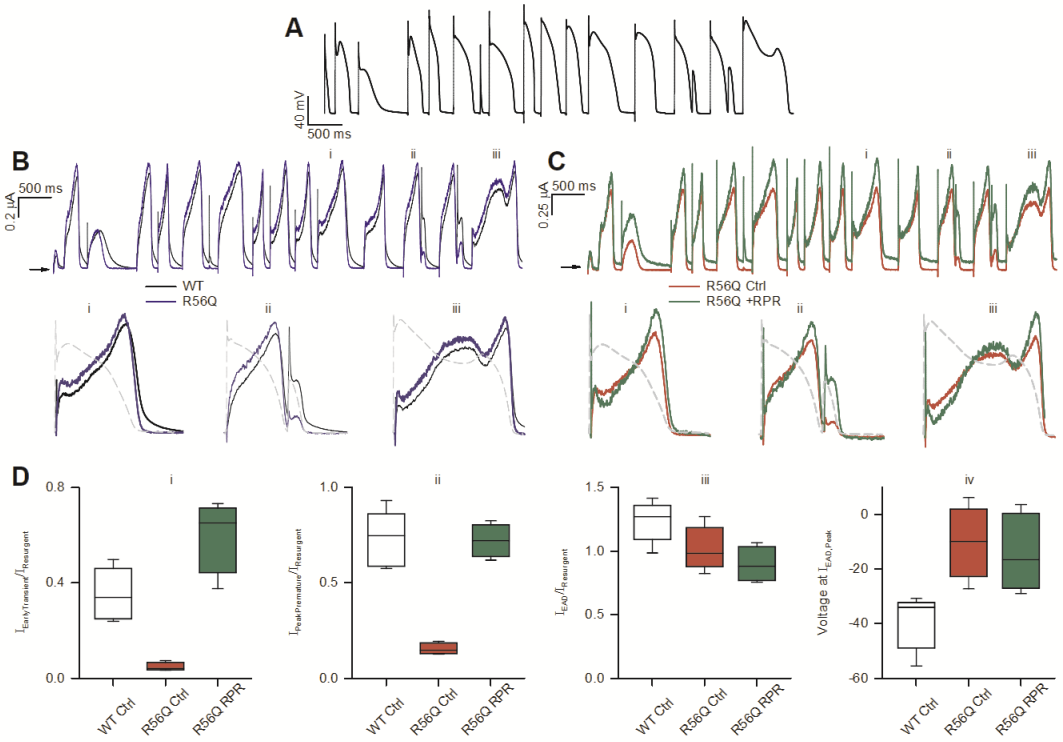

Figure 3.8 RPR260243 enhances attenuated protective repolarizing hERG current in R56Q mutant channels.

A. Complex action potential voltage waveform train used to assess repolarizing current under a variety of stimulation scenarios. **B**. Upper, typical current traces recorded from WT (black) and R56Q mutant (blue) channels at 37 °C in response to the waveform in A. Lower, selected action potentials from the train (indicated by i-iii) highlight repolarizing current in WT and R56Q mutant channels passed in response to a ventricular-like action potential waveform (i, left), a premature depolarization arriving early in the refractory period (ii, middle), and an EAD (iii, right). **C**. As in B, but with typical traces recorded from R56Q mutant channels in the absence (Ctrl, control; blue) and presence (+RPR260243; red) of 10 µM RPR260243. **D**. Plots of mean repolarizing current parameters from i-iii in WT under control conditions (WT Ctrl; open boxes; n=5) and R56Q mutant channels in the absence (R56Q Ctrl; blue boxes; n=5) and presence of 10 µM RPR260243 (R56Q RPR260243; red boxes; n=5). Plots show the amplitude of the early transient current relative to the peak resurgent current (i), the amplitude of the protective current in response to premature depolarization relative to the peak resurgent current (ii), the peak amplitude of repolarizing current during an EAD relative to the peak resurgent current (iii, left), and the voltage at which the peak repolarizing current during an EAD occurred (iv, right).

3.2.5. WT hERG Concentration-Response Curve at 21 °C

Having established the utility of RPR260243 for increasing repolarization reserve by slowing deactivation kinetics and increasing open channel availability, I aimed to

assess the concentration-response relationship of the effect of RPR260243 on protective current magnitude. Mean WT protective currents at a coupling interval of 100 ms were expressed as fold-change from control recordings and plotted against the concentration of RPR260243 applied. Data were fit using the Hill equation: $y = 1 + ax^b / (c^b x^b)$, where y is the fractional conductance, a is (I_{max} - I_{min}), c is the EC_{50} value, and b is the Hill coefficient. Fits revealed that RPR260243 has an EC_{50} value of 18.2 µM at a temperature of 21 °C with regard to WT hERG protective current magnitude at a coupling interval of 100 ms (Fig. 3.9). Hill fits were conducted for data at 21 °C but not 37 °C. To construct concentration-response curves at physiological temperature experiments should be conducted at 30 µM RPR260243, consistent with work conducted previously (Kang et al., 2005, Perry et al., 2007). Additionally, RPR260243 has been shown to exhibit temperature dependence with regard to its effect on hERG channels, which would likely affect the observed EC_{50} (Kang et al., 2005).

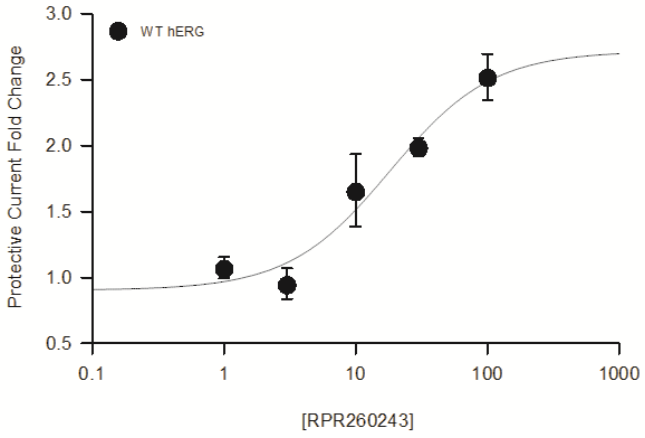

Figure 3.9 21 °C WT hERG concentration-response curve at a coupling interval of 100 ms.

Mean protective current amplitudes at a coupling interval of 100 ms plotted against the concentration of RPR260243 applied. Data were fit with the Hill equation (outlined above) (n=5 for all conditions except 30 µM and 100 µM, where n=4, 2, respectively).

3.2.6. Kinetic modelling recapitulates protective currents in both WT and R56Q at 21 °C.

Dr. Gary Mirams and Dr. Dominic Whittaker of the University of Nottingham have an interest in assessing the ability of different mathematical models to recapitulate hERG channel behaviour, and recent work from their group suggests a novel approach to kinetic modelling. The Beattie model is a four state Markov model comprised of an inactivated state, an open state, a closed state, and an inactivated closed state (Figure 3.10). Using kinetically rich data derived from sine wave recordings described previously, the Beattie model emphasizes kinetic contributions and limits reliance on steady-state parameters (Beattie et al., 2018). This differs from the five state Wang model, which is widely used and relies on steady-state behaviour to make predictions. This approach developed by Beattie et. al. is unique in that it takes advantage of large, single sweep, information-rich composite voltage protocols, as described previously. This means that data from specific regions of the complex protocol can be used to train the model, leaving other portions, such as complex AP waveforms, to test the predictive power of the model in the same cell. Dr. Whittaker performed the modelling experiments using data collected using both the TEVC and patch clamp methods. Using activation and deactivation recordings in response to the protocols described previously, along with a complex sine wave protocol provided by Dr. Mirams (Fig. 3.11), the model was trained and assessed for its predictive ability. This means steady-state data from our square wave voltage protocols along with the kinetic data provided by the sine wave protocol were used to derive rate constants (Figure 3.10) for the Beattie model, before applying the kinetic model to predict channel behavior during a premature stimulation. The Beattie model was able to accurately reproduce current waveforms observed in both sine wave repeats (Fig. 3.11). The primary difference between WT and R56Q was the deactivation rate constant, which was accelerated under R56Q conditions (Figure 3.10). This four state model with one significant perturbation was able to recapitulate channel behaviour observed in both WT and R56Q premature stimulation recordings (Fig. 3.12). These modelling data support the idea that accelerated deactivation in R56Q channels is the primary cause of the observed loss of protective current.

Using the approach outlined previously, we also wished to examine the ability of the Beattie model to recapitulate channel behaviour at 37 °C in response to the AP Train protocol described earlier. Using data recorded from the same cell, model parameters were derived using the square wave and sine wave portions of the protocol before using the model to predict current flow during the portion of the protocol exhibiting the action potential train. Figure 3.13 shows that using this approach, both WT hERG and R56Q mutant channel behavior is recapitulated. Indeed, the Beattie model appears robust and able to recapitulate channel behaviour at both 21 °C and 37 °C, in spite of its relative simplicity. These results are preliminary and this work is ongoing, as we wish to assess the ability of the model to reproduce channel behaviour in the presence of RPR260243. Preliminary results suggest that the Beattie model can achieve this; however, further study is warranted before the authors draw any conclusions in this regard.

Satisfied with the predictive power of this modelling approach, we next integrated the Beattie model describing hERG channel behaviour into two models of the human ventricular action potential, the Grandi model, and the Ord model (Fig. 3.14)(Grandi et al., 2010; O'Hara et al., 2011). WT hERG, hERG R56Q, and R56Q-r conditions were included. The R56Q-r condition was a reflection of recent reports that R56Q channel expression at the membrane is reduced by 20-50% (Foo et al., 2019; Kanner et al., 2018). This R56Q-r condition was used to address this, and reflected a 50% reduction in channel conductance. At this stage, we wished to examine the susceptibility of the myocardium to EAD formation. Model outputs shown in Figure 3.14 confirm that in both models, the R56Q mutation alone did not result in EAD formation. However, small hyperpolarizing shifts in the activation $V_{1/2}$ of the human cardiac L-type calcium channel were sufficient to induce EAD formation in both models under R56Q conditions, without the need for reduced conductance (Fig. 3.14). The reduced expression R56Q condition required the smallest shift to activation gating, and left the myocardium most susceptible to EAD formation (Fig. 3.14).

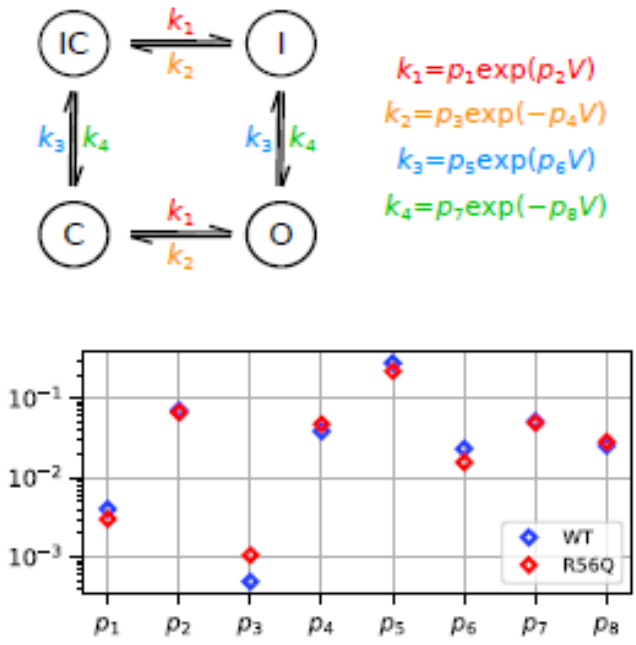

Figure 3.10 Beattie Model Schematic and Parameters.
Top, Markov schematic outlining gating transitions of the Beattie model (Beattie et al., 2018). Bottom, schematic showing model parameters for WT hERG (blue) and R56Q mutant channels (red).

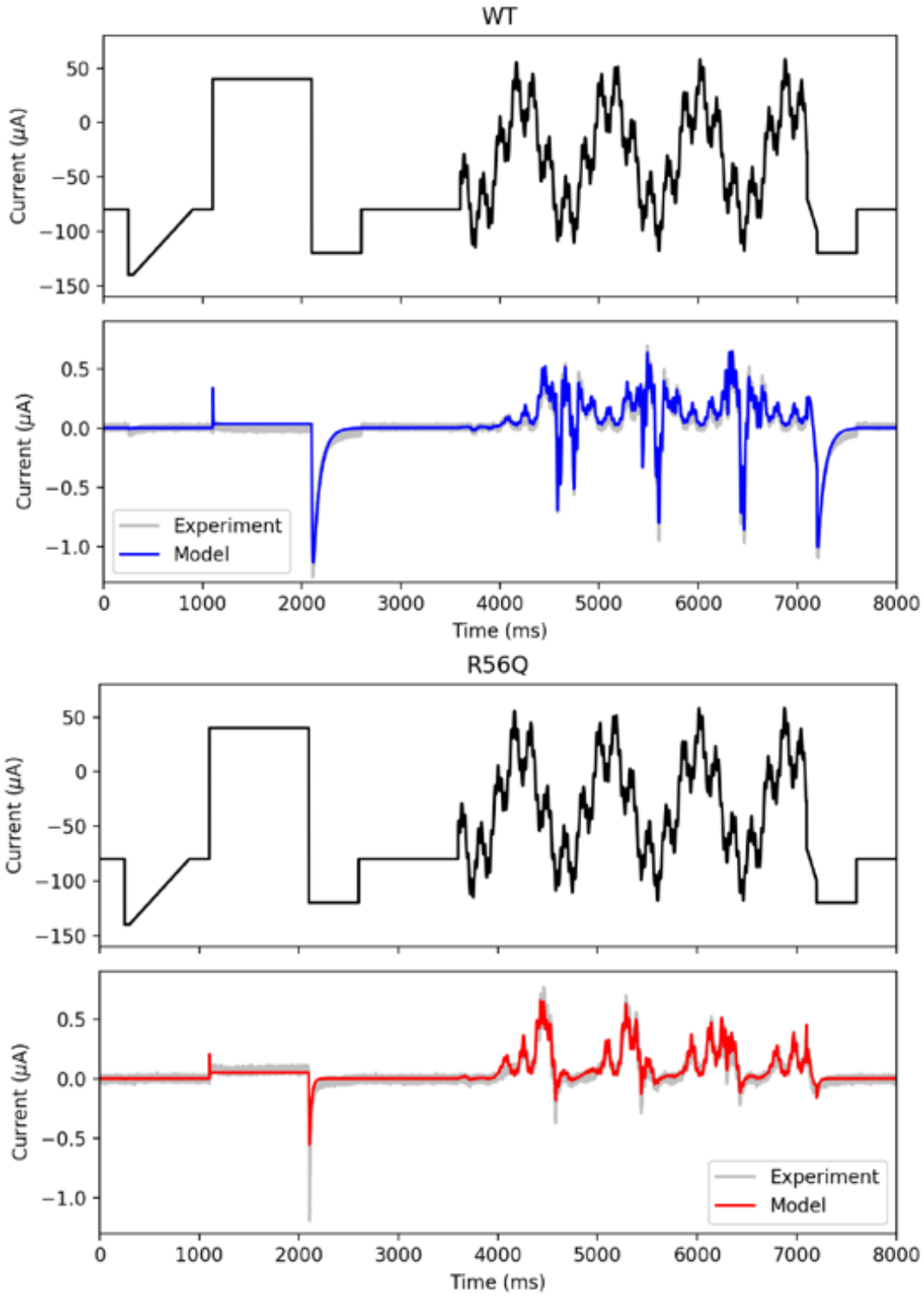

Figure 3.11 Sine wave voltage protocol used to model complex channel behaviour. Top, typical WT hERG recording in response to the protocol shown above. Experiment is in light grey with model overlayed in blue. Bottom, as top, for R56Q mutant channels.

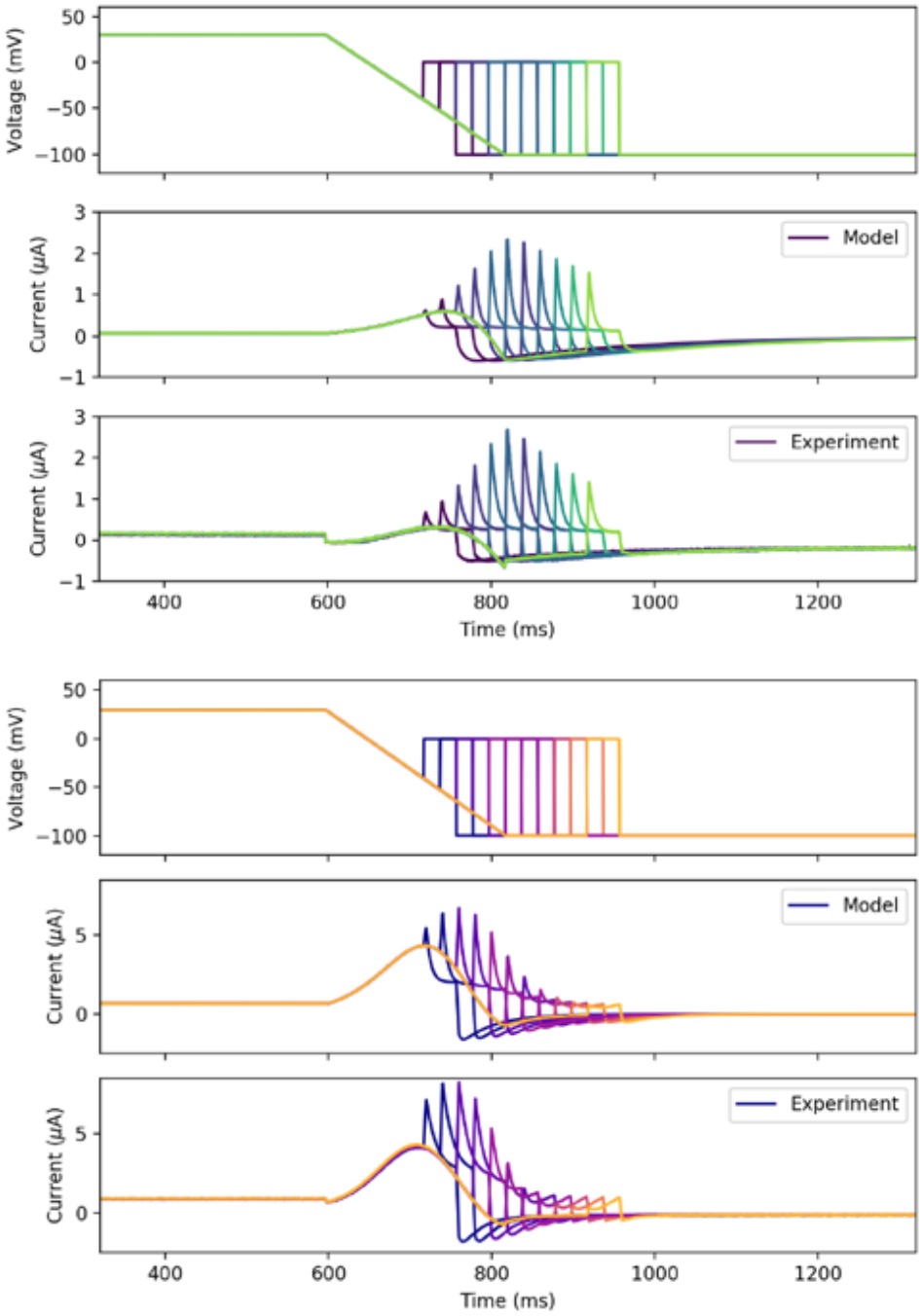

Figure 3.12 Mathematical modelling recapitulates protective currents seen in WT and R56Q mutant channels at 21 °C.

Top. Voltage protocol (adapted from Perry et. al. 2016) used to record protective currents in hERG. Middle. Model output based on parameters derived from control recordings in WT channels, using activation and deactivation protocols recorded using TEVC at 21 °C, along with the sine wave protocol shown earlier. Bottom, experimental data recorded in response to the protocol at top. Qualitative comparison of model and experiment shows good agreement. Shown below WT hERG experiment panel are R56Q conditions.

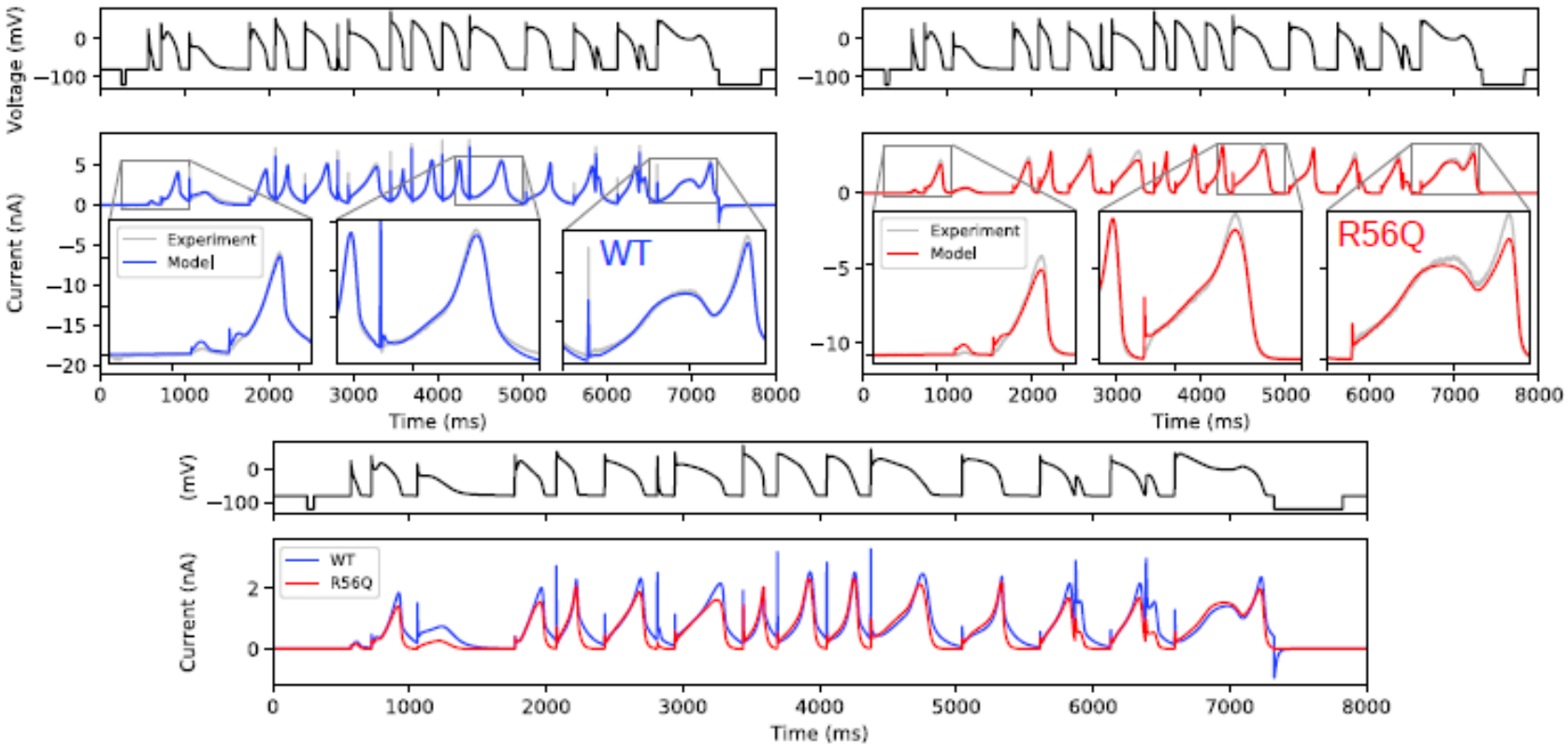

Figure 3.13 Kinetic modelling using the Beattie model recapitulates WT hERG and hERG R56Q channel behavior during a complex AP waveform at 37 °C.

Top left, schematic showing experiment in grey with Beattie model overlayed in blue, with voltage protocol shown above. Top right, as in top left, but R56Q mutant channels. Bottom, model outputs of both WT hERG and R56Q mutant channels overlayed for comparison. (Adapted from Whittaker et. al. 2019).

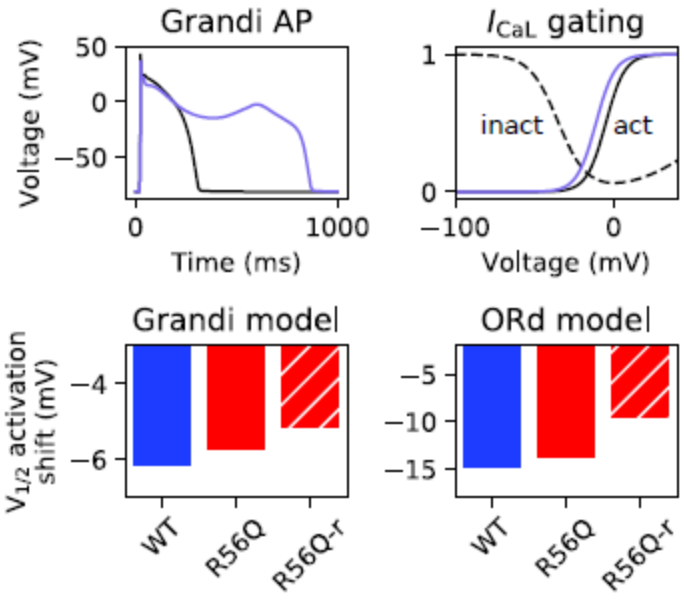

Figure 3.14 The R56Q mutation leaves the myocardium susceptible to EAD formation with small shifts in I_{CaL} gating.

The Beattie model used to predict hERG channel behavior was integrated into the Grandi and ORd models of the human ventricular AP. WT, R56Q, and R56Q-r (reduced surface expression) parameters were included. Top Left, WT hERG (Black) and WT hERG in the presence of a 6 mV hyperpolarizing shift in the activation $V_{1/2}$ of the cardiac L-type calcium channel. Note incidence of EAD even with WT hERG presence. Top Right, panel shows the shift in activation voltage dependency of the cardiac L-type calcium channel applied to elicit the EAD shown at Top Left. Bottom Left, summary of the required shift in voltage dependency of I_{CaL} to elicit EAD formation in using the Grandi model. Bottom Right, as bottom left, using the Ord model (Adapted from Whittaker et. al. 2019).

3.3. Discussion

The R56Q mutation exhibits significantly accelerated deactivation gating relative to WT hERG, while having minimal effects on other gating processes. Premature stimulation recordings revealed that R56Q channels exhibit significantly reduced protective currents, with a reduced peak protective current that occurs earlier in the AP. Loss of function in this regard has been posited to leave affected individuals susceptible to afterdepolarizations and subsequent arrhythmia. The small molecule activator, RPR260243, selectively slows deactivation kinetics primarily through effects on τ_{Slow}, with only a mild attenuation of inactivation and acceleration of recovery from inactivation. We hypothesized that application of the Type I activator, RPR260243, would selectively slow deactivation in R56Q channels, thereby providing a targeted rescue of function. We

observed that application of RPR260243 increased protective current magnitude in a concentration-dependent manner, with effects observed primarily in the refractory period, where deactivation gating predominates. High concentrations of RPR260243 were able to increase the peak protective current in R56Q channels and shift the peak to a shorter coupling interval, resulting in more WT-like behaviour, but this was not observed in WT channels. Using a train of complex AP waveforms, we observed significant differences between WT and R56Q constructs. While the characteristic bolus of hERG resurgent current was largely similar between the two, the early transient current in R56Q mutant channels was significantly reduced, consistent with accelerated deactivation reducing channel availability. Additionally, in response to premature stimulation, WT channels mediated robust currents, while R56Q channels showed significantly decreased current magnitude, again consistent with the accelerated deactivation observed in the mutant. Application of 10 μM RPR260243 was sufficient to restore the early transient current to WT levels, providing further evidence that rapid deactivation is causing loss of protective current. Additionally, in R56Q channels, 10 μM RPR260243 was able to increase resurgent current in response to premature stimulation 4.5-fold. Taken together, these data provide evidence that supports our hypothesis that accelerated deactivation drives a loss of protective current. Further, our RPR260243 data provide evidence that selective slowing of deactivation may provide targeted benefit while leaving the resurgent current during a normal AP waveform largely untouched. This contrasts heavily with Type II activators, and suggests that Type I activators may have a lower risk of overcorrection that could lead to short QT syndrome. *In silico* modelling using the four state Beattie model (Beattie et al., 2018) provides further evidence in support of our hypothesis. An accelerated deactivation rate constant was able to account for the differences in the observed current waveforms in R56Q channels. Able to accurately recapitulate both activation and deactivation protocols, the model was also able to accurately reproduce the protective currents elicited in response to premature stimulation.

With the slowing of deactivation kinetics resulting in the rescue of attenuated protective currents, the question is inherently raised as to whether rescue may be achieved via application of hERG channel activators targeting other gating parameters. With this in mind, the next chapter will examine the effects of the Type II hERG channel activator, ML-T531, on protective currents mediated by WT hERG and hERG R56Q mutant channels.

Chapter 4. The Type II hERG Activator, ML-T531, Significantly Attenuates Inactivation and may also Rescue Loss of Protective Current.

Acknowledgement: All data collection, analysis, and subsequent figure generation pertaining to this chapter was performed by the author.

4.1. Introduction

In the previous chapter, I showed that the accelerated time course of deactivation observed in R56Q mutant channels results in a dramatic loss of protective current, especially in the early refractory period. As a consequence, early transient hERG currents were significantly reduced in the mutant. In contrast, hERG resurgent current during an AP waveform was largely unchanged by the R56Q mutation. Application of the Type I activator, RPR260243, restored R56Q protective currents, especially during the refractory period, as well as the transient hERG current. Having demonstrated the potential utility of a Type I activator targeting deactivation, we next examined the effects of a Type II activator on protective currents mediated by hERG channels. Largely targeting inactivation gating, Type II activators attenuate the process and result in large outward currents during depolarized potentials (Gerlach et al., 2010; Vandenberg et al., 2012; Zhang et al., 2012; Zhou et al., 2005). First discovered in 2012 as part of a compound library screen, ML-T531 was shown to potentiate hERG function (Zhang et al., 2012). With no significant effects on activation gating, application of ML-T531 has modest effects on deactivation gating, slowing both the fast and slow time constants at a test concentration of 10 μM (Zhang et al., 2012). However, the primary effect of ML-T531 is a significant depolarizing-shift in the voltage dependency of inactivation. Consistent with Type II activator classification, we selected ML-T531 for this part of the study. While there are several other Type II activators that may be applicable, the most well characterized of these may be inappropriate for this study. For example, ICA-105574 displays complex effects on hERG channels. Similarly to ML-T531 it slows deactivation kinetics. However, its effect on inactivation is so profound, that channels are essentially rendered non-inactivating (Gerlach et al., 2010). Mutations resulting in this effect have been shown to cause SQT1, and so we felt that this activator was inappropriate for this study. Additionally, the well described NS-1643, while classified as a Type II activator, also blocks hERG channels at

higher concentrations (Casis et al., 2005). This precludes it from inclusion in our study, as we wished to focus on activator compounds and this would have been a confounding factor. Lastly, PD-118057 is also a potential candidate for this stage of the study. However, PD-118057 has effects on channel activation as well those observed on inactivation (Perry et al., 2009; Zhou et al., 2005). Additionally, similar to the reported effect of RPR260243, an earlier report found no significant changes to inactivation gating (Zhou et. al. 2005). While the effect of PD-118057 on inactivation has since been confirmed, the compound also appears to influence the single channel open probability of hERG (Zhou et al., 2005). For these reasons, we limited this portion of the study to ML-T531, as there are fewer effects on other gating parameters observed with application of this compound. We aimed to assess the effects of ML-T531 on gating in the R56Q mutant, and whether application of ML-T531 could rescue the loss of protective current observed in the mutant. As a Type II activator with a small effect on deactivation gating, we hypothesized that ML-T531 would exert its greatest effects on currents during the action potential, as opposed to during the refractory period. In particular, considering the increase in outward currents at depolarized potentials that result from the attenuation of inactivation, we proposed that ML-T531 application would increase the attenuated peak protective current amplitude observed in R56Q channels. The rest of this chapter will detail experimental results of the study, and a comparison between the effects of RPR260243 and ML-T531 on protective currents mediated by WT hERG and R56Q mutant channels. These experiments were conducted using the TEVC technique at 21 °C.

4.2. Results

4.2.1. ML-T531 significantly attenuates inactivation gating in WT hERG and R56Q mutant channels.

Similar to Chapter 3, this study began with characterizing the effects of ML-T531 on both WT hERG and R56Q mutant channels. Voltage protocols used to assess activation, deactivation, and inactivation processes in these channels were consistent with our experiments described in Chapter 3. Figure 4.1A shows representative current traces recorded at 21 °C from *Xenopus* oocytes expressing WT or mutant channels using the TEVC technique. Current traces were recorded in response to the activation protocol shown in the inset, in the absence and presence of 3 µM ML-T531. This concentration was selected due to the reported EC_{50} value of 3.13 µM, first published upon discovery of

the compound (Zhang et al., 2012). Tail currents were measured and normalized to the peak tail current elicited during the -110 mV test pulse, and plotted against the test voltage to generate activation conductance-voltage relationships. Data were fit with a single Boltzmann equation to afford activation $V_{1/2}$ values and the slope factor, *k.* Consistent with data in Chapter 3, WT hERG and R56Q mutant channels exhibited similar voltage dependency of activation (Fig. 4.1B, Table 2). Application of 3 µM ML-T531 produced no change in the $V_{1/2}$ of activation in either construct (Fig. 4.1B, Table 2; P=0.15, two-way ANOVA). However, it is worth noting that R56Q channels showed an approximately 5 mV hyperpolarizing shift that failed to reach significance. Slope factors were unchanged for all conditions (WT vs. R56Q, P=0.474, two-way ANOVA; Control vs. 3 µM ML-T531, P=0.538, two way ANOVA, Table 2).

We next assessed the effects of 3 µM ML-T531 on deactivation kinetics and the voltage dependency of inactivation. Figure 4.2A shows representative current traces recorded in response to the protocol shown in the inset, in the absence and presence of 3 µM ML-T531. Bi-exponential fits of current decays during the repolarizing step pulse afforded a fast and slow time constant to describe deactivation kinetics (Fig. 4.2C, Table 2). Consistent with previous reports, and as described in Chapter 3, R56Q mutant channels exhibited significantly accelerated deactivation kinetics relative to WT control, with effects on both time constants (Fig. 4.2C, Table 2; τ_{fast} P<0.001, τ_{slow} P=0.015, two way ANOVA). Application of 3 µM ML-T531 resulted in no significant changes to either the fast or slow time constant in both constructs at -120 mV (Fig. 4.2C, Table 2; WT τ_{fast} P=0.431, τ_{slow} P=0.357, R56Q τ_{fast} P=0.779, τ_{slow} P=0.607, two way ANOVA for all comparisons). The portion of current decay mediated by the fast time constant ($\%A_{Fast}$) was significantly increased in R56Q channels, consistent with data shown in Chapter 3. Interestingly, while both time constants showed no significant changes, the portion of current decay mediated by the fast component was significantly reduced upon application of 3 µM ML-T531 in WT hERG, but not R56Q (Table 2; WT P=0.005, R56Q P=0.319, two way ANOVA).

Single exponential fits of the rising phase of current during the variable step pulse afforded recovery from inactivation τ values, as outlined previously. Comparison of mutation and drug effects at -120 mV revealed that R56Q displays accelerated kinetics of recovery from inactivation, consistent with that observed in Chapter 3 (Table 2; P=0.033,

two way ANOVA). Application of 3 μM ML-T531 produced no change to the time constant of recovery from inactivation (Table 2, WT P=0.767, R56Q P=0.699, two way ANOVA).

The voltage dependence of inactivation was determined as outlined in previous Chapters using the Rectification Factor method (Sanguinetti et al., 1995). Consistent with data shown in Chapter 3, the R56Q mutation displayed attenuated inactivation relative to WT hERG, showing an approximately 13.5 mV depolarizing shift in the voltage dependence (Fig. 4.2B, Table 2; P<0.001, two way ANOVA). Application of 3 μM ML-T531 resulted in significant increases in outward current at depolarized potentials, consistent with an attenuation of inactivation (Fig. 4.2A). Conductance-voltage relationships revealed that application of 3 μM ML-T531 produced a 25.4 ± 2.4 mV depolarizing shift in WT hERG, and a 31.4 ± 2.4 mV depolarizing shift in R56Q mutant channels (Fig. 4.2B, Table 2; WT P<0.001, R56Q P<0.001, two way ANOVA). Thus, consistent with Type II activator activity and previous reports, 3 μM ML-T531 significantly attenuated inactivation gating in both WT and R56Q mutant channels (Zhang et al., 2012).

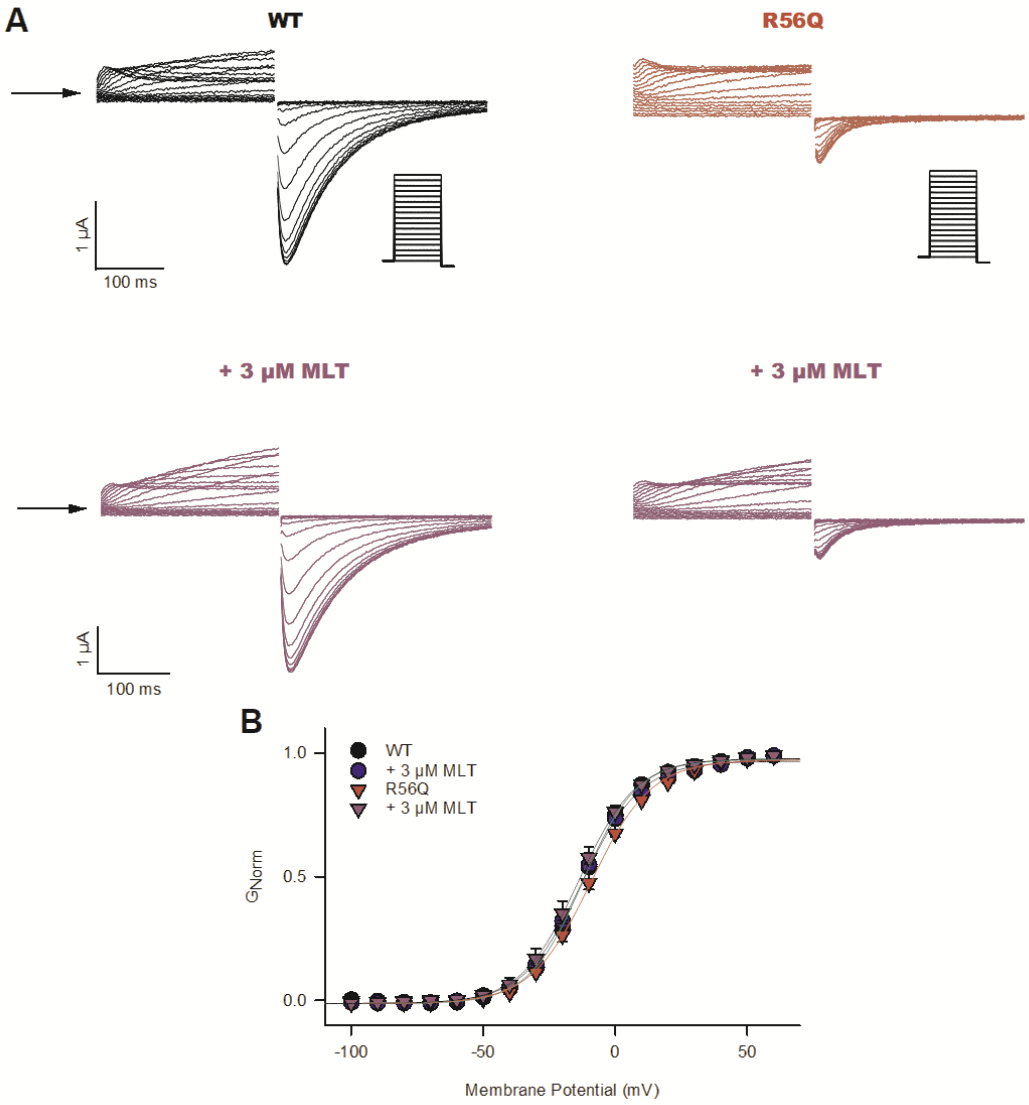

Figure 4.1 3 µM ML-T531 has no significant effects on activation gating.
A. Representative current traces recorded in response to the voltage protocol shown in the inset. Top-left, WT hERG Control; bottom-left, WT hERG +3 µM ML-T531; top-right, R56Q mutant channels control; bottom-right, R56Q in the presence of 3 µM ML-T531. **B**. Activation G-V relationships constructed from peak tail currents elicited in response to the -110 mV test pulse, normalized to peak tail current and fit with a single Boltzmann function (*n*=5 for all conditions).

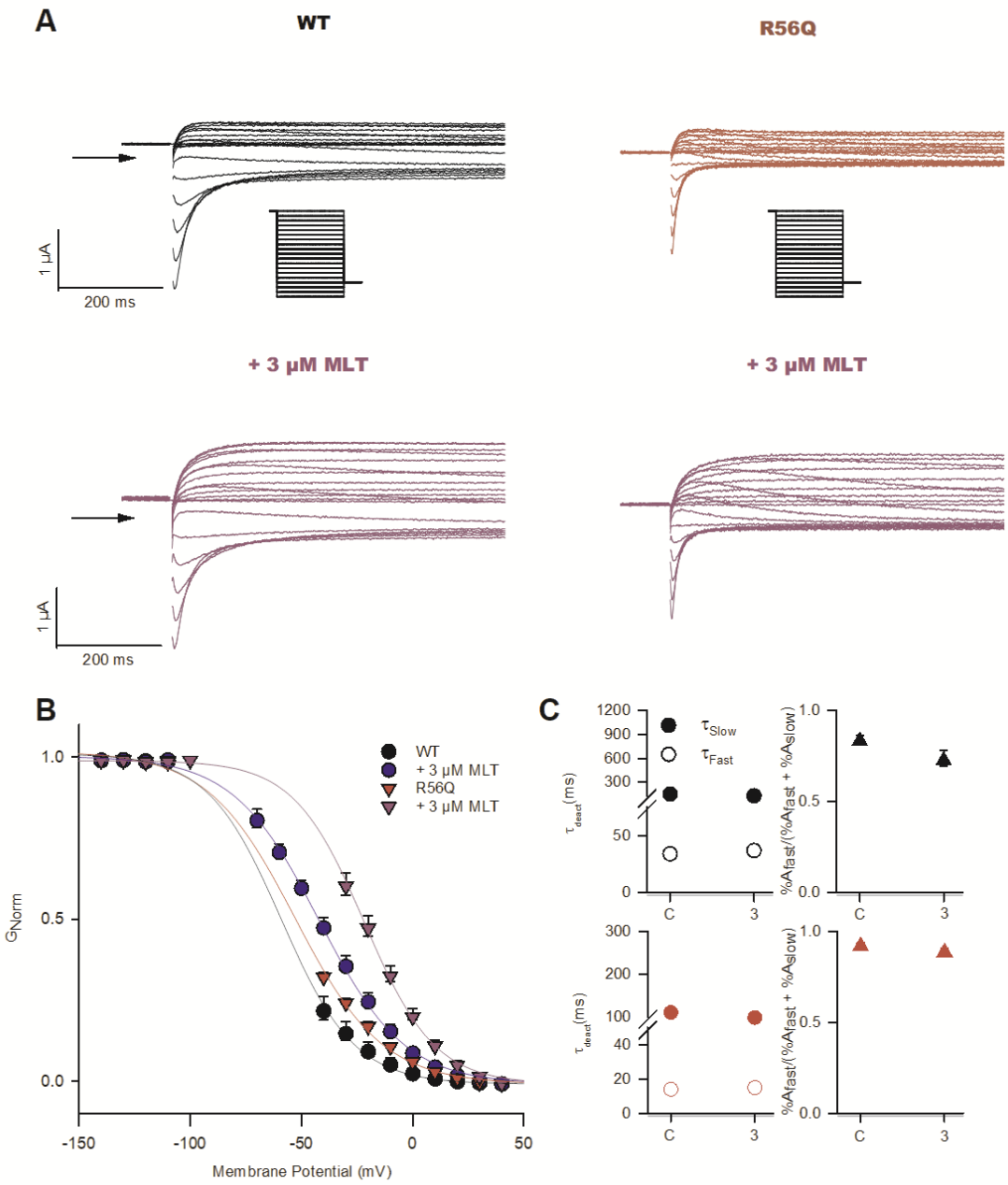

Figure 4.2 3 µM ML-T531 significantly attenuates inactivation gating in both WT hERG and R56Q mutant channels.

A. Representative current traces elicited in response to the voltage protocol shown in the inset. Top-left, WT hERG Control; bottom-left, WT hERG +3 µM ML-T531; top-right, R56Q mutant channels control; bottom-right, R56Q in the presence of 3 µM ML-T531. **B**. Mean inactivation G-V relationships constructed using the Rectification Factor method outlined previously. **C**. Scatter plots of deactivation time constants and percent amplitude contributions. Top-left, Mean WT hERG deactivation time constants. Top-right, mean plot of WT hERG $\%A_{Fast}$. Bottom-left, mean R56Q deactivation time constants. Bottom-right, mean plot of hERG R56Q $\%A_{Fast}$ (*n*=5 for all conditions).

Table 2. Biophysical characteristics of WT and R56Q mutant channels in the absence and presence of ML-T531 at 21 °C

		ML-T531	Activation		Deactivation (at -120 mV for 21 °C)			Inactivation		Inactivation Recovery
			$V_{1/2}$ (mV)	k (mV)	τ_{fast} (ms)	τ_{slow} (ms)	% A_{fast}	$V_{1/2}$ (mV)	k (mV)	τ_{-120mV} (ms)
21°C	WT	Ctrl	-12.2 ± 1.6	10.1 ± 0.4	36.0 ± 2.9	179 ± 25	84.4 ± 0.02	-67.0 ± 2.4	-19.5 ± 0.7	2.4 ± 0.2
		3 mM	-12.4 ± 1.6	11.0 ± 0.4	38.9 ± 3.4	157 ± 19	73.7 ± 0.04*	-41.5 ± 2.4*	-18.6 ± 0.7	2.5 ± 0.2
	R56Q	Ctrl	-9.34 ± 1.6	11.0 ± 0.4	15.5 ± 0.5**	115 ± 5.6**	93.0 ± 0.05**	-53.4 ± 2.4**	-20.0 ± 0.7	1.7 ± 0.2**
		3 mM	-14.0 ± 1.6	10.6 ± 0.4	16.4 ± 0.6	103 ± 5.8	89.7 ± 0.07	-22.0 ± 2.4*	-15.9 ± 0.7*	1.6 ± 0.2

*= sig dif compared to control (drug vs. control)

**= sig dif compared to construct (R56Q vs. WT hERG)

4.2.2. Loss of protective current in R56Q is rescued in a concentration-dependent manner by ML-T531.

Consistent with data in Chapter 3, the R56Q mutation resulted in significant changes to hERG protective currents (Fig. 4.3A, B). Quantification of protective current amplitude at a coupling interval of 100 ms, peak protective current elicited, and timing of peak protective current were all affected as described in Chapter 3 (Fig. 4.3E). R56Q mutant channels showed a significant reduction in both peak protective current, and protective current at 100 ms coupling interval when normalized to whole-cell conductance and compared with WT hERG (PPC $P<0.001$, PC_{100} $P<0.001$, two way ANOVA). Additionally, we observed that the timing of the peak protective current occurred significantly earlier than that observed in WT hERG, consistent with our previous findings ($P<0.001$, two way ANOVA).

Application of ML-T531 to WT hERG channels at various concentrations increased protective current amplitude in a concentration-dependent manner (Fig. 4.3A, C). Application of 3 µM ML-T531 increased both peak protective current, and the protective current at a coupling interval of 100 ms (Fig. 4.3A, C, E; PPC $P<0.001$, PC_{100} $P<0.001$, two way ANOVA). Protective current at a coupling interval of 100 ms normalized to whole cell conductance was increased from a value of 0.359 ± 0.06 that of the peak protective current mediated under control conditions to 1.12 ± 0.09 that of the control value, a more than 3 fold increase. Peak protective currents were also significantly increased, with application of 10 µM ML-T531 resulting in a 1.55 ± 0.06 fold increase in WT hERG peak protective current (Fig. 4.3C, E). It is worth noting that the effect of ML-T351 on the peak protective current was significant even at lower concentrations, which contrasts with the effects of RPR260243 that are largely limited to the refractory period. Interestingly, there was no significant difference observed in peak protective current amplitude between 3 µM and 10 µM ML-T531 ($P=0.14$, two way ANOVA) suggesting a saturating effect at the higher concentrations used. The timing of the peak protective current was consistent with that observed in Chapter 3, with WT hERG exhibiting peak protective currents at +20.7 ± 2.1 ms from the timing of 90% repolarization. Application of ML-T531 produced no change in this regard, with 3 µM ML-T531 resulting in peak protective currents mediated by WT hERG at a coupling interval of +24.1 ± 3.4 ms ($P=0.787$, two way ANOVA).

These effects of ML-T531 on WT channels were largely conserved in R56Q mutant channels, with some notable exceptions. Application of ML-T531 rescued the observed loss of peak protective current in R56Q mutant channels in a concentration-dependent manner (Fig. 4.3B, D, E). As observed with WT hERG channels, application of 3 μM ML-T531 significantly increased peak protective current in R56Q channels from 0.66 ± 0.02 that of WT control to 1.09 ± 0.09 that of WT, providing rescue above and beyond WT levels (Fig. 4.3D, E; $P<0.001$, two way ANOVA). The timing of the peak protective current in R56Q channels under control conditions was consistent with that in Chapter 3, with the peak protective current mediated by R56Q mutant channels occurring at a coupling interval of -22.9 ± 2.1 ms. Consistent with effects on WT hERG channels, application of 3 μM ML-T531 did not shift this timing significantly, with timing of the peak occurring at a coupling interval of -13.3 ± 3.8 ms in the presence of ML-T531 (Fig 4.3E, $P=0.094$, two way ANOVA). Interestingly, application of 1 μM ML-T531 to R56Q mutant channels resulted in a statistically significant shift in the timing of the peak to an earlier coupling interval, from -22.9 ± 2.1 to -35.9 ± 3.4 (Fig. 4.3E, right; $P=0.009$, two way ANOVA). While WT hERG also exhibited a similar shift, it failed to reach significance, shifting from +20.7 ± 2.1 to +12.7 ± 4.4 ($P=0.361$, two way ANOVA).

Interestingly, and in contrast to WT, the application of 3 μM ML-T531 did not significantly increase R56Q mutant channel protective currents at a coupling interval of 100 ms, with mean values of 0.12 ± 0.02 that of WT under control conditions, and 0.27 ± 0.01 that of WT in the presence of 3 μM ML-T531 ($P=0.273$, two way ANOVA). Additionally, 3 μM ML-T531 did not rescue protective currents further out in the refractory period, with no appreciable rescue of protective currents mediated at coupling intervals longer than 160 ms. At coupling intervals exceeding 160 ms, R56Q mutant channel protective currents were comparable in magnitude to those measured in control conditions at a coupling interval of 100 ms, which indicates minimal channel availability consistent with reduced protective currents in the R56Q mutant, and no drug effects. Application of 3 μM ML-T531 resulted in a protective current 0.11 ± 0.01 that of WT at 160 ms coupling interval, contrasting with the effects of the Type I activator, RPR260243, described in Chapter 3 (Figs. 3.4, 3.5). Protective currents mediated by R56Q channels at coupling intervals beyond 160 ms were too small to accurately measure. Higher concentrations of ML-T531 (10 μM), however, did increase protective currents at the longest coupling

interval tested, suggesting a lower affinity effect of the activator to affect protective currents during the refractory period than those during the action potential.

Taken together, these observations show that the Type II activator ML-T531 significantly attenuates inactivation in both WT and R56Q channels. This effect, observed even at 3 μM ML-T531, is robust enough to result in significant rescue of hERG protective currents mediated by R56Q mutant channels (Fig. 4.3B, E). Indeed, peak protective currents mediated by R56Q mutant channels were rescued to WT-like levels upon application of 3 μM ML-T531 (Fig. 4.3E, centre). In contrast, protective currents in the early refractory period, i.e., at a coupling interval of 100 ms, were not restored to WT-like levels and the effect of ML-T531 was not statistically significant. These data lead us to propose that the Type II activator, ML-T531, may restore lost repolarizing protective current during phase three of the action potential caused by the LQTS2-causing R56Q mutation. However, ML-T531 is unlikely to restore lost protective repolarizing drive during the refractory period as RPR260243 does.

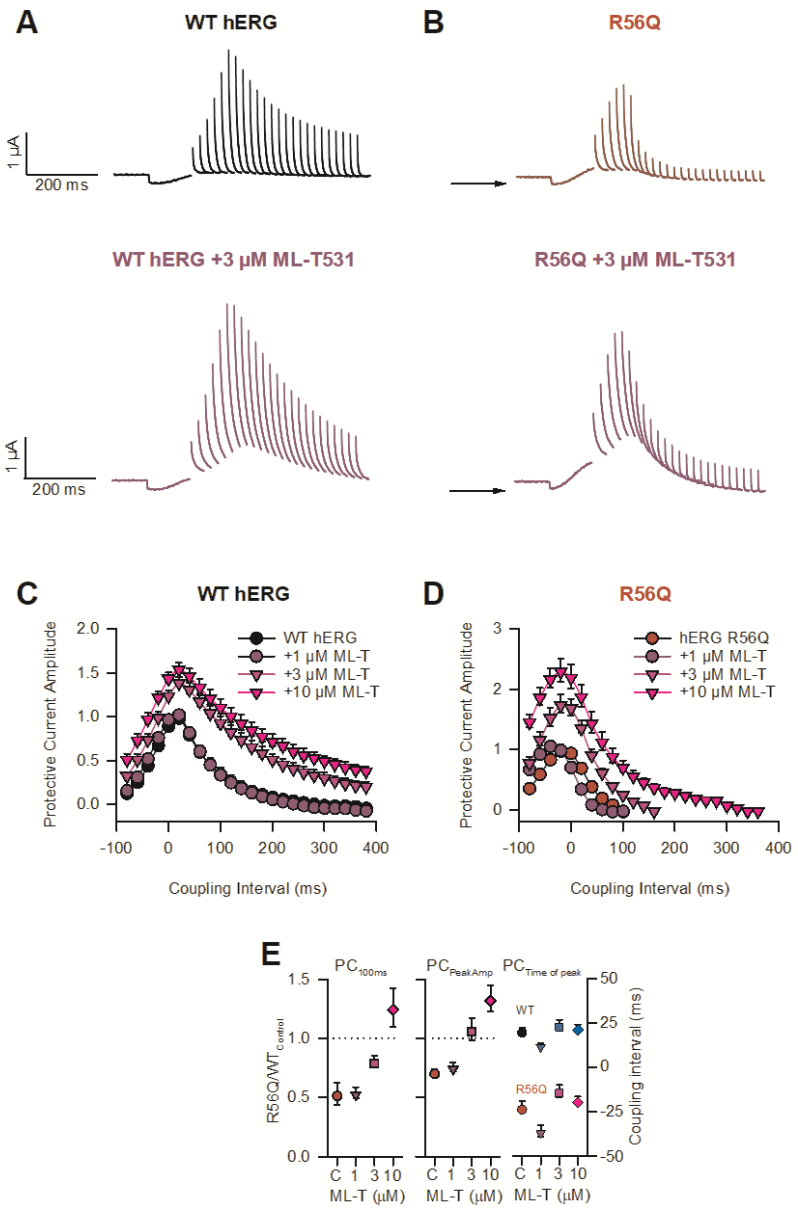

Figure 4.3 R56Q-mediated loss of protective current may be rescued by the type II activator, ML-T531.

A. Representative WT current traces recorded in response to the protocol shown in the inset. Top, WT hERG control; bottom, WT hERG +3 µM ML-T531. **B**. Representative R56Q current traces elicited in response to the protocol shown in the inset. Top, R56Q control; bottom, R56Q + 3 µM ML-T531. **C**. Mean plot of protective current amplitude against coupling interval for WT hERG, in the absence and presence of ML-T531 at increasing test concentrations. **D**. As in C., but under R56Q conditions. **E**. Left, mean scatter plot of protective current at 100 ms coupling interval, normalized to WT control value, plotted against concentration of ML-T531. Centre, mean plot of peak protective current elicited in R56Q channels, plotted as a fold change in amplitude from WT hERG against concentration of ML-T531. Right, mean scatter plot showing the timing of the peak protective current elicited (WT *n*=5; except 1 µM, *n*=3; R56Q *n*=5; except 10 µM, *n*=4)

4.3. Discussion

Type I and II hERG channel activators are relatively recent discoveries. While their therapeutic efficacy is unknown, as channel agonists that potentiate function, they may restore loss of function whether due to inherited mutation or high-affinity drug block. The data presented here support that potential, although the author would like to limit the scope of these conclusions to inherited mutations. Application of the Type I activator, RPR260243, selectively slows deactivation, while leaving other gating parameters largely unperturbed. This slowing of deactivation kinetics results in a greater number of channels residing in the open state during the refractory period, resulting in the increased protective currents described in Chapter 3. This increased protective current is largely limited to the refractory period, with increases in the peak protective current only observed at higher concentrations of RPR260243. Even at higher concentrations, this effect is limited, and may be related to the attenuation of inactivation observed at these drug concentrations. This contrasts significantly with the effects of the Type II activator, ML-T531.

Consistent with its classification as a Type II activator, application of ML-T531 causes a significant depolarizing-shift of the voltage dependence of inactivation. With limited effects on other gating parameters at the tested concentrations, ML-T531 was observed to rescue the loss of protective current caused by the R56Q mutation. Indeed, application of 3 μM ML-T531 was sufficient to induce robust increases in protective currents mediated during the ramp phase of the premature stimulation protocol. Peak protective currents mediated by R56Q channels were restored to WT-like levels, and although an increase in protective currents mediated at a coupling interval of 100 ms were observed, this effect failed to reach significance according to two-way ANOVA statistical analysis. However, qualitative observation of hERG R56Q protective currents at a coupling interval of 100 ms and beyond show what appears to be significant rescue. At coupling intervals of 120-160 ms protective currents were measurable where before they were not, suggesting a significant effect in refractory. However, this effect was not observed at any coupling intervals beyond 160 ms, and the magnitude of rescue decreased with increasing coupling interval. As such, it seems as though ML-T531 may produce effects in the refractory period, but these are limited and require channel availability. Additionally, the Type II activator ML-T531 did not elicit any significant changes to the timing of the peak protective current. With this in mind, a picture describing

the effects of activators on the protective currents mediated by hERG begins to emerge. Type I activators, such as RPR260243, primarily exert their effects on deactivation, slowing its kinetics. The profound slowing of deactivation increases channel availability in the refractory period, allowing for robust protective currents with only limited effects on the peak protective current. Type II activators on the other hand, such as ML-T531, primarily exert their effects on inactivation, reducing availability of inactivated states. Inhibition of inactivation increases channel availability during the action potential, allowing for significant increases in the peak protective current amplitude, with more muted effects on protective currents later in the refractory period.

The data presented here suggest that application of Type I activators targeting deactivation will result in rescue of protective currents largely in the refractory period, with limited effects on the peak protective current (Fig. 4.4A, B). This contrasts with Type II activators that target inactivation, which appear to result in rescue of protective currents during the repolarization phase of an action potential, increasing peak protective current amplitude (Fig. 4.4A, B). Type II activator rescue of repolarization reserve during the refractory period on the other hand appears limited. However, the effects of hERG activator compounds are seldom clear cut, as there is no pure activator that acts on one gating parameter. This is to be expected, as the effects of hERG mutations are equally diverse, and reflect the complex molecular interactions that occur throughout and across the protein (Wang et al., 2011). As shown here, effects on the peak protective current are observed upon application of 3 μM ML-T531, but not at a coupling interval of 100 ms. However, at the highest concentration tested here, one may observe rescue of protective current at and beyond a coupling interval of 100 ms (Fig. 4.3).

With the discovery of hERG channel agonists, the hypothesized holy grail of compounds was confirmed. Long known to be subject to block by a wide variety of molecular classes, hERG channel activators exert specific effects on the channel, likely reflective of distinct binding sites. Exceedingly rare, the therapeutic potential of these activators has yet to be fully explored. Classification based on dominant gating effects has revealed that Type II activators are relatively more common than Type I activators affecting deactivation kinetics, with arguably only one identified to date (Kang et al., 2005). Early work with regard to the effects of these activators raised significant concerns regarding overcorrection of APD_{90}, with a resulting short QT syndrome recently hypothesized to result (Perry et al., 2020). However, the work presented here highlights

that the therapeutic potential of activator compounds cannot be discarded. Application of both RPR260243 and ML-T531 resulted in the rescue of protective currents mediated by hERG, albeit in different capacities. Indeed, this highlights the importance of the continued study of activator compounds. Discovery or engineering of new activator compounds that strike a balance between effects during the AP and afterwards in the refractory period may be able to enhance the protective current without increasing the risk of arrhythmia. However, a complete understanding of the loss of function with regard to protective current would be required, e.g. the timing of the loss of protective current. This would permit the selective application of a hypothetical activator compound, providing targeted benefit in contrast to the current non-specific therapies.

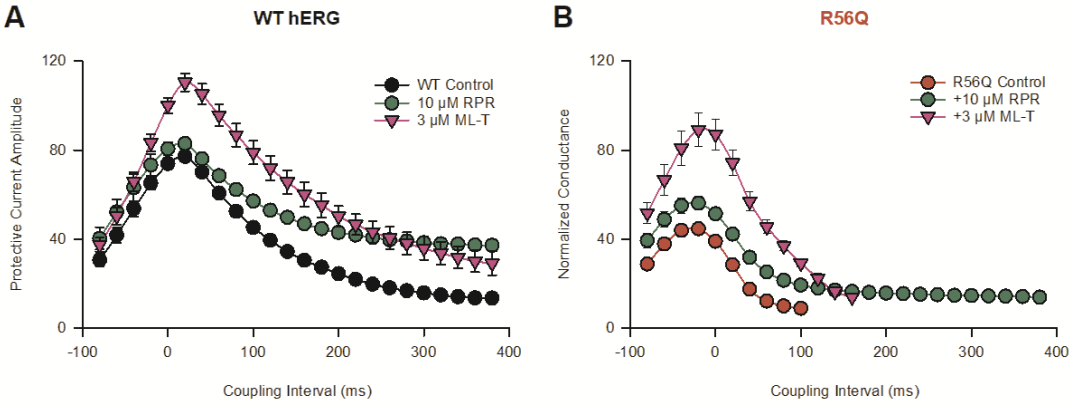

Figure 4.4 Comparison of the actions of RPR260243 and ML-T531.
A. Mean WT hERG protective current amplitude in response to premature stimulations plotted against coupling interval. Control conditions are plotted alongside test concentrations of RPR260243 and ML-T531. **B**. As in A, but in R56Q mutant channels.

Chapter 5. Discussion and Future Directions

5.1. Conclusions

The work presented here supports the idea that hERG activator compounds have novel therapeutic potential. While further study is certainly warranted, both Type I and II hERG channel agonists were able to rescue hERG protective currents lost due to inherited mutation, although the nature of this rescue differed between the classes. The Type I activator RPR260243 rescued loss of protective current largely in the refractory period, consistent with its effect on deactivation kinetics. This contrasts with the Type II activator ML-T531, application of which provided rescue largely during phase three repolarization and significantly increased the peak protective current mediated by hERG, with limited effects in the refractory period. It is worth mentioning that these results were presented in the context of an inherited mutation that resulted in significantly accelerated deactivation, hERG R56Q. This mutant mediated protective currents that were markedly reduced from those of WT hERG, with peak protective currents significantly reduced, and little meaningful protective current passed in the refractory period. Indeed, measurable currents were present only to a coupling interval of 100 ms. Additionally, the timing of the peak protective current in R56Q channels occurred significantly earlier than that of WT hERG channels. Application of 10 μM RPR260243 rescued the loss of protective current, with measurable protective current occurring at more extreme coupling intervals, and a shifting of the timing of the peak towards a more WT-like level.

These effects contrast with the effects of the Type II activator ML-T531, which significantly increased peak protective currents at a concentration of 3 μM, but did not result in significant changes to protective current magnitude during the refractory period. These results suggest that targeting the protective current as a therapeutic target requires characterization of the clinical phenotype, as the application of ML-T531 was unable to provide significant rescue in the refractory period, where loss of function is most apparent in the R56Q mutant. Indeed, the effects of RPR260243 on protective currents mediated during the refractory period, and the ability of RPR260243 to shift the timing of the peak protective current to greater coupling intervals would suggest that it is better suited in rescuing loss of function in R56Q channels than ML-T531. Further supporting this idea is the fact that application of ML-T531 was insufficient to produce changes in the timing of

the peak. However, this does not necessitate discarding ML-T531, or other Type II activators, as potential therapies. For mutations that may exhibit significantly reduced peak protective currents, but muted effects on protective currents mediated during refractory, Type II activators providing rescue largely during phase three repolarization may provide the necessary benefit without affecting the refractory period. This is especially apparent when considering the limited effects of the Type I activator RPR260243 on peak protective currents. Also suggestive of the importance of peak protective currents is the fact that protective currents in WT hERG peak at approximately 90% repolarization, equivalent to APD_{90}, the timing of the effective refractory period. As such, further study of Type II activators is certainly warranted, especially in light of the hypothesized risk of overcorrection. These studies would ideally elucidate the unique features of the compounds (Type I or II) that allow them to bind at sites distinct not only from one another, but also the hydrophobic residues of the pore known to mediate high affinity drug block. This may permit engineering of compounds that are closely related to those first discovered, but with more specific effects than those observed with activators at high concentrations.

5.2. Future Directions

Mutations occurring throughout the hERG protein are disease-causing. Able to affect any of the gating transitions, impaired function due to inherited mutation in any part of the hERG gating pathway can result in loss of function and loss of repolarizing current (Curran et al., 1995). Having demonstrated that rapid deactivation can result in the loss of protective current, ultimately resulting in susceptibility to afterdepolarizations, I would like to examine other mutations in the context of premature stimulation. The majority of hERG mutations result in defective trafficking as a result of protein misfolding (Perry et al., 2016, Vandenberg et al., 2012). Resulting in a haploinsufficiency in some cases, other mutations appear to exert a dominant negative effect, with expression (albeit reduced) at the membrane and aberrant gating mechanisms (Perry et al., 2016). One such mutation, E637K, has been identified and characterized as disease-causing, with reduced membrane expression and altered inactivation gating (Hayashi et al., 2002). Unable to form homotetramers alone, E637K is able to be incorporated into heterotetramers when co-expressed with WT hERG (Hayashi et al., 2002). When co-expressed, consistent with the location of the mutation around the outer mouth of the pore in the S6-P-loop, channels

exhibited accelerated activation and enhanced inactivation (Hayashi et al., 2002). Outward currents at depolarized potentials were reduced relative to WT alone, and tail currents were approximately 30% of those observed in WT (Hayashi et al., 2002). Such significant reductions in current magnitude raise questions regarding the protective current. Having established that rapid deactivation results in reduced protective current during early refractory, we wished to examine the effect of enhanced inactivation on protective currents. E637K provides an appropriate platform for this study, as it exerts a dominant negative effect on hERG currents and exhibits a significant left-shift in the voltage dependency of inactivation (Hayashi et al., 2002). While the mutation has been reported to result in a small but significant right shift in the voltage dependence of activation, deactivation kinetics are WT-like. This is key as it would be expected that the mutation would affect protective currents during repolarization as opposed to the early refractory period, due to the respective gating processes predominating over these two time periods. However, in light of the dominant negative effects on channel expression, it seems likely that protective currents will be reduced relative to WT at all coupling intervals. Examining effects of inactivation on protective currents would thus be most appropriate in mutations exhibiting WT-like deactivation, such as E637K.

Another mutation of interest is the V535M mutation, first associated with a family from China exhibiting a history of syncope and sudden cardiac death (Shao et al., 2011). Electrophysiological characterization revealed that the mutation expressed well at the membrane, but displayed altered gating parameters. The mutation was reported to have a significantly hyperpolarized $V_{1/2}$ of inactivation, consistent with loss of function observed in other mutations. However, the characterization of this mutation has recently come under some scrutiny. Before drawing any conclusions on the effect of the mutation on hERG channel gating, further characterization at 37 °C is required.

I have collected some preliminary data using E637K and V535M channels to explore their effect on the protective current, and whether the Type I activator RPR260243 influences protective currents mediated by these channels. I hypothesize that the enhanced inactivation gating will result in reduced peak protective currents, but those mediated in the refractory period would be less affected than those observed in R56Q. Additionally, I posit that as in R56Q, application of RPR260243 will rescue protective current in the refractory period, consistent with increased open channel availability as a result of slowed deactivation, but have little effect on the peak protective current. It is worth

noting that divorcing the effect of inactivation gating on protective currents from that of dominant negative suppression is difficult. With this in mind, I wished to assess the ability of RPR260243 to rescue protective currents lost due to mechanisms unrelated to deactivation gating. I present evidence here that the utility of RPR260243 is not limited to mutants exhibiting accelerated deactivation.

5.2.1. Loss of Protective Current is observed in both E637K/WT and V535M, and this may be rescued by the application of RPR260243

To assess if the previously discussed mutations exhibited a loss of protective current, I expressed mutant constructs in *Xenopus* oocytes for TEVC recordings. In response to the premature stimulation protocol shown previously, both the E637K/WT hERG co-expression and V535M construct showed loss of protective current, particularly in the refractory period (Fig. 5.1A, B, C). Application of RPR260243 appeared to provide significant benefit, rescuing protective currents in the refractory period as shown in Chapter 3 (Fig. 5.1A, B, C). Plots of protective current amplitude against coupling interval highlight this rescue, with notable effects in the refractory period, consistent with previous results. These data suggest that the utility of RPR260243 in the rescue of protective current is not limited to mutants exhibiting aberrant deactivation gating. However, these conclusions are preliminary and work is ongoing. Future work in this regard would assess the concentration-response relationship of RPR260243 for each mutant, as for R56Q. Additionally, as for the R56Q mutant, robust characterization at both 21 °C and 37 °C is ideal. Additionally, with the ability of the Beattie model to robustly predict channel behaviour at both 21 °C and 37°C in the R56Q mutant, assessing the ability of the model with regard to the mutations presented here would be fruitful.

The data presented here in this chapter, along with the methodologies employed in Chapter 3, provide a framework for future work in this regard. With each hERG mutation exhibiting unique effects on channel gating, exploring the effects of enhanced inactivation on protective currents mediated by hERG is a logical next step. Future work using these mutants would also be able to compare the utility of Type I vs. Type II activators in ameliorating the observed phenotype. The work presented here suggests that Type I activators may be better suited for rescue of protective current in the refractory period, whereas Type II activators may be better suited to rescue during phase three repolarization, and increasing the peak protective current magnitude. The work presented

here also suggests broad utility of the Type I activator RPR260243, but further experiments are required to fully describe this effect. We observed that application of 10 μM RPR260243 provided targeted rescue in refractory to both the E637K and V535M mutations. These mutations have been reported to result in mutant channels that display enhanced inactivation, resulting in a loss of repolarizing current and LQTS2. We report that both mutations resulted in reduced protective currents, both during phase three repolarization and the refractory period. Protective currents recorded in the presence of 10 μM RPR260243 were increased largely in the refractory period, consistent with previous results. However, the author declines to draw significant conclusions with regard to these mutants, as work remains preliminary. In any case, the data presented here suggest novel therapeutic potential for activator compounds, and the author is keen to see how the field develops.

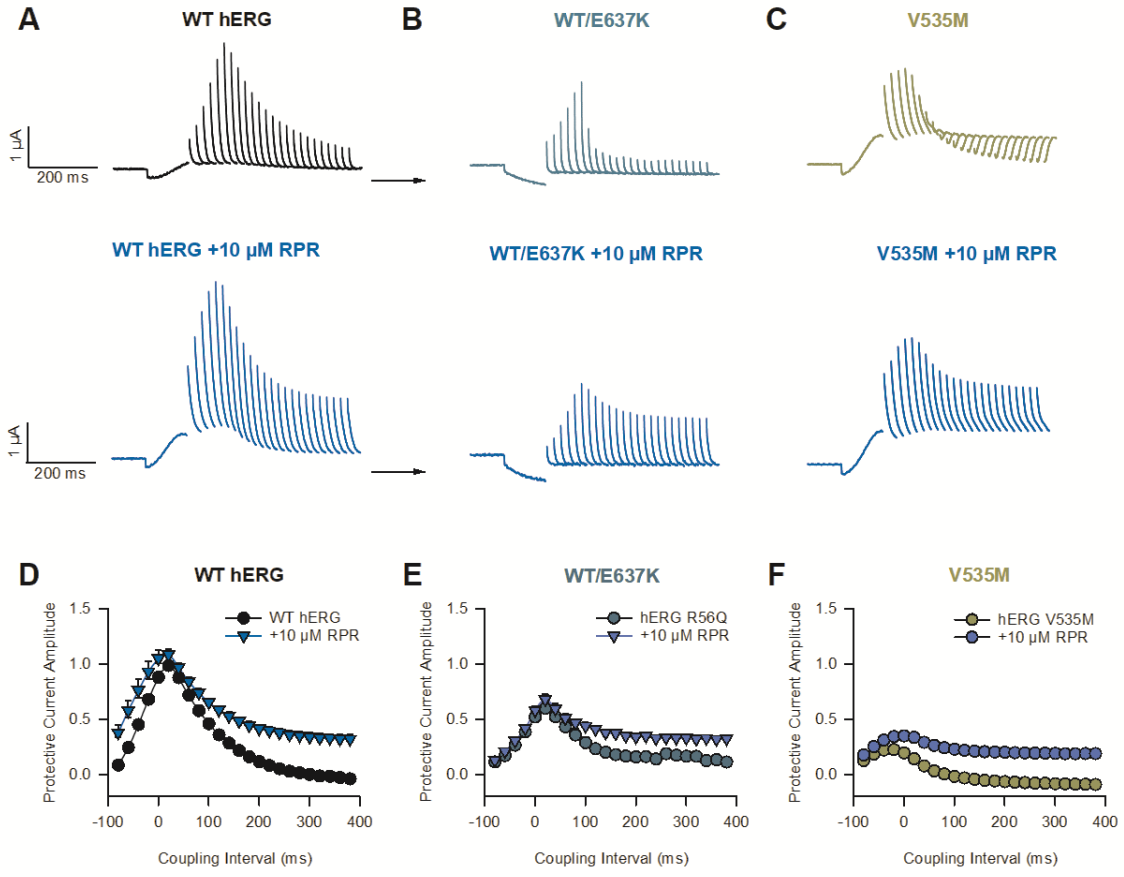

Figure 5.1 Mutations affecting hERG channel inactivation can reduce protective current, and this may be rescued with the application of the type I activator RPR260243.

A. Representative WT hERG current traces in response to the premature stimulation protocol shown previously. Top, control recording. Bottom, Recording in the presence of 10 μM RPR260243. **B, C.** As in A, for the E637K/WT hERG co-expression mutant and the V535M mutant, respectively. **D-F**. Mean plots of protective current amplitude against coupling interval. Protective currents were normalized to whole cell conductance and to the peak WT control protective current, as previously. (n=5 for WT, 4 for WT/E637K and V535M).

5.3. Limitations and Mitigating Factors

Regulation of the Protective Current

hERG protective currents are subject to regulation beyond that exerted by the normal gating mechanisms governing hERG channel availability (Du et al., 2010; Lu et al., 2001, 2003; Melgari et al., 2014). Co-expression studies of hERG with *KCNE2* revealed that mutations in the *KCNE2* protein known to result in LQTS were associated with significant changes in hERG gating (Lu et al., 2001). Deactivation was observed to slow significantly when hERG was co-expressed with all of the examined mutations, and when premature action potential stimuli were delivered, this was reflected in increased protective current magnitude relative to WT *KCNE2* (Lu et al., 2001). However, this increase in protective current may not be protective in nature. The mutations examined all exerted effects that resulted in increased protective current, especially at longer coupling intervals (Lu et al., 2001). While this intuitively seems to promote the protective function of hERG by allowing for greater repolarizing current, the authors took great care to make measured conclusions in this regard. They note that the electrical conduction system of the heart is complex and relies on the coordinated action of many different ion channels, and as such the response of the organ to a premature beat will depend also on the activity of other ion channels (Lu et al., 2001). Of particular importance is the voltage gated sodium channel and its recovery from inactivation. Subtle changes that manifest in both apparent gain of function and loss of function have been noted to result in increased risk of arrhythmia (Balser, 1999; Lu et al., 2001). Thus, they posit that it is conceivable that increases in the protective current magnitude during a premature stimulus may antagonize sodium channel activity and result in an apparent loss of function of sodium channel current in the early refractory period, which may also be pro-arrhythmic (Balser, 1999).

Additional regulatory elements include the closely related *KCNE1*, which has also been shown to associate with and modulate hERG (McDonald et al., 1997). Expressed in greater quantities than *KCNE2* in the myocardium and associated with LQTS, it has been posited that *KCNE2* may only form significant interactions with hERG in the cardiac conduction system (Bendahhou et al., 2005; Hancox et al., 2008; Pourrier et al., 2003; Sanguinetti & Tristani-Firouzi, 2006). Consistent with this suggestion, WT *KCNE1* increased outward current during the course of an action potential waveform compared with WT hERG (Du et al., 2013). Mutant *KCNE1* when co-expressed with WT hERG showed a significant reduction in outward current, consistent with a loss of function mediated by *KCNE1* (Du et al., 2013). Compared with WT *KCNE1*, co-expression of all mutants resulted in significant reductions in protective currents mediated by hERG channels (Du et al., 2013). Along with the *KCNE2* study, these data indicate the importance of hERG accessory subunits, and that loss of protective current may occur through mutations outside of the hERG channel itself.

These findings have implications for the work presented here. We selected the *Xenopus* oocyte heterologous expression system for our study, as its robustness in quantifying biophysical phenomena is noteworthy. However, the cells are amphibian, differing in significant ways from the mammalian cell lines often used in patch clamp techniques. As such, the interacting partners described above would not be present in *Xenopus* oocytes, and the differential effects observed using the patch clamp technique may be partially accounted for by this. However, confounding this potential effect is the different temperatures at which the two data sets were recorded. Gating transitions in hERG channels display different Q_{10} values, and this may also contribute to the difference in effects observed between the two systems.

Timing of the Peak Protective Current

In Chapter 3, we observed that R56Q mutant channels mediate peak protective currents at shorter coupling intervals than WT hERG channels. Application of 10 µM RPR260243 shifted the timing of this peak to a more WT-like coupling interval. This result, taken together with the accelerated deactivation observed in the R56Q mutant, suggests that the timing of the peak protective current may be subject to regulation by deactivation kinetics. However, based on the work presented here this conclusion may be inappropriate. While deactivation kinetics have correlated well with protective current

decay in refractory, it is worth mentioning that the rising phase of protective currents correlates well with recovery from inactivation kinetics. This, along with the observed acceleration of recovery from inactivation in both R56Q mutant channels and with the application of RPR260243, makes it difficult to draw conclusions as to which effect is shifting the timing of the peak. With both effects observed here, it seems likely that both recovery from inactivation and deactivation kinetics contribute to the timing of the peak protective current, with the peak shifting as the balance between the two processes shifts.

Effects of RPR260243 on Protective Currents During the Refractory Period and Subsequent Action Potentials

In Chapter 3, application of RPR260243 was shown to produce significant increases in the peak transient current in response to phase zero depolarization during an action potential waveform. This was interpreted as being reflective of RPR260243 slowing channel deactivation and increasing the number of open channels in the refractory period. Upon depolarization, these channels are thought to pass a large repolarizing current before rapidly inactivating in response to the same depolarization. As the holding potential used is reasonably close to the equilibrium potential, the electromotive force is rather small, and so directly assessing the number of open channels is difficult during the terminal stage of the refractory period prior to a subsequent action potential. A modified protocol in which a hyperpolarizing step is delivered prior to the upstroke could more directly assess this open probability in the presence of RPR260243. As the step is hyperpolarizing, an increase in the electromotive force would be expected to produce an inward current directly proportional to the number of channels remaining in the open state following the previous depolarization, as the effect of inactivation on the current decay would be minimal. This could inform on the steady-state open probability of hERG channels in the presence of RPR260243.

Large increases in the steady-state open probability of hERG channels may produce changes to the action potential. If the open probability is increased across all phases of the action potential, it seems intuitive that increased I_{Kr} magnitude would produce a shortened action potential. However, the application of RPR260243 produced apparently different effects on channel open probability in different phases of the AP waveform. Effects of RPR260243 on the protective current and the early peak transient current are suggestive of increased open probability; however, the current evoked during phase two of the cardiac AP was largely unchanged from WT conditions. This suggests

that steady-state open probability was not increased during phase two, or perhaps that the rapid inactivation kinetics of hERG channels overrides the effect of RPR260243 on steady-state open probability, thereby limiting the effects of RPR260243 to regions where deactivation kinetics are clearly dominant and the contribution of inactivation is negligible.

Canonical Action Potential Characterization vs. Pathological Variants

In Chapter 3, the characterization of mutation and drug effects on the current evoked in response to an action potential waveform used a canonical AP voltage protocol in which I_{Kr} would be expected to be mediated by WT hERG. With the application of our chosen activators, changes to hERG kinetics could produce significant changes to I_{Kr}, which would manifest as changes in action potential morphology. While the evidence presented here suggests that Type I activators may have limited effects in this regard, the effect of Type II activators on inactivation may produce significant changes. Thus, future work could make use of action potential waveforms that reflect these changes. For example, application of ML-T531 resulted in significantly attenuated inactivation and large outward currents during depolarized potentials. This would indicate that the contribution of I_{Kr} during phase two of the cardiac action potential is likely increased, due to kinetics favouring the open state over the inactivated state. Large increases in outward repolarizing currents during the plateau phase would be expected to prematurely depolarize the membrane, resulting in early termination of the cardiac AP. This would expose channels to more negative voltages earlier than desired, and could result in a hastening of deactivation, thereby removing channels from the open population in spite of the attenuation of inactivation. Thus, an apparent gain of function in one regard could conceivably produce a loss of function in another, as removal of channels from the open population would result in reduced protective currents. The degree to which this effect regulates protective current magnitude remains unknown, and future experiments utilizing pathological action potential waveforms may be informative.

Concentration-response Curve and Reported EC_{50}

In Chapter 3, a concentration-response curve was constructed and fit with a Hill function to determine an EC_{50} of RPR260243 at a coupling interval of 100 ms. We report an EC_{50} of 18.2 µM, which differs significantly from the value our group previously reported, 6.7 µM (Hull et al., 2019). This discrepancy could be attributed to the difference in methodologies used to assess response. In the earlier report, integrated tail currents

were normalized to peak tail current amplitude and fit with a Hill equation. The method reported here used protective current amplitude at a coupling interval of 100 ms to assess response, normalized to the control protective current amplitude. Due to the method presented here not requiring integration of the area under the current decay, it likely exhibits smaller error, as current decays between different cells may exhibit significant differences even under the same conditions. Additionally, it should be noted that the EC_{50} value reported here is consistent with that published by Perry et. al. (Perry et al., 2007). Perry et. al. report an EC_{50} value of 15.0 ± 2.6 μM RPR260243.

Effects of ML-T531 on Deactivation, Time of Peak

Previous reports have shown that application of 10 μM ML-T531 resulted in a slowing of deactivation kinetics, with effects observed on both the fast and slow time constants (Zhang et al., 2012). We report no such change in deactivation gating, although we did not assess this effect at a concentration of 10 μM ML-T531. The discrepancy could be due to concentration effects, with effects on deactivation only occurring at higher concentrations, similar to how RPR260243 affects inactivation, or NS-1643 blocks hERG channels at elevated concentrations. This discrepancy could also be due in part to different recording methodologies, as our experiments were conducted using the *Xenopus* oocyte heterologous expression system and two-electrode voltage clamp, whereas Zhang et. al. used the patch clamp technique on channels expressed in CHO cells. Regardless, the chosen test concentration of 3 μM ML-T531 achieved its purpose, as its application resulted in effects on inactivation, but not deactivation gating, and thus made drawing meaningful conclusions with regards to activator effects on protective current feasible.

The effect of ML-T531 on the timing of the peak protective current was for the most part nonexistent. However, both WT hERG and R56Q mutant channels exhibited a shift towards shorter coupling intervals upon application of 1 μM ML-T531. This contrasted with results of higher concentration solutions of ML-T531, which produced no significant shifts. This may be due to an unknown experimental effect, as 1 μM data were collected on the same day for both WT hERG and R56Q mutant channels. In both constructs, control recordings also showed an anomalous shift of the peak protective current timing to shorter coupling intervals. Statistical comparison of the 1 μM ML-T531 control group revealed no significant effects of 1 μM ML-T531 application. With this in mind, it seems as though

application of ML-T531 does not influence the timing of the peak protective current mediated by hERG channels.

Using the 'Beattie' Approach to Model Channel Behaviour in the Presence of RPR260243

With regard to the kinetic modelling of channel behaviour, work remains ongoing. We are currently focusing our efforts on modelling the behaviour of hERG channels in the presence of RPR260243. To date, the Beattie approach has been validated at both room and physiological temperature, and against the inherited mutation R56Q. However, it is conceivable that this approach may be unable to reproduce the observed behaviour, as it is well known that application of high concentrations of RPR260243 produces current decays that are not fit as well with a biexponential function as those recorded in control conditions. Should the approach be unable to reproduce channel behaviour under these conditions, it is possible that refining the Beattie approach may be warranted. Indeed, the initial publication suggested that refinement of the model may be required (Beattie et al. 2018). However, with its robust predictive ability shown to date, and in this thesis, adjusting the model to reflect kinetics observed in the presence of a single drug may be inappropriate.

Conversely, an inability to reproduce channel behaviour in the presence of RPR260243 could be explained by the presence of an unknown, or undescribed, effect on hERG channel gating. This would certainly suggest that the four-state Beattie approach may not capture the kinetics in question, and so may suggest a refinement of the model with the addition of another state is warranted. Comparison with the Wang model would also be informative, as the Wang model includes five states and is widely used under a variety of conditions. It is worth noting however, that previous comparisons with the Wang model at room temperature showed that the four-state Beattie approach outperformed the Wang model.

Xenopus Oocyte Heterologous Expression System

As discussed in brief previously, the *Xenopus* oocyte heterologous expression system, while robust, is not mammalian. This makes the translation of results to more complex human models inappropriate for several reasons. *Xenopus* oocytes, being amphibian, do not possess cellular constituents affecting hERG channels found in mammalian cells. However, our use of 37 °C patch clamp recordings using HEK-293 cells

addresses this, and we see a conservation of the main effect in the 37 °C system. Additionally, application of the Beattie model to both data sets suggest that the *Xenopus* system is appropriate. An additional consequence of the use of *Xenopus* oocytes is the potential for potassium accumulation on the extracellular membrane surface. *Xenopus* oocytes have many invaginations in their membrane, and during depolarizing steps with outward current, these folds in the membrane can accumulate potassium ions, leading to a local elevation of potassium in the extracellular compartment, which has been shown to paradoxically potentiate hERG function through effects on inactivation (Wang et al., 2011; Wang et al., 1996, 1997). This was of particular concern when conducting experiments with 10 µM ML-T531, as potassium accumulation in addition to the effect of the activator resulted in significant increases in outward current that made quantification of the effect of the activator essentially impossible. This, along with the reported EC_{50} of 3.13 µM, were factors in our decision to characterize the effect of ML-T531 at a concentration of 3 µM. However, it is worth noting that potassium accumulation was not an issue of concern for premature stimulation recordings. The shorter duration pulses did not appear to result in potassium accumulation, whereas the longer duration 750 ms pulse during deactivation protocols did. Future work concerning ML-T531, or any Type II activator, should take this into consideration.

R56Q Membrane Expression

While initial reports indicated that the R56Q mutation expressed well at the membrane, these findings have recently come under question. Initial characterization of the R56Q mutation indicated that the mutant channels expressed well at the membrane – robust currents were observed and co-expression with WT hERG was not required to elicit membrane currents (Chen et al., 1999). This was supported by a subsequent publication, which also observed robust membrane currents without co-expression (Berecki et al., 2005). While the initial report utilized the TEVC technique and the *Xenopus* oocyte heterologous expression system, the latter employed whole cell patch clamp techniques at both room and physiological temperature (Berecki et al., 2005; Chen et al., 1999). This would indicate that the lower temperature incubation of *Xenopus* oocytes had little effect on channel expression at the membrane relative to the physiological incubation temperature of HEK cells used by Berecki's group in 2005. However, it is worth noting that neither study set out to definitively answer the question of membrane expression. Rather, the focus was on the characterization of the effects of the mutation on hERG channel

function. As such, more recent reports describing the effects of the R56Q mutation on membrane surface expression have raised questions in this regard. Recently, two groups have reported that the R56Q mutation may result in reduced surface expression of between 20-50% (Foo et al., 2019; Kanner et al., 2018). However, it is worth noting that the R56Q mutant channels display glycosylation markers indicating successful protein folding and maturation, which would suggest that the channels are able to be inserted into the membrane (Foo et al., 2019). Indeed, it seems that the half-life of R56Q channels at the membrane is reduced relative to WT hERG, and that channels are able to express at the membrane but are quickly internalized and targeted for lysosomal degradation (Foo et al., 2019). In any case, in light of the majority of hERG mutations resulting in reduced channel expression at the membrane, it is possible that even mutations observed to mediate robust membrane currents may have altered expression profiles, similar to that recently observed in R56Q. This provides further support for the idea that robust phenotypic characterization should be carried out for any clinically relevant LQTS patient, as it is known that even family members carrying the same mutation may display significantly different phenotypes (Schwartz et al., 2009, 2012).

References

Al-Owais, Moza, Kate Bracey, and Dennis Wray. “Role of Intracellular Domains in the Function of the Herg Potassium Channel.” *European Biophysics Journal* 38, no. 5 (June 2009): 569–76. https://doi.org/10.1007/s00249-009-0408-2.

Anson, Blake D., Michael J. Ackerman, David J. Tester, Melissa L. Will, Brian P. Delisle, Corey L. Anderson, and Craig T. January. “Molecular and Functional Characterization of Common Polymorphisms in HERG (KCNH2) Potassium Channels.” *American Journal of Physiology-Heart and Circulatory Physiology* 286, no. 6 (June 2004): H2434–41. https://doi.org/10.1152/ajpheart.00891.2003.

Arnaout, R., T. Ferrer, J. Huisken, K. Spitzer, D. Y. R. Stainier, M. Tristani-Firouzi, and N. C. Chi. “Zebrafish Model for Human Long QT Syndrome.” *Proceedings of the National Academy of Sciences* 104, no. 27 (July 3, 2007): 11316–21. https://doi.org/10.1073/pnas.0702724104.

Balser, J. “Structure and Function of the Cardiac Sodium Channels.” *Cardiovascular Research* 42, no. 2 (May 1999): 327–38. https://doi.org/10.1016/S0008-6363(99)00031-0.

Barsheshet, Alon, Olena Dotsenko, and Ilan Goldenberg. “Genotype-Specific Risk Stratification and Management of Patients with Long QT Syndrome: Genotype-Specific Risk in LQTS.” *Annals of Noninvasive Electrocardiology* 18, no. 6 (November 2013): 499–509. https://doi.org/10.1111/anec.12117.

Beattie, Kylie A., Adam P. Hill, Rémi Bardenet, Yi Cui, Jamie I. Vandenberg, David J. Gavaghan, Teun P. de Boer, and Gary R. Mirams. “Sinusoidal Voltage Protocols for Rapid Characterisation of Ion Channel Kinetics: Sinusoidal Protocols to Capture Ion Channel Kinetics.” *The Journal of Physiology* 596, no. 10 (May 15, 2018): 1813–28. https://doi.org/10.1113/JP275733.

Bendahhou, S, C Marionneau, K Haurogne, M Larroque, R Derand, V Szuts, D Escande, S Demolombe, and J Barhanin. “In Vitro Molecular Interactions and Distribution of KCNE Family with KCNQ1 in the Human Heart.” *Cardiovascular Research* 67, no. 3 (August 15, 2005): 529–38. https://doi.org/10.1016/j.cardiores.2005.02.014.

Berecki, Géza, Jan G. Zegers, Arie O. Verkerk, Zahurul A. Bhuiyan, Berend de Jonge, Marieke W. Veldkamp, Ronald Wilders, and Antoni C.G. van Ginneken. “HERG Channel (Dys)Function Revealed by Dynamic Action Potential Clamp Technique.” *Biophysical Journal* 88, no. 1 (January 2005): 566–78. https://doi.org/10.1529/biophysj.104.047290.

Bezanilla, Francisco. “The Voltage Sensor in Voltage-Dependent Ion Channels.” *Physiological Reviews* 80, no. 2 (January 4, 2000): 555–92. https://doi.org/10.1152/physrev.2000.80.2.555.

Bezzina, C. “A Common Polymorphism in KCNH2 (HERG) Hastens Cardiac Repolarization.” *Cardiovascular Research* 59, no. 1 (July 1, 2003): 27–36. https://doi.org/10.1016/S0008-6363(03)00342-0.

Boukens, Bastiaan JD, Vincent Christoffels, Ruben Coronel, Antoon Moorman. “Developmental Basis for Electrophysiological Heterogeneity in the Ventricular and Outflow Tract Myocardium As a Substrate for Life-Threatening Ventricular Arrhythmias.” *Circulation Research* 104, no. 1 (January 2, 2009): 19-31. https://www.ahajournals.org/doi/pdf/10.1161/CIRCRESAHA.108.188698

Brugada, Ramon, Kui Hong, Robert Dumaine, Jonathan Cordeiro, Fiorenzo Gaita, Martin Borggrefe, Teresa M. Menendez, et al. “Sudden Death Associated With Short-QT Syndrome Linked to Mutations in HERG.” *Circulation* 109, no. 1 (January 6, 2004): 30–35. https://doi.org/10.1161/01.CIR.0000109482.92774.3A.

Butler, Andrew, Matthew V. Helliwell, Yihong Zhang, Jules C. Hancox, and Christopher E. Dempsey. “An Update on the Structure of HERG.” *Frontiers in Pharmacology* 10 (January 24, 2020): 1572. https://doi.org/10.3389/fphar.2019.01572.

Casis, Oscar, Søren-Peter Olesen, and Michael C. Sanguinetti. “Mechanism of Action of a Novel Human *Ether-a-Go-Go* -Related Gene Channel Activator.” *Molecular Pharmacology* 69, no. 2 (February 2006): 658–65. https://doi.org/10.1124/mol.105.019943.

Chen, J., G. Seebohm, and M. C. Sanguinetti. “Position of Aromatic Residues in the S6 Domain, Not Inactivation, Dictates Cisapride Sensitivity of HERG and Eag Potassium Channels.” *Proceedings of the National Academy of Sciences* 99, no. 19 (September 17, 2002): 12461–66. https://doi.org/10.1073/pnas.192367299.

Chen, Jun, Anrou Zou, Igor Splawski, Mark T. Keating, and Michael C. Sanguinetti. “Long QT Syndrome-Associated Mutations in the Per-Arnt-Sim (PAS) Domain of HERG Potassium Channels Accelerate Channel Deactivation.” *Journal of Biological Chemistry* 274, no. 15 (April 9, 1999): 10113–18. https://doi.org/10.1074/jbc.274.15.10113.

Cheng, Yen May, and Tom W. Claydon. “Voltage-Dependent Gating of HERG Potassium Channels.” *Frontiers in Pharmacology* 3 (2012). https://doi.org/10.3389/fphar.2012.00083.

Cheng, Yen May, Christina M. Hull, Christine M. Niven, Ji Qi, Charlene R. Allard, and Tom W. Claydon. “Functional Interactions of Voltage Sensor Charges with an S2 Hydrophobic Plug in HERG Channels.” *The Journal of General Physiology* 142, no. 3 (September 1, 2013): 289–303. https://doi.org/10.1085/jgp.201310992.

Cho, Yongkeun. “Management of Patients with Long QT Syndrome.” *Korean Circulation Journal* 46, no. 6 (2016): 747. https://doi.org/10.4070/kcj.2016.46.6.747.

Chockalingam, Priya, Lia Crotti, Giulia Girardengo, Jonathan N. Johnson, Katy M. Harris, Jeroen F. van der Heijden, Richard N.W. Hauer, et al. “Not All Beta-Blockers Are Equal in the Management of Long QT Syndrome Types 1 and 2.” *Journal of the American College of Cardiology* 60, no. 20 (November 2012): 2092–99. https://doi.org/10.1016/j.jacc.2012.07.046.

Codding, Sara J., and Matthew C. Trudeau. “The HERG Potassium Channel Intrinsic Ligand Regulates N- and C-Terminal Interactions and Channel Closure.” *Journal of General Physiology* 151, no. 4 (April 1, 2019): 478–88. https://doi.org/10.1085/jgp.201812129.

Curran, Mark E, Igor Splawski, Katherine W Timothy, G.Michael Vincen, Eric D Green, and Mark T Keating. “A Molecular Basis for Cardiac Arrhythmia: HERG Mutations Cause Long QT Syndrome.” *Cell* 80, no. 5 (March 1995): 795–803. https://doi.org/10.1016/0092-8674(95)90358-5.

DiMarco, John P. “Implantable Cardioverter–Defibrillators.” *The New England Journal of Medicine*, 2003, 12.

Doyle, D. A. “The Structure of the Potassium Channel: Molecular Basis of K+ Conduction and Selectivity.” *Science* 280, no. 5360 (April 3, 1998): 69–77. https://doi.org/10.1126/science.280.5360.69.

Du, Chun Yun, Ismail Adeniran, Hongwei Cheng, Yi Hong Zhang, Aziza El Harchi, Mark J. Mcpate, Henggui Zhang, Clive H. Orchard, and Jules C. Hancox. “Acidosis Impairs the Protective Role of HERG K+ Channels Against Premature Stimulation.” *Journal of Cardiovascular Electrophysiology* 21, no. 10 (October 2010): 1160–69. https://doi.org/10.1111/j.1540-8167.2010.01772.x.

Du, Chunyun, Aziza El Harchi, Henggui Zhang, and Jules C. Hancox. “Modification by KCNE1 Variants of the HERG Potassium Channel Response to Premature Stimulation and to Pharmacological Inhibition.” *Physiological Reports* 1, no. 6 (November 2013): e00175. https://doi.org/10.1002/phy2.175.

Elliott, David J. S., Naciye Y. Dondas, Tim S. Munsey, and Asipu Sivaprasadarao. “Movement of the S4 Segment in the HERG Potassium Channel during Membrane Depolarization.” *Molecular Membrane Biology* 26, no. 8 (December 2009): 435–47. https://doi.org/10.3109/09687680903321081.

Es-Salah-Lamoureux, Zeineb, Robert Fougere, Ping Yu Xiong, Gail A. Robertson, and David Fedida. “Fluorescence-Tracking of Activation Gating in Human ERG Channels Reveals Rapid S4 Movement and Slow Pore Opening.” Edited by Michael N. Nitabach. *PLoS ONE* 5, no. 5 (May 28, 2010): e10876. https://doi.org/10.1371/journal.pone.0010876.

Ferrer, Tania, Jason Rupp, David R. Piper, and Martin Tristani-Firouzi. “The S4-S5 Linker Directly Couples Voltage Sensor Movement to the Activation Gate in the Human Ether-á-Go-Go-Related Gene (HERG) K^+ Channel.” *Journal of Biological Chemistry* 281, no. 18 (May 5, 2006): 12858–64. https://doi.org/10.1074/jbc.M513518200.

Foo, Brian, Camille Barbier, Kevin Guo, Jaminie Vasantharuban, Gergely L. Lukacs, and Alvin Shrier. “Mutation-Specific Peripheral and ER Quality Control of HERG Channel Cell-Surface Expression.” *Scientific Reports* 9, no. 1 (December 2019): 6066. https://doi.org/10.1038/s41598-019-42331-6.

Gardner, Alison, and Michael C. Sanguinetti. “C-Linker Accounts for Differential Sensitivity of ERG1 and ERG2 K $^{+}$ Channels to RPR260243-Induced Slow Deactivation.” *Molecular Pharmacology* 88, no. 1 (July 2015): 19–28. https://doi.org/10.1124/mol.115.098384.

Gerlach, Aaron C., Sally J. Stoehr, and Neil A. Castle. “Pharmacological Removal of Human *Ether-à-Go-Go* -Related Gene Potassium Channel Inactivation by 3-Nitro- *N* -(4-Phenoxyphenyl) Benzamide (ICA-105574).” *Molecular Pharmacology* 77, no. 1 (January 2010): 58–68. https://doi.org/10.1124/mol.109.059543.

Gianulis, Elena C., and Matthew C. Trudeau. “Rescue of Aberrant Gating by a Genetically Encoded PAS (Per-Arnt-Sim) Domain in Several Long QT Syndrome Mutant Human *Ether-á-Go-Go* -Related Gene Potassium Channels.” *Journal of Biological Chemistry* 286, no. 25 (June 24, 2011): 22160–69. https://doi.org/10.1074/jbc.M110.205948.

Giudicessi, John R., and Michael J. Ackerman. “Genotype- and Phenotype-Guided Management of Congenital Long QT Syndrome.” *Current Problems in Cardiology* 38, no. 10 (October 2013): 417–55. https://doi.org/10.1016/j.cpcardiol.2013.08.001.

Goodchild, Samuel J., Logan C. Macdonald, and David Fedida. “Sequence of Gating Charge Movement and Pore Gating in HERG Activation and Deactivation Pathways.” *Biophysical Journal* 108, no. 6 (March 2015): 1435–47. https://doi.org/10.1016/j.bpj.2015.02.014.

Grandi, Eleonora, Francesco S. Pasqualini, and Donald M. Bers. “A Novel Computational Model of the Human Ventricular Action Potential and Ca Transient.” *Journal of Molecular and Cellular Cardiology* 48, no. 1 (January 2010): 112–21. https://doi.org/10.1016/j.yjmcc.2009.09.019.

Gustina, A. S., and M. C. Trudeau. “A Recombinant N-Terminal Domain Fully Restores Deactivation Gating in N-Truncated and Long QT Syndrome Mutant HERG Potassium Channels.” *Proceedings of the National Academy of Sciences* 106, no. 31 (August 4, 2009): 13082–87. https://doi.org/10.1073/pnas.0900180106.

Gustina, Ahleah S., and Matthew C. Trudeau. “HERG Potassium Channel Gating Is Mediated by N- and C-Terminal Region Interactions.” *The Journal of General Physiology* 137, no. 3 (March 1, 2011): 315–25. https://doi.org/10.1085/jgp.201010582.

———. “HERG Potassium Channel Regulation by the N-Terminal Eag Domain.” *Cellular Signalling* 24, no. 8 (August 2012): 1592–98. https://doi.org/10.1016/j.cellsig.2012.04.004.

Hancox, Jules C., Mark J. McPate, Aziza El Harchi, and Yi hong Zhang. “The HERG Potassium Channel and HERG Screening for Drug-Induced Torsades de Pointes.” *Pharmacology & Therapeutics* 119, no. 2 (August 2008): 118–32. https://doi.org/10.1016/j.pharmthera.2008.05.009.

Hardman, Rachael M., Phillip J. Stansfeld, Sarah Dalibalta, Michael J. Sutcliffe, and John S. Mitcheson. “Activation Gating of HERG Potassium Channels: *S6 GLYCINES ARE NOT REQUIRED AS GATING HINGES*.” *Journal of Biological Chemistry* 282, no. 44 (November 2, 2007): 31972–81. https://doi.org/10.1074/jbc.M705835200.

Hayashi, K. “Characterization of a Novel Missense Mutation E637K in the Pore-S6 Loop of HERG in a Patient with Long QT Syndrome.” *Cardiovascular Research* 54, no. 1 (April 2002): 67–76. https://doi.org/10.1016/S0008-6363(02)00240-7.

Helliwell, Matthew V., Yihong Zhang, Aziza El Harchi, Chunyun Du, Jules C. Hancox, and Christopher E. Dempsey. “Structural Implications of HERG K $^{+}$ Channel Block by a High-Affinity Minimally Structured Blocker.” *Journal of Biological Chemistry* 293, no. 18 (May 4, 2018): 7040–57. https://doi.org/10.1074/jbc.RA117.000363.

Hodgkin, A. L., and A. F. Huxley. “Currents Carried by Sodium and Potassium Ions through the Membrane of the Giant Axon of *Loligo*.” *The Journal of Physiology* 116, no. 4 (April 28, 1952): 449–72. https://doi.org/10.1113/jphysiol.1952.sp004717.

———. “The Components of Membrane Conductance in the Giant Axon of *Loligo*.” *The Journal of Physiology* 116, no. 4 (April 28, 1952): 473–96. https://doi.org/10.1113/jphysiol.1952.sp004718.

———. “The Dual Effect of Membrane Potential on Sodium Conductance in the Giant Axon of *Loligo*.” *The Journal of Physiology* 116, no. 4 (April 28, 1952): 497–506. https://doi.org/10.1113/jphysiol.1952.sp004719.

Hodgkin A.L., Huxley A.F., Katz B. Measurement of current-voltage relations in the membrane of the giant axon of Loligo. *J Physiol.* 1952 Apr;**116**(4):424–448.

Hoshi, T., W. Zagotta, and R. Aldrich “Two types of inactivation in Shaker K+ channels: effects of alterations in the carboxy-terminal region.” *Neuron* vol. 7,4 (1991): 547-56. doi:10.1016/0896-6273(91)90367-9

Hoshi, T., W. Zagotta, and R. Aldrich. “Biophysical and Molecular Mechanisms of Shaker Potassium Channel Inactivation.” *Science* 250, no. 4980 (October 26, 1990): 533–38. https://doi.org/10.1126/science.2122519.

Hua, Fei, and Robert F. Gilmour. “Contribution of I_{Kr} to Rate-Dependent Action Potential Dynamics in Canine Endocardium.” *Circulation Research* 94, no. 6 (April 2, 2004): 810–19. https://doi.org/10.1161/01.RES.0000121102.24277.89.

Hull, Christina M., Christine E. Genge, Yuki Hobbs, Kaveh Rayani, Eric Lin, Marvin Gunawan, Sanam Shafaattalab, Glen F. Tibbits, and Tom W. Claydon. “Investigating the Utility of Adult Zebrafish Ex Vivo Whole Hearts to Pharmacologically Screen HERG Channel Activator Compounds.” *American Journal of Physiology-Regulatory, Integrative and Comparative Physiology* 317, no. 6 (December 1, 2019): R921–31. https://doi.org/10.1152/ajpregu.00190.2019.

Hull, Christina M., Stanislav Sokolov, Aaron C. Van Slyke, and Tom W. Claydon. “Regional Flexibility in the S4–S5 Linker Regulates HERG Channel Closed-State Stabilization.” *Pflügers Archiv - European Journal of Physiology* 466, no. 10 (October 2014): 1911–19. https://doi.org/10.1007/s00424-013-1431-9.

Benhorin Jesaia & Aharon Medina. “Congenital Long-QT Syndrome,” *New England Journal of Medicine* 336, no. 1568 (May 29, 1997)

Jiang, Qiang, Kai Li, Wen-Jing Lu, Shuang Li, Xin Chen, Xi-Juan Liu, Jie Yuan, Qiurong Ding, Feng Lan, and Shi-Qing Cai. “Identification of Small-Molecule Ion Channel Modulators in C. Elegans Channelopathy Models.” *Nature Communications* 9, no. 1 (December 2018): 3941. https://doi.org/10.1038/s41467-018-06514-5.

Jiang, Youxing, Alice Lee, Jiayun Chen, Martine Cadene, Brian T. Chait, and Roderick MacKinnon. “Crystal Structure and Mechanism of a Calcium-Gated Potassium Channel.” *Nature* 417, no. 6888 (May 2002): 515–22. https://doi.org/10.1038/417515a.

———. “The Open Pore Conformation of Potassium Channels.” *Nature* 417, no. 6888 (May 2002): 523–26. https://doi.org/10.1038/417523a.

Jiang, Youxing, Alice Lee, Jiayun Chen, Vanessa Ruta, Martine Cadene, Brian T. Chait, and Roderick MacKinnon. “X-Ray Structure of a Voltage-Dependent K+ Channel.” *Nature* 423, no. 6935 (May 2003): 33–41. https://doi.org/10.1038/nature01580.

Jones, Eugenia M. C., Elon C. Roti Roti, Jinling Wang, Samantha A. Delfosse, and Gail A. Robertson. “Cardiac I_{Kr} Channels Minimally Comprise HERG 1a and 1b Subunits.” *Journal of Biological Chemistry* 279, no. 43 (October 22, 2004): 44690–94. https://doi.org/10.1074/jbc.M408344200.

Kang, Jiesheng, Xiao-Liang Chen, Hongge Wang, Junzhi Ji, Hsien Cheng, Josephine Incardona, William Reynolds, Fabrice Viviani, Michel Tabart, and David Rampe. “Discovery of a Small Molecule Activator of the Human *Ether-a-Go-Go* -Related Gene (HERG) Cardiac K^+ Channel.” *Molecular Pharmacology* 67, no. 3 (March 2005): 827–36. https://doi.org/10.1124/mol.104.006577.

Kannankeril, Prince, Dan M. Roden, and Dawood Darbar. “Drug-Induced Long QT Syndrome.” Edited by David Sibley. *Pharmacological Reviews* 62, no. 4 (December 2010): 760–81. https://doi.org/10.1124/pr.110.003723.

Kanner, Scott A., Ananya Jain, and Henry M. Colecraft. “Development of a High-Throughput Flow Cytometry Assay to Monitor Defective Trafficking and Rescue of Long QT2 Mutant HERG Channels.” *Frontiers in Physiology* 9 (April 19, 2018): 397. https://doi.org/10.3389/fphys.2018.00397.

Kaplan, W D, and W E Trout 3rd. “The behavior of four neurological mutants of Drosophila.” *Genetics* vol. 61,2 (1969): 399-409.

Kapplinger, Jamie D., David J. Tester, Benjamin A. Salisbury, Janet L. Carr, Carole Harris-Kerr, Guido D. Pollevick, Arthur A.M. Wilde, and Michael J. Ackerman. “Spectrum and Prevalence of Mutations from the First 2,500 Consecutive Unrelated Patients Referred for the FAMILION® Long QT Syndrome Genetic Test.” *Heart Rhythm* 6, no. 9 (September 2009): 1297–1303. https://doi.org/10.1016/j.hrthm.2009.05.021.

Lacroix, Jérôme J., Alain J. Labro, and Francisco Bezanilla. “Properties of Deactivation Gating Currents in Shaker Channels.” *Biophysical Journal* 100, no. 5 (March 2011): L28–30. https://doi.org/10.1016/j.bpj.2011.01.043.

Liu, Qiang-ni, and Matthew C. Trudeau. “Eag Domains Regulate LQT Mutant HERG Channels in Human Induced Pluripotent Stem Cell-Derived Cardiomyocytes.” Edited by Katriina Aalto-Setala. *PLOS ONE* 10, no. 4 (April 29, 2015): e0123951. https://doi.org/10.1371/journal.pone.0123951.

Liu, S., R.L. Rasmusson, D.L. Campbell, S. Wang, and H.C. Strauss. “Activation and Inactivation Kinetics of an E-4031-Sensitive Current from Single Ferret Atrial Myocytes.” *Biophysical Journal* 70, no. 6 (June 1996): 2704–15. https://doi.org/10.1016/S0006-3495(96)79840-5.

Long, S. B. “Crystal Structure of a Mammalian Voltage-Dependent Shaker Family K+ Channel.” *Science* 309, no. 5736 (August 5, 2005): 897–903. https://doi.org/10.1126/science.1116269.

López-Barneo, J, H. Toshinori, S. Heinemann, R. Aldrich. Aldrich, Richard. “Effects of external cations and mutations in the pore region on C-type inactivation of Shaker potassium channels.” *Receptors & Channels* 1. (1993):61-71.

Lu, Y., M. P Mahaut-Smith, C. L-H Huang, and J. I Vandenberg. “Mutant MiRP1 Subunits Modulate HERG K+ Channel Gating: A Mechanism for pro-Arrhythmia in Long QT Syndrome Type 6.” *The Journal of Physiology* 551, no. 1 (August 15, 2003): 253–62. https://doi.org/10.1113/jphysiol.2003.046045.

Lu, Yu, P. Mahaut-Smith, Anthony Varghese, Christopher L.-H. Huang, Paul R. Kemp, and Jamie I. Vandenberg. “Effects of Premature Stimulation on HERG K $^{+}$ Channels.” *The Journal of Physiology* 537, no. 3 (December 2001): 843–51. https://doi.org/10.1111/j.1469-7793.2001.00843.x.

Mao, Haiyan, Xiaoli Lu, Justin Michael Karush, Xiaoyan Huang, Xi Yang, Yanna Ba, Ying Wang, Ningsheng Liu, Jianqing Zhou, and Jiangfang Lian. “Pharmacologic Approach to Defective Protein Trafficking in the E637K-HERG Mutant with PD-118057 and Thapsigargin.” Edited by Andrea Cavalli. *PLoS ONE* 8, no. 6 (June 19, 2013): e65481. https://doi.org/10.1371/journal.pone.0065481.

Matsuura, Hiroshi, Tsuguhisa Ehara, and Yutaka Imoto. “An Analysis of the Delayed Outward Current in Single Ventricular Cells of the Guinea-Pig.” *Pfl*[illegible]*gers Archiv European Journal of Physiology* 410, no. 6 (December 1987): 596–603. https://doi.org/10.1007/BF00581319.

McDonald, Thomas V., Zhihui Yu, Zhen Ming, Eugen Palma, Marian B. Meyers, Ke-Wei Wang, Steve A. N. Goldstein, and Glenn I. Fishman. “A MinK–HERG Complex Regulates the Cardiac Potassium Current IKr.” *Nature* 388, no. 6639 (July 1997): 289–92. https://doi.org/10.1038/40882.

McPate, M.J., H. Zhang, I. Adeniran, J.M. Cordeiro, H.J. Witchel, J.C. Hancox. “Comparative effects of the short QT N588K mutation at 37 degrees C on hERG K+ channel current during ventricular, Purkinje fibre and atrial action potentials: an action potential clamp study.” *Journal of physiology and pharmacology : an official journal of the Polish Physiological Society* vol. 60,1 (2009): 23-41.

McPate, Mark J., Rona S. Duncan, James T. Milnes, Harry J. Witchel, and Jules C. Hancox. “The N588K-HERG K+ Channel Mutation in the ‘Short QT Syndrome’: Mechanism of Gain-in-Function Determined at 37°C.” *Biochemical and Biophysical Research Communications* 334, no. 2 (August 2005): 441–49. https://doi.org/10.1016/j.bbrc.2005.06.112.

Melgari, Dario, Chunyun Du, Aziza El Harchi, Yihong Zhang, and Jules C. Hancox. “Suppression of the HERG Potassium Channel Response to Premature Stimulation by Reduction in Extracellular Potassium Concentration.” *Physiological Reports* 2, no. 10 (October 2014): e12165. https://doi.org/10.14814/phy2.12165.

Mitcheson, J. S., J. Chen, M. Lin, C. Culberson, and M. C. Sanguinetti. “A Structural Basis for Drug-Induced Long QT Syndrome.” *Proceedings of the National Academy of Sciences* 97, no. 22 (October 24, 2000): 12329–33. https://doi.org/10.1073/pnas.210244497.

Modell, Stephen M, and Michael H Lehmann. “The Long QT Syndrome Family of Cardiac Ion Channelopathies: A HuGE Review*.” *Genetics in Medicine* 8, no. 3 (March 2006): 143–55. https://doi.org/10.1097/01.gim.0000204468.85308.86.

Morais Cabral, J H et al. “Crystal structure and functional analysis of the HERG potassium channel N terminus: a eukaryotic PAS domain.” *Cell* vol. 95,5 (1998): 649-55. doi:10.1016/s0092-8674(00)81635-9.

Ng, Chai Ann, Matthew D. Perry, Peter S. Tan, Adam P. Hill, Philip W. Kuchel, and Jamie I. Vandenberg. “The S4–S5 Linker Acts as a Signal Integrator for HERG K+ Channel Activation and Deactivation Gating.” Edited by Bernard Attali. *PLoS ONE* 7, no. 2 (February 16, 2012): e31640. https://doi.org/10.1371/journal.pone.0031640.

Ng, Chai Ann, Kevin Phan, Adam P. Hill, Jamie I. Vandenberg, and Matthew D. Perry. “Multiple Interactions between Cytoplasmic Domains Regulate Slow Deactivation of Kv11.1 Channels.” *Journal of Biological Chemistry* 289, no. 37 (September 12, 2014): 25822–32. https://doi.org/10.1074/jbc.M114.558379.

Noble, D, and R W Tsien. “Outward membrane currents activated in the plateau range of potentials in cardiac Purkinje fibres.” *The Journal of physiology* vol. 200,1 (1969): 205-31. doi:10.1113/jphysiol.1969.sp008689

Nuss, H. Bradley, Eduardo Marbán, and David C. Johns. “Overexpression of a Human Potassium Channel Suppresses Cardiac Hyperexcitability in Rabbit Ventricular Myocytes.” *Journal of Clinical Investigation* 103, no. 6 (March 15, 1999): 889–96. https://doi.org/10.1172/JCI5073.

O’Hara, Thomas, László Virág, András Varró, and Yoram Rudy. “Simulation of the Undiseased Human Cardiac Ventricular Action Potential: Model Formulation and Experimental Validation.” Edited by Andrew D. McCulloch. *PLoS Computational Biology* 7, no. 5 (May 26, 2011): e1002061. https://doi.org/10.1371/journal.pcbi.1002061.

Pages, Guilhem, Allan M. Torres, Pengchu Ju, Paramjit S. Bansal, Paul F. Alewood, Philip W. Kuchel, and Jamie I. Vandenberg. “Structure of the Pore-Helix of the HERG K+ Channel.” *European Biophysics Journal* 39, no. 1 (December 2009): 111–20. https://doi.org/10.1007/s00249-009-0433-1.

Papazian DM, Schwarz TL, Tempel BL, Jan YN, Jan LY. “Cloning of genomic and complementary DNA from Shaker, a putative potassium channel gene from Drosophila.” *Science*. 1987;237(4816):749-753. doi:10.1126/science.2441470

Peña, Pilar de la, Pedro Domínguez, and Francisco Barros. “Gating Mechanism of Kv11.1 (HERG) K+ Channels without Covalent Connection between Voltage Sensor and Pore Domains.” *Pflügers Archiv - European Journal of Physiology* 470, no. 3 (March 2018): 517–36. https://doi.org/10.1007/s00424-017-2093-9.

Perozo, E., D.M. Papazian, E. Stefani, and F. Bezanilla. “Gating Currents in Shaker K+ Channels. Implications for Activation and Inactivation Models.” *Biophysical Journal* 62, no. 1 (April 1992): 160–71. https://doi.org/10.1016/S0006-3495(92)81802-7.

Perrin, Mark J., Rajesh N. Subbiah, Jamie I. Vandenberg, and Adam P. Hill. “Human Ether-a-Go-Go Related Gene (HERG) K+ Channels: Function and Dysfunction.” *Progress in Biophysics and Molecular Biology* 98, no. 2–3 (October 2008): 137–48. https://doi.org/10.1016/j.pbiomolbio.2008.10.006.

Perry, M., F. B. Sachse, J. Abbruzzese, and M. C. Sanguinetti. “PD-118057 Contacts the Pore Helix of HERG1 Channels to Attenuate Inactivation and Enhance K+ Conductance.” *Proceedings of the National Academy of Sciences* 106, no. 47 (November 24, 2009): 20075–80. https://doi.org/10.1073/pnas.0906597106.

Perry, M., F. B. Sachse, and M. C. Sanguinetti. “Structural Basis of Action for a Human Ether-a-Go-Go-Related Gene 1 Potassium Channel Activator.” *Proceedings of the National Academy of Sciences* 104, no. 34 (August 21, 2007): 13827–32. https://doi.org/10.1073/pnas.0703934104.

Perry, Matthew D., Chai Ann Ng, Kevin Phan, Erikka David, Kieran Steer, Mark J. Hunter, Stefan A. Mann, et al. “Rescue of Protein Expression Defects May Not Be Enough to Abolish the Pro-Arrhythmic Phenotype of Long QT Type 2 Mutations: Functional Defects of LQTS2 Mutations.” *The Journal of Physiology* 594, no. 14 (July 15, 2016): 4031–49. https://doi.org/10.1113/JP271805.

Perry, Matthew D, Chai-Ann Ng, Melissa M Mangala, Timothy Y M Ng, Adam D Hines, Whitney Liang, Michelle J O Xu, Adam P Hill, and Jamie I Vandenberg. “Pharmacological Activation of IKr in Models of Long QT Type 2 Risks Overcorrection of Repolarization.” *Cardiovascular Research* 116, no. 8 (July 1, 2020): 1434–45. https://doi.org/10.1093/cvr/cvz247.

Perry, Matthew D., Chai-Ann Ng, Stefan A. Mann, Arash Sadrieh, Mohammad Imtiaz, Adam P. Hill, and Jamie I. Vandenberg. “Getting to the Heart of HERG K $^{+}$ Channel Gating: Getting to the Heart of HERG K+ Channel Gating.” *The Journal of Physiology* 593, no. 12 (June 15, 2015): 2575–85. https://doi.org/10.1113/JP270095.

Perry, Matthew, Marcel J. de Groot, Ray Helliwell, Derek Leishman, Martin Tristani-Firouzi, Michael C. Sanguinetti, and John Mitcheson. “Structural Determinants of HERG Channel Block by Clofilium and Ibutilide.” *Molecular Pharmacology* 66, no. 2 (August 2004): 240–49. https://doi.org/10.1124/mol.104.000117.

Perry, Matthew, and Michael C. Sanguinetti. “A Single Amino Acid Difference between *Ether-a-Go-Go-* Related Gene Channel Subtypes Determines Differential Sensitivity to a Small Molecule Activator.” *Molecular Pharmacology* 73, no. 4 (April 2008): 1044–51. https://doi.org/10.1124/mol.107.043018.

Perry, Matthew, Michael Sanguinetti, and John Mitcheson. “SYMPOSIUM REVIEW: Revealing the Structural Basis of Action of HERG Potassium Channel Activators and Blockers: HERG Channel Blockers and Activators.” *The Journal of Physiology* 588, no. 17 (September 1, 2010): 3157–67. https://doi.org/10.1113/jphysiol.2010.194670.

Piper, D. R., A. Varghese, M. C. Sanguinetti, and M. Tristani-Firouzi. “Gating Currents Associated with Intramembrane Charge Displacement in HERG Potassium Channels.” *Proceedings of the National Academy of Sciences* 100, no. 18 (September 2, 2003): 10534–39. https://doi.org/10.1073/pnas.1832721100.

Piper, David R., William A. Hinz, Chandra K. Tallurri, Michael C. Sanguinetti, and Martin Tristani-Firouzi. “Regional Specificity of Human *Ether-a’-Go-Go* -Related Gene Channel Activation and Inactivation Gating.” *Journal of Biological Chemistry* 280, no. 8 (February 25, 2005): 7206–17. https://doi.org/10.1074/jbc.M411042200.

Potet, Franck, Amanda N. Lorinc, Sebastien Chaigne, Corey R. Hopkins, Raghav Venkataraman, Svetlana Z. Stepanovic, L. Michelle Lewis, et al. “Identification and Characterization of a Compound That Protects Cardiac Tissue from Human Ether-à-Go-Go-Related Gene (HERG)-Related Drug-Induced Arrhythmias.” *Journal of Biological Chemistry* 287, no. 47 (November 16, 2012): 39613–25. https://doi.org/10.1074/jbc.M112.380162.

Pourrier, Marc, Stephen Zicha, Joachim Ehrlich, Wei Han, and Stanley Nattel. “Canine Ventricular KCNE2 Expression Resides Predominantly in Purkinje Fibers.” *Circulation Research* 93, no. 3 (August 8, 2003): 189–91. https://doi.org/10.1161/01.RES.0000084851.60947.B5.

Rasmusson, Randall L., and Justus M. Anumonwo. “Activation of HERG Channels: Opening New Applications for the Biophysics of Antiarrhythmic Therapy.” *Biophysical Journal* 108, no. 6 (March 2015): 1309–11. https://doi.org/10.1016/j.bpj.2015.01.011.

Robertson, Gail A., and João H. Morais-Cabral. “HERG Function in Light of Structure.” *Biophysical Journal* 118, no. 4 (February 2020): 790–97. https://doi.org/10.1016/j.bpj.2019.10.010.

Royer, A, S Demolombe, A Elharchi, K Lequang, J Piron, G Toumaniantz, D Mazurais, C Bellocq, G Lande, and C Terrenoire. “Expression of Human ERG K Channels in the Mouse Heart Exerts Anti-Arrhythmic Activity.” *Cardiovascular Research* 65, no. 1 (January 1, 2005): 128–37. https://doi.org/10.1016/j.cardiores.2004.09.030.

Sale, Harinath, Jinling Wang, Thomas J. O’Hara, David J. Tester, Pallavi Phartiyal, Jia-Qiang He, Yoram Rudy, Michael J. Ackerman, and Gail A. Robertson. “Physiological Properties of HERG 1a/1b Heteromeric Currents and a HERG 1b-Specific Mutation Associated With Long-QT Syndrome.” *Circulation Research* 103, no. 7 (September 26, 2008). https://doi.org/10.1161/CIRCRESAHA.108.185249.

Sanguinetti, M.C., M. E. Curran, P. S. Spector, and M. T. Keating. “Spectrum of HERG K+-Channel Dysfunction in an Inherited Cardiac Arrhythmia.” *Proceedings of the National Academy of Sciences* 93, no. 5 (March 5, 1996): 2208–12. https://doi.org/10.1073/pnas.93.5.2208.

Sanguinetti, M.C., and N.K. Jurkiewicz. “Two Components of Cardiac Delayed Rectifier K+ Current. Differential Sensitivity to Block by Class III Antiarrhythmic Agents.” *The Journal of General Physiology* 96, no. 1 (July 1, 1990): 195–215. https://doi.org/10.1085/jgp.96.1.195.

Sanguinetti, M.C., C. Jiang, M.E. Curran, and M.T. Keating. “A Mechanistic Link between an Inherited and an Acquired Cardiac Arrhythmia: HERG Encodes the IKr Potassium Channel,” Cell 81, no 2 (April 21, 1995): 299-307.

Sanguinetti, Michael C., and Martin Tristani-Firouzi. “HERG Potassium Channels and Cardiac Arrhythmia.” *Nature* 440, no. 7083 (March 2006): 463–69. https://doi.org/10.1038/nature04710.

Sanguinetti, M C, and Q P Xu. “Mutations of the S4-S5 linker alter activation properties of HERG potassium channels expressed in Xenopus oocytes.” *The Journal of physiology* vol. 514 (Pt 3),Pt 3 (1999): 667-75. doi:10.1111/j.1469-7793.1999.667ad.x.

Schönherr, R, and S H Heinemann. “Molecular Determinants for Activation and Inactivation of HERG, a Human Inward Rectifier Potassium Channel.” *The Journal of Physiology* 493, no. 3 (June 15, 1996): 635–42. https://doi.org/10.1113/jphysiol.1996.sp021410.

Schwartz, Peter J., Lia Crotti, and Roberto Insolia. “Long-QT Syndrome: From Genetics to Management.” *Circulation: Arrhythmia and Electrophysiology* 5, no. 4 (August 2012): 868–77. https://doi.org/10.1161/CIRCEP.111.962019.

Schwartz, Peter J., Marco Stramba-Badiale, Lia Crotti, Matteo Pedrazzini, Alessandra Besana, Giuliano Bosi, Fulvio Gabbarini, et al. “Prevalence of the Congenital Long-QT Syndrome.” *Circulation* 120, no. 18 (November 3, 2009): 1761–67. https://doi.org/10.1161/CIRCULATIONAHA.109.863209.

Shao, Chunyan, Yan Lu, Mohan Liu, Qi Chen, Yunfeng Lan, Yan Liu, Min Lin, and Yang Li. “Electrophysiological Study of V535M HERG Mutation of LQT2.” *Journal of Huazhong University of Science and Technology [Medical Sciences]* 31, no. 6 (December 2011): 741–48. https://doi.org/10.1007/s11596-011-0670-2.

Shi, Yu Patrick, Yen May Cheng, Aaron C. Van Slyke, and Tom W. Claydon. “External Protons Destabilize the Activated Voltage Sensor in HERG Channels.” *European Biophysics Journal* 43, no. 2–3 (March 2014): 59–69. https://doi.org/10.1007/s00249-013-0940-y.

Shi, Yu Patrick, Samrat Thouta, Yen May Cheng, and Tom W. Claydon. “Extracellular Protons Accelerate HERG Channel Deactivation by Destabilizing Voltage Sensor Relaxation.” *Journal of General Physiology* 151, no. 2 (February 4, 2019): 231–46. https://doi.org/10.1085/jgp.201812137.

Smith, Paula L., Thomas Baukrowitz, and Gary Yellen. “The Inward Rectification Mechanism of the HERG Cardiac Potassium Channel.” *Nature* 379, no. 6568 (February 1996): 833–36. https://doi.org/10.1038/379833a0.

Smith, Paula L, and Gary Yellen. “Fast and slow voltage sensor movements in HERG potassium channels.” *The Journal of general physiology* vol. 119,3 (2002): 275-93. doi:10.1085/jgp.20028534

Spector, P S, M E Curran, A Zou, M T Keating, and M C Sanguinetti. “Fast Inactivation Causes Rectification of the IKr Channel.” *The Journal of General Physiology* 107, no. 5 (May 1, 1996): 611–19. https://doi.org/10.1085/jgp.107.5.611.

Stefani, Enrico, Ligia Toro, Eduardo Perozo, and Francisco Bezanillat. “Gating of Shaker K+ Channels: 1. Ionic and Gating Currents.” *Biophysical Journal* 66 (1994): 15.

Stühmer, Walter, Franco Conti, Harukazu Suzuki, Xiaodong Wang, Masaharu Noda, Naoki Yahagi, Hideo Kubo, and Shosaku Numa. “Structural Parts Involved in Activation and Inactivation of the Sodium Channel.” *Nature* 339, no. 6226 (June 1989): 597–603. https://doi.org/10.1038/339597a0.

Subbiah, Rajesh N., Catherine E. Clarke, David J. Smith, JingTing Zhao, Terence J. Campbell, and Jamie I. Vandenberg. “Molecular Basis of Slow Activation of the Human *Ether-á-Go-Go* Related Gene Potassium Channel: Molecular Basis of Slow Activation of HERG Channels.” *The Journal of Physiology* 558, no. 2 (July 2004): 417–31. https://doi.org/10.1113/jphysiol.2004.062588.

Sun, Yaxun, Xiao-Qing Quan, Samantha Fromme, Robert H. Cox, Ping Zhang, Li Zhang, Donglin Guo, et al. “A Novel Mutation in the KCNH2 Gene Associated with Short QT Syndrome.” *Journal of Molecular and Cellular Cardiology* 50, no. 3 (March 2011): 433–41. https://doi.org/10.1016/j.yjmcc.2010.11.017.

Szabo, G., V. Farkas, M. Grunnet, A. Mohacsi, and P. P. Nanasi. “Enhanced Repolarization Capacity: New Potential Antiarrhythmic Strategy Based on HERG Channel Activation.” *Current Medicinal Chemistry* 18, no. 24 (August 1, 2011): 3607–21. https://doi.org/10.2174/092986711796642382.

Tester, D.J., and M.J. Ackerman. “Genetics of long QT syndrome.” *Methodist DeBakey cardiovascular journal* vol. 10,1 (2014): 29-33. doi:10.14797/mdcj-10-1-29

Thouta, Samrat, Christina M. Hull, Yu Patrick Shi, Valentine Sergeev, James Young, Yen M. Cheng, and Thomas W. Claydon. “Stabilization of the Activated HERG Channel Voltage Sensor by Depolarization Involves the S4-S5 Linker.” *Biophysical Journal* 112, no. 2 (January 2017): 300–312. https://doi.org/10.1016/j.bpj.2016.12.021.

Tristani-Firouzi, Martin, Jun Chen, and Michael C. Sanguinetti. “Interactions between S4-S5 Linker and S6 Transmembrane Domain Modulate Gating of HERG K $^{+}$ Channels.” *Journal of Biological Chemistry* 277, no. 21 (May 24, 2002): 18994–0. https://doi.org/10.1074/jbc.M200410200.

Trudeau, M., J. Warmke, B Ganetzky, and G. Robertson. “HERG, a Human Inward Rectifier in the Voltage-Gated Potassium Channel Family.” *Science* 269, no. 5220 (July 7, 1995): 92–95. https://doi.org/10.1126/science.7604285.

Van Slyke, Aaron C., Saman Rezazadeh, Mischa Snopkowski, Patrick Shi, Charlene R. Allard, and Tom W. Claydon. “Mutations within the S4–S5 Linker Alter Voltage Sensor Constraints in HERG K+ Channels.” *Biophysical Journal* 99, no. 9 (November 2010): 2841–52. https://doi.org/10.1016/j.bpj.2010.08.030.

Vandenberg, Jamie I., Matthew D. Perry, Mark J. Perrin, Stefan A. Mann, Ying Ke, and Adam P. Hill. “HERG K $^{+}$ Channels: Structure, Function, and Clinical Significance.” *Physiological Reviews* 92, no. 3 (July 2012): 1393–1478. https://doi.org/10.1152/physrev.00036.2011.

Villalba-Galea, C. A., W. Sandtner, D. M. Starace, and F. Bezanilla. “S4-Based Voltage Sensors Have Three Major Conformations.” *Proceedings of the National Academy of Sciences* 105, no. 46 (November 18, 2008): 17600–607. https://doi.org/10.1073/pnas.0807387105.

Waddell-Smith, Kathryn E, and Jonathan R Skinner. “Update on the Diagnosis and Management of Familial Long QT Syndrome.” *Heart, Lung and Circulation* 25, no. 8 (August 2016): 769–76. https://doi.org/10.1016/j.hlc.2016.01.020.

Wang, David T, Adam P Hill, Stefan A Mann, Peter S Tan, and Jamie I Vandenberg. "Mapping the Sequence of Conformational Changes Underlying Selectivity Filter Gating in the Kv11.1 Potassium Channel." *Nature Structural & Molecular Biology* 18, no. 1 (January 2011): 35–41. https://doi.org/10.1038/nsmb.1966.

Wang, Shimin, Shuguang Liu, Michael J. Morales, Harold C. Strauss, and Randall L. Rasmusson. "A Quantitative Analysis of the Activation and Inactivation Kinetics of *HERG* Expressed in *Xenopus* Oocytes." *The Journal of Physiology* 502, no. 1 (July 1997): 45–60. https://doi.org/10.1111/j.1469-7793.1997.045bl.x.

Wang, Shimin, Shuguang Liu, Michael J Morales, Harold C Strauss, and Randall L Rasmusson. "A Quantitative Analysis of the Activation and Inactivation Kinetics of SHEROG Expressed in Xenopus Oocytes." *J Physiol.*, n.d., 16.

Wang, Shimin, Michael J. Morales, Shuguang Liu, Harold C. Strauss, and Randall L. Rasmusson. "Time, Voltage and Ionic Concentration Dependence of Rectification of h-*Er* g Expressed in *Xenopus* Oocytes." *FEBS Letters* 389, no. 2 (July 1, 1996): 167–73. https://doi.org/10.1016/0014-5793(96)00570-4.

Wang, Weiwei, and Roderick MacKinnon. "Cryo-EM Structure of the Open Human Ether-à-Go-Go -Related K + Channel HERG." *Cell* 169, no. 3 (April 2017): 422-430.e10. https://doi.org/10.1016/j.cell.2017.03.048.

Warmke, J., R. Drysdale, and B. Ganetzky. "A Distinct Potassium Channel Polypeptide Encoded by the Drosophila Eag Locus." *Science* 252, no. 5012 (June 14, 1991): 1560–62. https://doi.org/10.1126/science.1840699.

Warmke, Jeffrey W, and Barry Ganetzky. "A Family of Potassium Channel Genes Related to Eag in Drophila and Mammals," n.d., 5.

Weiss, James N., Alan Garfinkel, Hrayr S. Karagueuzian, Peng-Sheng Chen, and Zhilin Qu. "Early Afterdepolarizations and Cardiac Arrhythmias." *Heart Rhythm* 7, no. 12 (December 2010): 1891–99. https://doi.org/10.1016/j.hrthm.2010.09.017.

Whicher, J. R., and R. MacKinnon. "Structure of the Voltage-Gated K+ Channel Eag1 Reveals an Alternative Voltage Sensing Mechanism." *Science* 353, no. 6300 (August 12, 2016): 664–69. https://doi.org/10.1126/science.aaf8070.

Wu, Wei, Alison Gardner, and Michael C. Sanguinetti. “Concatenated HERG1 Tetramers Reveal Stoichiometry of Altered Channel Gating by RPR-260243.” *Molecular Pharmacology* 87, no. 3 (March 2015): 401–9. https://doi.org/10.1124/mol.114.096693.

Wynia-Smith, Sarah L., Anne Lynn Gillian-Daniel, Kenneth A. Satyshur, and Gail A. Robertson. “HERG Gating Microdomains Defined by S6 Mutagenesis and Molecular Modeling.” *Journal of General Physiology* 132, no. 5 (November 1, 2008): 507–20. https://doi.org/10.1085/jgp.200810083.

Zeng, Haoyu, Irina M. Lozinskaya, Zuojun Lin, Robert N. Willette, David P. Brooks, and Xiaoping Xu. “Mallotoxin Is a Novel Human *Ether-a-Go-Go* -Related Gene (HERG) Potassium Channel Activator.” *Journal of Pharmacology and Experimental Therapeutics* 319, no. 2 (November 2006): 957–62. https://doi.org/10.1124/jpet.106.110593.

Zhang, H., B. Zou, H. Yu, A. Moretti, X. Wang, W. Yan, J. J. Babcock, et al. “Modulation of HERG Potassium Channel Gating Normalizes Action Potential Duration Prolonged by Dysfunctional KCNQ1 Potassium Channel.” *Proceedings of the National Academy of Sciences* 109, no. 29 (July 17, 2012): 11866–71. https://doi.org/10.1073/pnas.1205266109.

Zhang, M., J. Liu, M. Jiang, D.-M. Wu, K. Sonawane, H.R. Guy, and G.-N. Tseng. “Interactions Between Charged Residues in the Transmembrane Segments of the Voltage-Sensing Domain in the HERG Channel.” *Journal of Membrane Biology* 207, no. 3 (October 2005): 169–81. https://doi.org/10.1007/s00232-005-0812-1.

Zhou, Jun, Corinne E. Augelli-Szafran, Jenifer A. Bradley, Xian Chen, Bryan J. Koci, Walter A. Volberg, Zhuoqian Sun, and Jason S. Cordes. “Novel Potent Human *Ether-à-Go-Go* -Related Gene (*HERG*) Potassium Channel Enhancers and Their in Vitro Antiarrhythmic Activity.” *Molecular Pharmacology* 68, no. 3 (September 2005): 876–84. https://doi.org/10.1124/mol.105.014035.

Zhou, Ping-zheng, Joseph Babcock, Lian-qing Liu, Min Li, and Zhao-bing Gao. “Activation of Human Ether-a-Go-Go Related Gene (HERG) Potassium Channels by Small Molecules.” *Acta Pharmacologica Sinica* 32, no. 6 (June 2011): 781–88. https://doi.org/10.1038/aps.2011.70.

Zhou W, Cayabyab FS, Pennefather PS, Schlichter LC, DeCoursey TE. HERG-like K+ channels in microglia. J Gen Physiol. 1998 Jun;111(6):781-94. doi: 10.1085/jgp.111.6.781. PMID: 9607936; PMCID: PMC2217149.

Zhou, Y., J.H. Morais-Cabral, A. Kaufmann, R. MacKinnon “Chemistry of ion coordination and hydration revealed by a K+ channel-Fab complex at 2.0 A resolution.” *Nature* vol. 414,6859 (2001): 43-8. doi:10.1038/35102009